Electrochemical Investigations on the Reduction of Short Chain SAMs from a Au(111) Electrode

by

Gabriele Hager
M.Sc., University of Waterloo, 2001
B.Sc., University of Waterloo, 1998

A Thesis Submitted in Partial Fulfillment
of the Requirements for the Degree of

DOCTOR OF PHILOSOPHY

in the Department of Chemistry

Supervisory Committee

Electrochemical Investigations on the Reduction of Short Chain SAMs from a Au(111) Electrode

by

Gabriele Hager
M.Sc., University of Waterloo, 2001
B.Sc., University of Waterloo, 1998

Supervisory Committee

Dr. Alexandre G. Brolo, (Department of Chemistry)
Supervisor

Dr. David Harrington, (Department of Chemistry)
Departmental Member

Dr. Tom Fyles, (Department of Chemistry)
Departmental Member

Dr. Sadik Dost, (Department of Mechanical Engineering)
Outside Member

Dr. Dan Bizzotto, (Department of Chemistry)
External Examiner

Abstract

Supervisory Committee
Dr. Alexandre G. Brolo, (Department of Chemistry)
Supervisor
Dr. David Harrington, (Department of Chemistry)
Departmental Member
Dr. Tom Fyles, (Department of Chemistry)
Departmental Member
Dr. Sadik Dost, (Department of Mechanical Engineering)
Outside Member
Dr. Dan Bizzotto, (Department of Chemistry)
Additional Member

Self-assembled monolayers (SAMs) derived from long chain alkanethiols are known to exhibit generalized trends as a function of chain length where *n* denotes the number of methylene units (CH_2). For $n \leq 3$, these trends are no longer manifest. It can be shown that SAMs of short chain lengths are much more affected by the presence and type of functional group. The reduction of electrochemically induced SAMs derived from cysteine (cys), cystine ($(cys)_2$), mercaptopropionic acid (MPA) and mercaptoethylamine (MEA) from Au(111) highlight the effect of the two functional groups evaluated ($R\text{-}CO_2^-$ and $R\text{-}NH_2$). The reductive desorption of these species was monitored by cyclic voltammetry and electrochemical impedance spectroscopy (EIS) in 0.1 M $KClO_4$ and 0.1 M NaOH. The work presented herein demonstrates that under short time frames of immobilization, the presence of NH_2 provides a stabilizing effect to the SAM.

Cys and $(cys)_2$ SAMs that maintain both functional groups are generally found to provide the lowest surface coverage under the short term conditions of assembly. The thiol derived monolayers (cys) are consistently higher packed than the disulfide SAMs

from $(cys)_2$ in both media evaluated. In 0.1 M NaOH however, cys coverage is consistent with coverages obtained from very long incubation times. In the presence of the strong base the disulfide species, $(cys)_2$, desorbs at potentials that are always more positive than those of the thiol species (cys), further supporting poor monolayer formation. Additionally, these monolayers also exhibit the presence of two separate processes in 0.1 M $KClO_4$, whereas only desorption is noted in 0.1 M NaOH. It is likely that a de-protonation of the amine group occurs prior to the desorption of the SAM. The SAM desorption occurs near -0.65 V vs. SCE, and the de-protonation at about -0.50 V vs. SCE. Since the monolayers formed from cys are better formed than those from $(cys)_2$, this de-protonation is much more pronounced in the cys SAMs.

The presence of only the CO_2^- group (MPA) on the SAM, yields surface coverage that is intermediate compared to the bi-functionalized SAMs formed from cys and $(cys)_2$ and the NH_2 containing SAMs of MEA. In the potential region up to and prior to desorption, only one process is noted in both media.

SAMs derived from MEA provide the highest surface coverage of the four species, approximating theoretical values. The presence of two surface species is observed in both media, as a result of trans and gauche binding. Of the four species evaluated, MEA appears to be most suitable for rapid SAM formation. The disulfide species, $(cys)_2$, is found to be unsuitable for short-term preparation of SAMs.

Table of Contents

Acknowledgments

Having at some point convinced myself that “higher education” was indeed feasible, I needed those with strength and patience to guide me along the way. First and foremost I would like to give my heartfelt gratitude to my supervisor, Dr. A. G. Brolo, for his extended tolerance and continual encouragement these past years (even though most times I drove him crazy). I could not imagine having accomplished this type of feat without him. I am also indebted to Dr. D. Harrington for not only assisting me in gaining further insights into the methods of impedance spectroscopy, but also for numerous philosophical discussions (and allowing me to drive him crazy as well). Special thanks are given to Loel Horvey, for obtaining the MPA and MEA data, and permitting me the opportunity to be in a supervisory role. I could not have had a better student!

I also had the pure joy of working with some of the wildest characters imaginable, and thoroughly relished getting to know past and present members of the Brolo research group: Aaron Sanderson, Chris Addison, Meikun Fan, Jason Anema, Simon Birnie-Lefcovitch, Patrick Germain, Anderson Smith, Allison Jones, Yanhong Yang, Adam Roe, Shing Kwok, Sharon Sharma, Jacy Lee, Claire Mocock, Erin Arctander, Matt Cooper and Winnie Chan. It is a sure sign to finish my degree at this point, as I seem to have outlasted them all! It was also a great pleasure to learn from the Brolo group’s international visitors: Joon-Hyung Jin (Korea), Mohammad Pourhoussein (Iran), Marcos Jose Leite Santos (Brazil) and Jacqueline Ferreira (Brazil).

Not only has my group been extremely encouraging and supportive, but I thank the entire chemistry department for being beyond amazing. This has truly been one of the greatest experiences in my life.

Dedication

For my family for unconditional love and support through all my wild endeavours:

My son, Kylan

My parents, Rolf and Hannelore

My sister and her husband, Claudia and Dave

And my little nephews, Mason and Ethan

I thank you all

List of Figures

List of Tables

Chapter 1: Introduction

1.1 Research Objectives

Advancements in the development of electrochemical biosensors aim at improvements in the selectivity, sensitivity, reproducibility, and stability of the working electrode (or sensor). In general, an electrochemical biosensor consists of a metallic surface modified by adsorbed species that serve as the recognition element for the biomolecule of interest (target analyte). A simple schematic of a typical biosensor is shown in Figure 1.1. An understanding of the structure and behaviour of the adsorbed species is important to further optimize the analytical capabilities of the biosensor. Although numerous substrates (metallic surfaces) are employed as working electrodes for biosensors, gold is generally preferred due to its chemical stability. Moreover, gold surfaces are known to support the formation of self-assembled monolayers (SAMs).

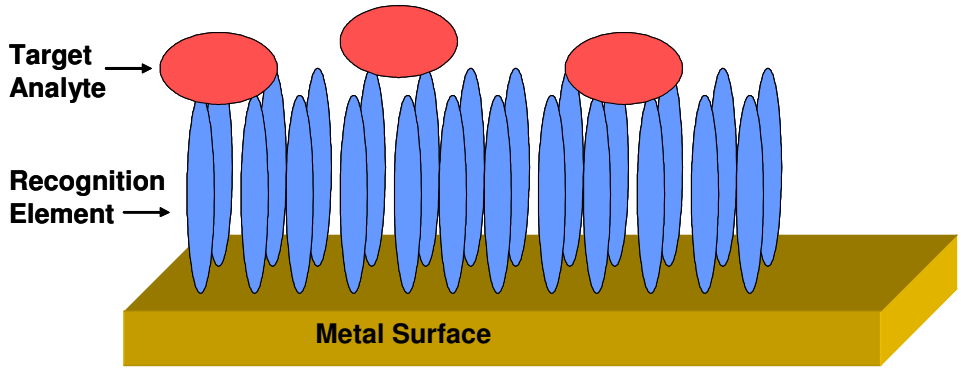

Figure 1.1: Schematic of a simplified biosensor.

.

The general objective of this thesis is to study the structure and electrochemical behaviour of SAMs formed by the adsorption of cysteine (cys), cystine ($(cys)_2$), mercaptopropionic acid (MPA) and mercaptoethylamine (MEA) on a Au(111) electrode.

These molecular species have a thiol group (in the case of $(cys)_2$ a disulfide) that binds to the gold surface, leaving the functional group(s) at the other end of the molecule exposed to the solution side. The chemical structures of all four molecules are shown in Figure 1.2.

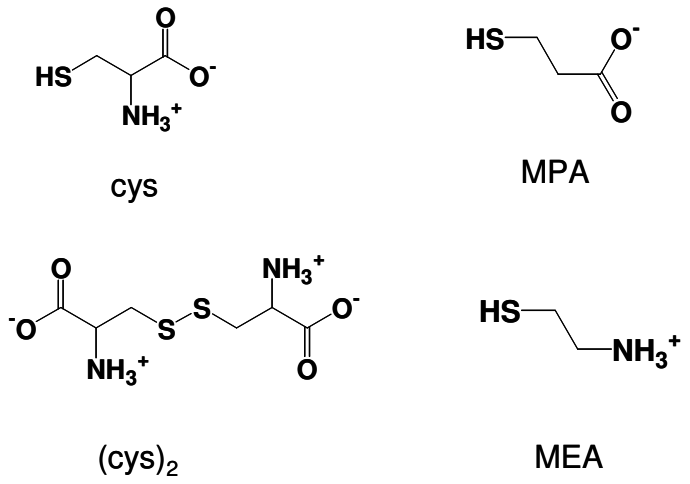

Figure 1.2: The chemical structures of the molecules used for SAM formation.

The SAMs formed from these species serve as a basis for more complex biosensor preparation by permitting further attachments of biological molecules to the pendant functional group. An amicable characteristic of these SAMs is the suitability to immobilization of enzymes and proteins [1, 2, 3, 4, 5, 6, 7, 8]. They are promising for the development of sensors for such uses as rapid glucose determination and antibody detection [9, 10, 11, 12]. Therefore, a better understanding of these SAMs may allow one to develop optimized methods when generating a basic platform for biosensors. Great emphasis has been placed on the study of SAMs formed from long chain thiols, yet the characterization of short chain SAMs, particularly the role of their pendant functional groups, is an area lacking in theory and experimental work. It has also recently been confirmed (for a long-chain SAM of $C_{18}SH$) that the general assumptions for the

reduction of SAMs from gold are not valid [13]. The work presented herein will provide further insight towards a more fundamental understanding of the complex molecular processes and interactions existing at electrified metal surfaces modified by short chain SAMs. Stable working potential regions are identified for the various systems, and short term immobilization is evaluated.

1.2 Organization of the Thesis

This thesis is divided into six chapters, including this introduction (Chapter 1) and a general conclusion chapter (Chapter 6). The main results are presented in chapters 2 through 5. Each results chapter is self-contained, with its own introduction, containing a literature review pertinent to the subject of the chapter, a description of the experimental details, a results section and a conclusion summary. Chapter 2 introduces the initial cyclic voltammetry (CV) experiments employing cys and $(cys)_2$ monolayers, where different enantiomers were used in an attempt to electrochemically distinguish SAMs of varying orientations. This endeavour provided insights into distinctions between the thiol and disulfide based species, as well as indicating that an additional surface process was evident. In Chapter 3, following up on the observations from Chapter 2, electrochemical impedance spectroscopy (EIS) is used to evaluate the more complex reduction of the monolayers of cys and $(cys)_2$ from gold. A de-protonation process prior to the monolayer desorption appears to be evident. The impedance of a Au(111) electrode modified by cys and $(cys)_2$ in basic conditions, where the monolayer reduction (desorption) is uncomplicated, is discussed in Chapter 4. Chapter 5 summarizes the findings for MPA

and MEA, which are model systems chosen to complement the data interpretations of cys and $(cys)_2$.

Although each results Chapter has its own introduction, the next section will present some general background with an overview of the main concepts and techniques used in this work. The objective of the general background is to help the reader with a broad overview of the main concepts and the experimental methods. Further details on these concepts and methods can be found in comprehensive reviews and books that are cited in the reference list.

1.3 General Background

This section will provide information about the gold surface (Au(111)) used in this work; general points regarding SAMs; an introduction to the species of interest as well as the electrochemical methods used. Additionally, the concept of protonation and de-protonation of surface bound species at electrified interfaces will be discussed.

1.3.1 Gold Single Crystal Electrodes

Gold, like other metals such as platinum, silver and copper, belongs to the fcc (face-centered cubic) family of crystals. The atoms in the bulk crystal have a specified arrangement as shown in Figure 1.3a [14]. This packing of the atoms will yield many different atomic-scale surface arrangements depending on the exact cleavage of the crystallized metal. The resultant surface structures (faces) are classified by what are known as Miller indices. To obtain the Miller index for a specified plane, one merely uses the reciprocal integer values of the intercepts on the crystallographic axes.

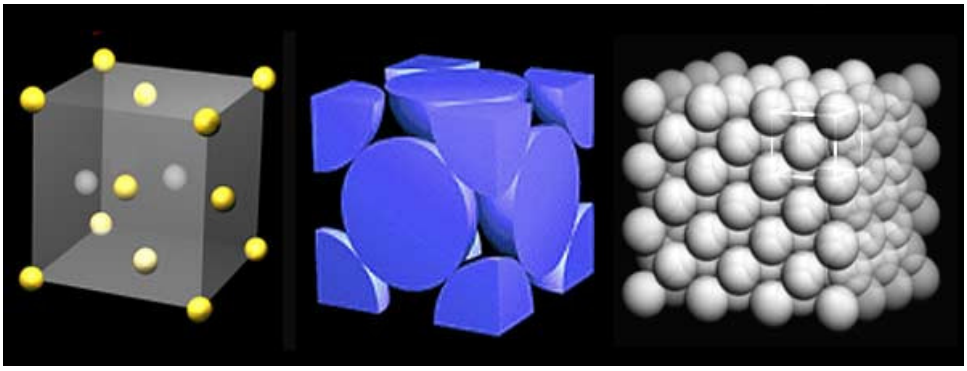

a)

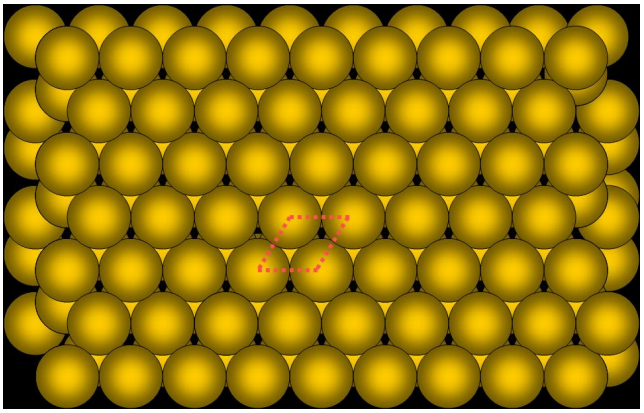

b)

Figure 1.3: a) unit cell showing atom arrangement for fcc packing[14] (reprinted with copyright permission from Iowa State University) and b) Au(111) surface showing the 1x1 repeating surface unit cell.

Most commonly evaluated and established are the three low-index faces, Au(111), Au(100) and Au(110). Of these, Au(111) has the highest work function, smoothest, most densely packed surface, and consequently the most positive pzc (potential of zero charge).[15] The pzc is the potential at which there is no net charge on the surface of the metal. The surface arrangement of the (111) face is referred to as hexagonal close packing, with a repeating surface unit cell of 1 x 1 (Figure 1.3b). At potentials more positive than the pzc, the (111) surface is considered to be un-reconstructed, and the 1x1 surface atom packing is evident. However, all three low-index faces of gold are known to

reconstruct, which results in changes of the surface atom packing to a thermodynamically favoured structure.

1.3.1.1 Reconstruction of Au(111)

When gold is annealed, at temperatures below the melting point (1064ºC), enough energy is provided to the surface atoms to overcome a kinetic barrier to form a surface structure of net lower energy. In the case of Au(111), this results in a slight lateral compression of the already densely packed surface by about 4.4% [16]. The resultant structure is referred to as the ($\sqrt{3}$ x 22) reconstructed surface, and every 23rd surface atom is then in registry with every 22nd underlying bulk atom. Although the reconstructed surface is prepared by annealing, application of a net positive potential results in the surface de-constructing, resulting in the 1 x 1 structure. In either case, the surface structure is well-defined, and for a well-prepared electrode, there should be minimal surface defects.

1.3.1.2 Single Crystal Electrode Pre-treatments

However, in actuality, even the best prepared single crystal surfaces contain natural defects. There are ample reference guides for the electrochemical responses of bare gold surfaces in various media, and each gold face displays discrete electrochemical behaviour [15, 17, 18, 19, 20]. Figure 1.4 indicates the current responses of the three low-index faces of gold for two different electrolyte conditions.[18] Deviation from the standard responses under controlled conditions is quite indicative that the desired surface is not perfect and that sources of contamination are present. Various cleaning treatments to reduce sources of contamination or defects of the surface are available [15, 21].

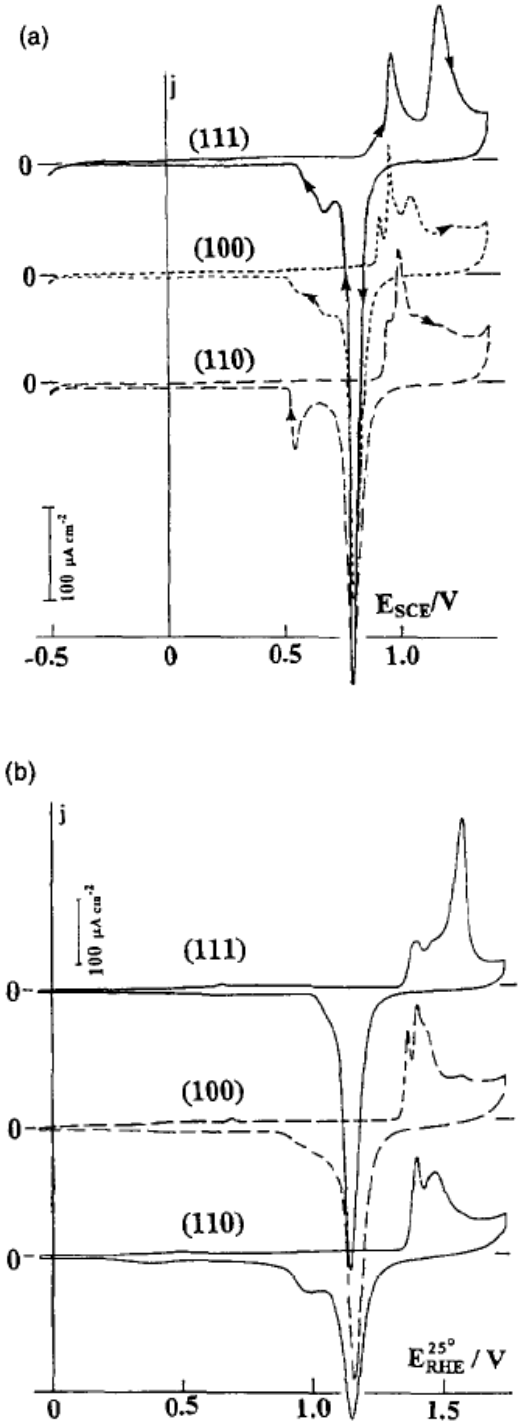

Figure 1.4: The current responses of Au(111), Au(110) and Au(100) in the presence of a) 0.09 M $NaClO_4$ + 0.01 M $HClO_4$ and b) 0.1 M H_2SO_4.[18] (reprinted with full copyright permission from Elsevier Publishing)

Since Au(111) is extremely sensitive to the presence of contaminants, it is extremely important to ensure the cleanliness and well ordered nature of the surface and solution cell prior to any experimental work. The Au(111) electrochemical signature in 0.1 M H_2SO_4 is considered a good standard, and is characterized by the phase transition of the adsorbed sulphate layer at +0.78 V vs. SCE, which Figure 1.5 indicates as a pronounced spike [16, 22]. The presence of this reversible current spike, is considered validation that indeed the Au(111) surface, which is desired, is present.

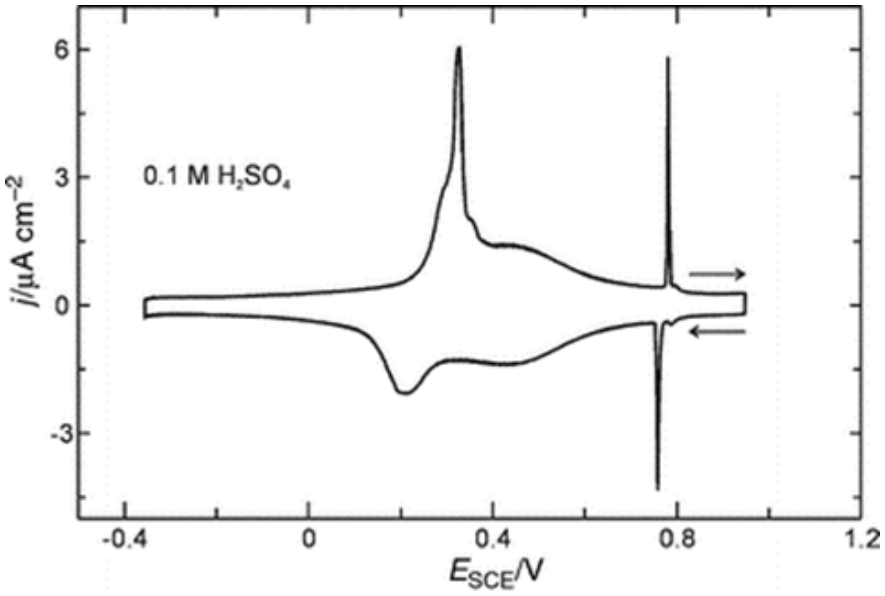

Figure 1.5: Cyclic voltammograms of Au(111) in 0.1 M H_2SO_4 at positive applied potentials indicating the sulphate adlayer transition near 0.8 V [22]. (reprinted with permission from RSC publishing)

1.3.2 Self Assembled Monolayers (SAMs)

Self assembly is a natural process whereby molecules spontaneously adsorb, and with sufficient time form ordered structures at the surface of the electrode. In particular, thiols (as well as disulfides), will form very strong sulfur-gold bonds, and are often used as the anchor for further molecular modifications. The self-assembly process is most

commonly achieved by incubating the gold surface in a thiol or disulfide solution for approximately 24 hours. This extended period permits not only the binding to the substrate (which is very rapid and may occur on the order of milliseconds [23]), but ample time for molecular re-organization on the surface as well. However, the use of different techniques to evaluate SAM formation, suggest that the process requires time on the order of 100-800 seconds to hours [24]. Alternatively, SAMs may be formed under electrochemical potential control [25]. In this case, the electrode potential is held to a pre-determined value that facilitates the adsorption of the organic species. It has been suggested that electrochemically-prepared SAMs have the same quality as those prepared by several hours of incubation. High quality SAMs have been achieved much faster using electrochemical deposition of long chain thiols.

The structures of the SAMs are dependant on the packing of the substrate surface atoms, the local ”solvent” environment (for example pH) and electrode potential to name a few variables. It is thus necessary to understand the mechanisms involved for self-assembly, as well as the disassembly of the SAMs when conditions such as pH or potential are changed.

1.3.2.1 Long Chain SAMs

The most stable and best characterized monolayers have been achieved employing long chain alkanethiols. These types of SAMs are found to be very well insulating as they afford the highest packing density on the order of 8 - 10 x 10^{-10} mol cm^{-2}. Due to this insulating quality, the capacitance of these SAMs is found to be quite low. An inverse relationship exists between the capacitance and the chain length. In fact, numerous parameters are found to demonstrate a linear relationship with the carbon chain

length [23, 26, 27, 28, 29, 30]. This may be understood in terms of the strong intermolecular forces which contribute to the stability of the SAM. As the chain length decreases, the degree of intermolecular interactions also decreases. A very good example is the correlation of the desorption potential, the energy required to desorb the monolayer, with chain length. Particularly in basic or ethanolic solutions, this can be described as a change of approximately 15 – 30 mV per methylene unit [26, 27, 28]. However, when the chain length becomes too small, circa n=3 (where n is the number of methylene units) then the desorption potential becomes independent of the chain length.

1.3.2.2 Short Chain SAMs

SAMs formed from short-chain alkanethiols have predominantly been utilized in the fabrication of biosensors [10, 11, 12]. However, unlike their long-chain counterparts, these monolayers are not as densely packed, and consequently do not offer low capacitance values. Yet, these SAMs are still effectively employed for biosensor development. Likely the most common utilized modifier or linker is cysteine. Cys SAMs are particularly suited to biological applications such as: selective detection of cytochrome *c* in the presence of cytochrome b_5 [31], evaluating the electron transfer of promoter-protein complexes [8], and chiral discrimination of 3,4-dihydroxyphenylalanine [32]. Hence, cys is chosen in this work as the primary analyte, as well as its oxidized form, $(cys)_2$. Representative known surface structures for cys are shown in Figure 1.6, which clearly indicate the degree of exposed surface area [33, 34, 35].

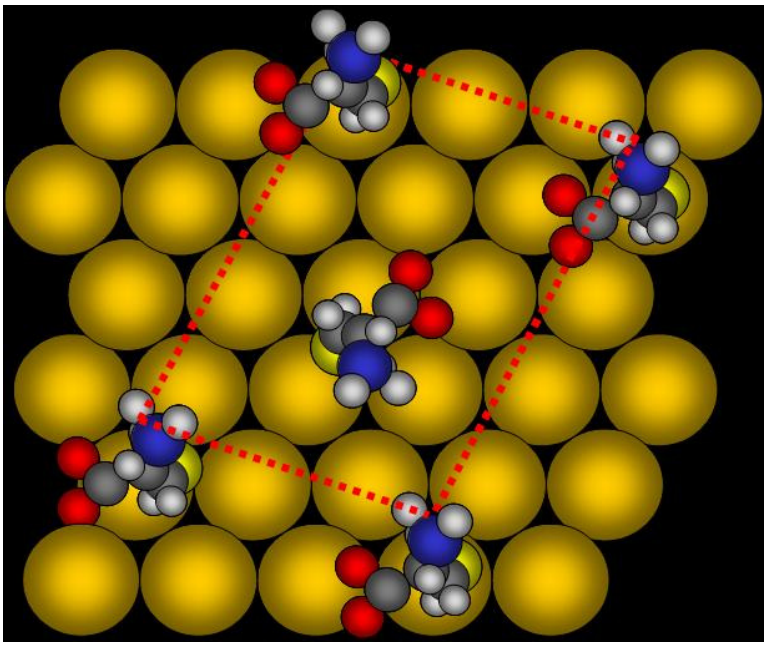

a)

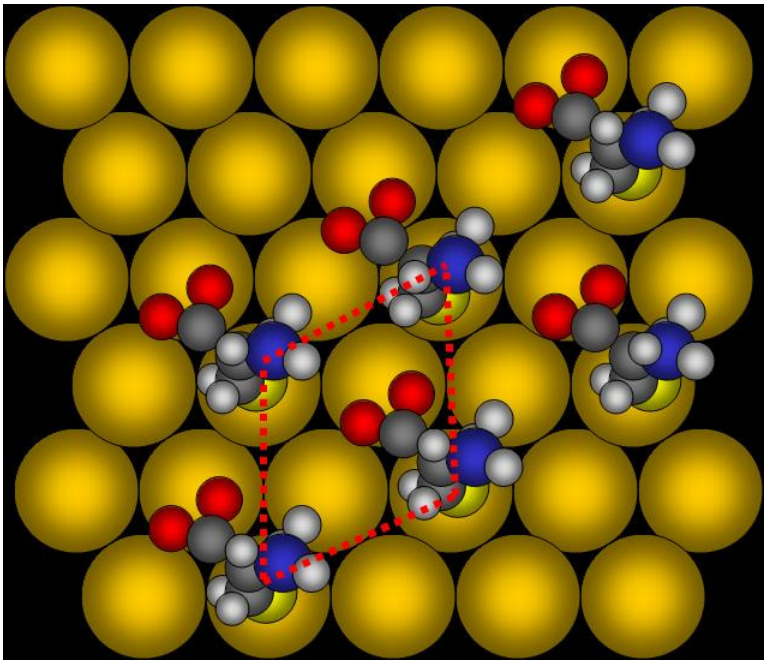

b)

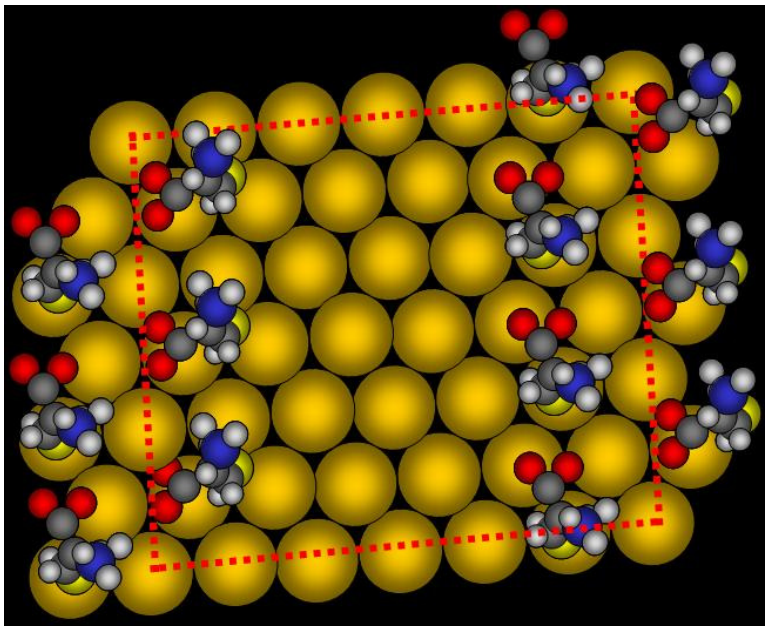

c)

Figure 1.6: Reported model structures determined by STM images for various surface formations of cys on Au(111) given different electrolyte conditions: a) 0.1 M $HClO_4$, (4 x $\sqrt{7}$)R19º[33], b) 0.1 M $KClO_4$ + 1 mM $HClO_4$, ($\sqrt{3}$ x $\sqrt{3}$)R30º [34] and c) 50 mM NH_4Ac, (3$\sqrt{3}$ x 6)R30º [35].

Cysteine (cys, $HSCH_2CHNH_3^+COO^-$), is a non-essential amino acid which is easily available commercially. The thiol group facilitates binding to gold substrates, whereas either the amino or carboxylic moieties are oriented away from the surface. Cys further contains a chiral carbon, and is thus available as both L and D isomers. The designation of L and D is based on the derivation of the species in relation to glyceraldehyde (since these are biological molecules, a biological standard is used), with L being the biologically relevant isomer. There is a tendency for cysteine to readily oxidize to the dimer form cystine ($(cys)_2$, $(SCH_2CHNH_3^+COO^-)_2$) according to:

$$2RSH \longrightarrow RSSR + 2H^+ + 2e^- \qquad \text{Scheme 1.1}$$

For surface modification, both cys and $(cys)_2$ essentially yield the same anchored species. However, differences in binding between a free thiol and disulfide have shown

to result in much better formed SAMs from the thiol-based species [36]. Whereas the thiol binds directly to gold in a one-step mechanism, disulfide binding is a multi-step reaction. Other work has indicated that thiol and disulfide derived monolayers are indistinguishable once formed, although the rate of formation of the SAM is about 40% slower for a disulfide [37, 38]. Since most studies have focused on the characterization of SAMs formed from cys and $(cys)_2$ at longer incubation times, differences between the two have barely been noted.

MPA ($SHCH_2CH_2COO^-$) and MEA ($SHCH_2CH_2NH_3^+$) were also investigated in this thesis to aid in characterizing and interpreting the results for cys and $(cys)_2$. These molecules are structurally related to cys as MPA is cys without the amino group and MEA is cys without the carboxylic acid functionality. Therefore comparisons of the four species through relation of the similar structures should provide further insights into their electrochemical behaviour.

It has been noted that SAMs formed from short-chain functionalized thiols are much more sensitive to changes in the local environment than their long-chain counterparts [39]. Hence, evaluations of short-chain functionalized SAMs under controlled conditions may provide an amplification of measurable parameters. This type of information may further contribute to reducing the time of standard methods for the preparation of biosensors in the case where monolayers are deemed indistinguishable from those prepared over long incubation times. In the case of poor monolayer formation, possible influences attributed to the functional groups may be identified.

1.3.3 Electrochemical Methods

Three major electrochemical techniques, cyclic voltammetry (CV), chrono-amperometry (or chrono-coulometry) and electrochemical impedance spectroscopy (EIS), were used to provide mechanistic and kinetic information. A typical electrochemical cell consists of a reliable reference electrode (RE), an auxiliary or counter electrode (CE) and the working electrode (WE). A schematic of the actual cell set-up used is shown in Figure 1.7. The WE was a Au(111) single crystal electrode, the RE was typically a saturated calomel electrode (SCE), although some experiments utilized a reversible hydrogen electrode. The reference electrode was maintained in a separate compartment, and brought near the WE with a Luggin capillary. The CE was always a platinum (Pt) mesh electrode, separated by a glass frit arm to the main cell. For either technique, the resultant current at the WE is monitored relative to an applied potential (sinusoidal voltage for EIS). The measured current may be the result of a charging or capacitive process or a Faradaic process which results from electron transfer. Whereas CV methods are dynamic measurements, EIS probes the system under steady state conditions.

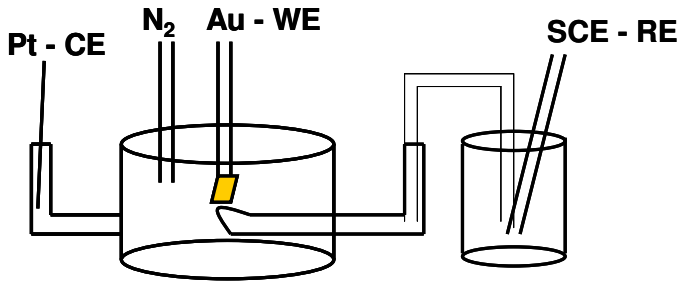

Figure 1.7: Schematic of electrochemical cell showing positions of working electrode (WE), reference electrode (RE) and counter electrode (CE).

1.3.3.1 Cyclic Voltammetry

In CV methods, an applied potential is ramped at a given scan rate (in V s^{-1}) from the starting potential to an apex potential, and then returned to the initial potential. A stylized schematic of this is shown in Figure 1.8. The monitored current, which is a result of both the charging and Faradaic components, results in current peaks at the DC potential where either a solution or surface process is occurring at the working electrode.

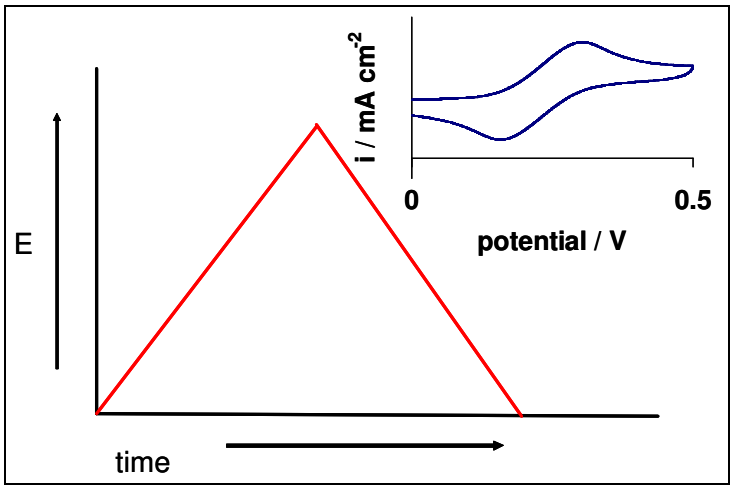

Figure 1.8: The change of the applied potential as a function of time for cyclic voltammetry. The inset indicates the CV obtained for a solution redox active species.

The inset of Figure 1.8 shows the typical current response for a reversible redox active species in solution. Charging currents are the result of changes in the electron density at the interphase, whereas Faradaic currents are the direct result of electron transfer to or from the working electrode of a redox active species. Potential excursions may cover the entire available potential range for the working electrode. This range is determined by water reduction to yield hydrogen (also known as hydrogen evolution) at the most negative potentials, which lead to very large cathodic currents, and oxidation

processes at the most positive potentials indicated by very large anodic currents. Since this work is focused on the reduction of SAMs from Au(111), only the potential range from near the open circuit potential (OCP) to the initiation of hydrogen evolution was evaluated.

1.3.3.2 Chrono-Methods

Any technique referred to as a chrono method, is the measurement of a parameter with time (chrono is derived from the Greek word *khrono* meaning time). In the case of chrono-amperometry, the current at the WE is measured as a function of time. Chrono-coulometry is the measurement of the total charge that is passed, and chrono-potentiometry is the measurement of the potential. These measurements can be performed with or without potential control. For a system at rest, addition of an analyte may be monitored as current, charge or potential changes. One may also induce changes to a system, and measure the desired parameter as a function of an applied potential or applied current. In the case of step-experiments, a condition is set, such as an applied potential, and the current or charge at the given potential is measured. This is immediately followed by a change or step of the potential, and the resultant change in current or charge is measured as a function of time.

1.3.3.3 Electrochemical Impedance Spectroscopy (EIS)

Impedance methods, unlike CV techniques, probe the system of interest under steady conditions. At each applied DC potential, an AC signal typically between 5 and 10 mV root mean square (rms) is superimposed spanning a range of applicable

frequencies as indicated in Figure 1.9. The frequency range is determined experimentally and varies with the configuration of the actual working cell. The AC signal can be represented in terms of voltage as a rotating vector by [40, 41]:

$$E = \Delta E \sin \omega t \qquad \text{Equation 1.1}$$

Here, E is the observed voltage, ΔE is the potential amplitude, ω is $2\pi f$ (where f is the frequency in Hz) and t is time. The measured or observed current (i) will also be sinusoidal, and will either lead or lag in phase with the potential by an angle, ϕ, as:

$$i = \Delta i \sin(\omega t + \phi) \qquad \text{Equation 1.2}$$

Using the relations from Ohm's Law, ϕ is shown to be 0º for a pure resistor (R) since:

$$i = \frac{E}{R} \qquad \text{Equation 1.3}$$

In the case of a pure capacitor (C), ϕ can be shown to be 90º, since the charge on two parallel plates is related to the potential according to:

$$q = CE \qquad \text{Equation 1.4}$$

The current, obtained by differentiation is:

$$i = \frac{dq}{dt} = C\frac{dE}{dt} \qquad \text{Equation 1.5}$$

By using Equation 1.1, the current for a capacitor is then shown to be:

$$i = \omega C \Delta E \cos \omega t \qquad \text{Equation 1.6}$$

Substitution of the capacitive reactance, X_c, defined as $1/\omega C$, leads to the final expression with ϕ equal to 90º for a pure capacitor:

$$i = \frac{\Delta E}{X_C}\sin(\omega t + \pi/2) \qquad \text{Equation 1.7}$$

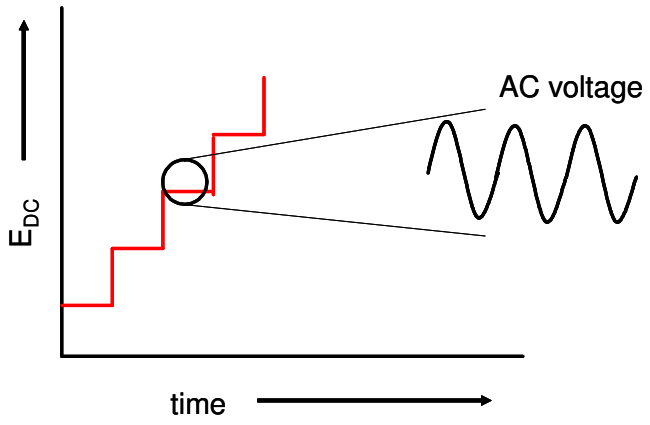

Figure 1.9: The application of a sinusoidal voltage in AC voltammetry.

However, real systems tend to exhibit phase angles that are between 0º and 90º, and the value of ϕ indicates the net contributions of the combination of the resistive and capacitive components. To extract meaningful information from the EIS data, the system may be represented by an equivalent circuit. Equivalent circuits are the combination (in series or parallel) of resistors and capacitors which represent different elements of the system. In all cases, since the current must pass through the solution, the circuit will have a solution resistance (R_S) in series with any other components.

The electrochemical double layer is typically represented by a capacitor (C_{DL}), which results from charging of the interphase that is in series with R_S. For a simplified equivalent circuit, such as a resistor and capacitor in series as in Figure 1.10, one may represent the overall impedance (Z) in terms of real and imaginary components:

$$Z(\omega) = Z' - jZ''$$ Equation 1.8

The current from EIS, measured both in-phase (real component, Z') and out-of-phase (imaginary component, Z") with the applied AC perturbation, is plotted as a function of frequency. Data analysis proceeds by plotting the imaginary impedance (Z") as the ordinate, and the real impedance (Z') as the abscissa, for the given range of frequencies evaluated. This form of graph is known as a Nyquist plot, and Figure 1.10 shows the response in the case of a series combination of R_S and C_{DL}.

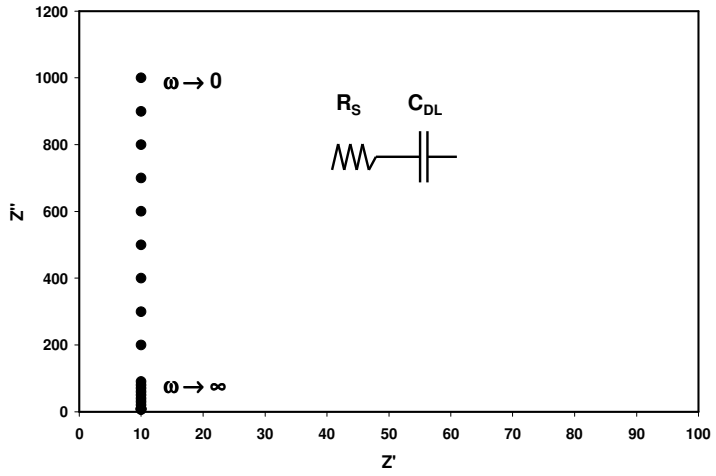

Figure 1.10: Nyquist plot for a circuit consisting of R_S and C_{DL} in series.

In the case of a Faradaic process, an additional element in the form of a charge transfer resistance (R_{CT}) is incorporated parallel to the C_{DL} as in Figure 1.11. The typical Nyquist representation is also shown in Figure 1.11, and the charge-transfer is evident as a distinct semi-circle. The real and imaginary components are then given by:

$$Z' = R_s + \frac{R_{CT}}{1 + \omega^2 C_{DL}^2 R_{CT}^2}$$ Equation 1.9

$$Z'' = \frac{\omega C_{DL} R_{CT}^2}{1 + \omega^2 C_{CL}^2 R_{CT}^2}$$ Equation 1.10

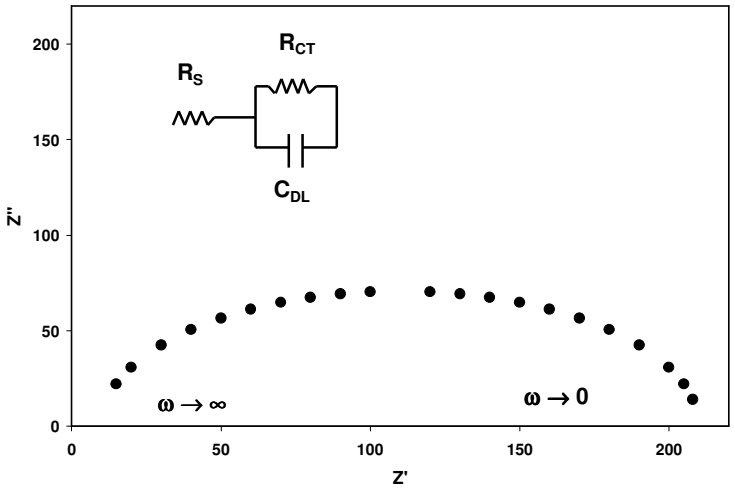

Figure 1.11: Nyquist plot representing a simple charge transfer process, with R_{CT} and C_{DL} in parallel.

Considering now that for a self-assembled monolayer the molecules are strongly adsorbed, then additional components such as an adsorbate capacitance (C_{ad}) and resistance (R_{ad}) associated with the bound species are incorporated. For short-chain SAMs, the surface is not completely covered, and in essence they may be considered as monolayers with large defects. In practice, monolayers with defects can be modeled by equivalent circuits incorporating a constant phase element (CPE).[42] For single crystal electrodes, the C_{DL} is also often represented by a CPE, which accounts for any surface defects and inherent inhomogeneity [43]. In terms of admittance, Y (which is the inverse of the impedance Z^{-1}), the CPE can be defined as:

$$Y(\omega) = Q(i\omega)^{\alpha_f}$$ Equation 1.11

Where Q is the CPE parameter (S cm^{-2} s^{α}), and α_f is the CPE exponent. It is common to consider the values obtained for the CPE parameter as approaching C_{DL}, as long as α^f is equal to or greater than 0.95.

The technique is complementary to the dynamic measurements, but has the added strength of separating charging (or capacitive) processes from Faradaic.

1.3.4 Choice of Electrolytes

Potassium perchlorate is a typical electrolyte employed in characterizing Au electrodes when aqueous conditions are used. It is well known that the ClO_4^- anions are a weakly binding species, and use of 0.1 M $KClO_4$ would thus be anticipated to not complicate the desorption process, as any current which is monitored should be directly related to the adsorbed species only. It is also an easily purified solid, and all experiments were performed employing high-grade, doubly re-crystallized product. Additionally, the pH range of electrolyte only solutions was experimentally determined to fall between 5 and 6 pH units. However, as $KClO_4$ is an unbuffered solution, addition of analyte directly impacts the solution pH. In the case of cys and $(cys)_2$ solutions, analyte addition does not greatly influence the pH as the carboxyl and amino groups constituted a 1:1 ratio. Addition of MPA results in a net pH shift to more acidic values (~3-4) and the addition of MEA shifts the solution pH to more basic values (~7-8).

NaOH was employed to evaluate the SAMs under basic conditions. Unlike perchlorate, hydroxide is known as a strongly binding electrolyte. However, it is widely used in studying the desorption of all types of SAMs from gold surfaces, mostly due to the increase of solubility which is noted for highly basic conditions. To ensure utmost

cleanliness, only the highest-grade NaOH (99.998%) commercially available was employed. For bare Au(111), potassium hydroxide (KOH, 98%) was also employed. However, a number of problems associated with hydroxide solutions can not be completely prevented. These would primarily be the potential etching of the glassware during any experiment as well as the phenomena of creeping. Hydroxide solutions will with time creep up along the edges of the single crystal electrode. As a consequence, not only will the electrochemical signal be a result of the structured (111) surface, but over time contributions from the outer edges (random orientations) may manifest.

Increasing the basicity also leads to the increase of the rate of bulk thiol oxidation. The conversion of thiols to subsequent disulfide species in basic solution has been noted to occur at rates of almost 15-20 times that of equivalent conversion in more acidic media.[44]

1.3.5 Protonation and De-protonation

An interesting attribute of adsorbed functionalized species is the protonation and de-protonation of carboxylic and amino terminal groups. Whereas the solution species exhibit protonation and de-protonation strictly as a function of pH, the adsorbed species are affected by both solution pH and the applied potential (which affects the local pH environment). In this regard, the pK_a values of adsorbed carboxylic groups are found to shift towards more alkaline values for adsorbed molecules relative to the solution species at potentials near the OCP [39, 45]. Similarly, surface bound amine groups tend towards more acidic pK_a values relative to their solution counterparts [39,45]. Since the change of the protonation state directly affects the dielectric constant, ε_r, of the interphase, this process can be observed using techniques such as Surface Plasmon Resonance (SPR) [46,

47] or capacitance titrations for surface bound species [39]. Measuring the capacitance is quite effective at distinguishing such effects (much more so for short chain SAMs), as the capacitance (C) is directly related to the relative permittivity of the SAM, ε_r according to:

$$C = \frac{\varepsilon_r \varepsilon_o}{d} \qquad \text{Equation 1.12}$$

Where ε_o is the permittivity of free space, and d is the thickness of the SAM.

Other methods such as Raman or Fourier Transform Infrared Spectroscopy have also been used, by monitoring the changes of the vibrational modes associated with the protonated and deprotonated forms of the functional groups or by monitoring counter ion species [48, 49, 50, 51]. The protonation state of the SAM may also be evaluated based on contact angle measurements [52, 53, 54].

Theoretical models for the protonation or de-protonation at the surface have been developed considering the SAM as being irreversibly bound to the metal [55, 56, 57]. These models have primarily focused on considering long-chain SAMs, where the surface of the electrode is essentially blocked. For simplicity, an acid functional group is considered. Hence, depending on the level of intermolecular interactions, the solution pH and applied electrochemical potential, one can describe the total surface excess of the adsorbed layer (Γ_T mol cm^{-2}) as comprised of protonated and deprotonated species:

$$\Gamma_T = \Gamma_{AH} + \Gamma_{A^-} \qquad \text{Equation 1.13}$$

Considering now an equilibrium for the acid group on the adsorbed species as:

$$HA \rightleftharpoons H^+ + A^- \qquad \text{Equation 1.14}$$

Further, assuming an equilibrium between protons that are adsorbed (a) and in solution (s), then the electrochemical potentials of the adsorbed species can be presented as:

$$\overline{\mu}_{AH}{}^{a} = \overline{\mu}_{A^-}{}^{a} + \overline{\mu}_{H^+}{}^{s} \qquad \text{Equation 1.15}$$

Converting the electrochemical potentials to the respective chemical and electrostatic components, results in:[55, 56, 57]

$$\overline{\mu}_{AH}{}^{a} = \mu_{AH}{}^{o} + RT \ln \Gamma_{AH} \qquad \text{Equation 1.16}$$

$$\overline{\mu}_{H^+}{}^{s} = \mu_{H^+}{}^{o} + RT \ln a_{H^+} \qquad \text{Equation 1.17}$$

and

$$\overline{\mu}_{A^-}{}^{a} = \mu_{A^-}{}^{o} + RT \ln \Gamma_{A^-} - F\Psi^{a} \qquad \text{Equation 1.18}$$

Where Ψ^a is the local potential of the charged adsorbed functional group, relative to the average potential of the bulk solution, ϕ^s, T defines the temperature (in units of K), R is the molar gas constant (8.31451 J mol^{-1} K^{-1}) and F is the Faraday constant (9.64853 x 10^4 C mol^{-1}).

Combining the above equations, results in the equilibrium equation:

$$RT \ln\left(\frac{\Gamma_{HA}}{\Gamma_{A^-}}\right) = -RT \ln K_a + RT \ln a_{H+} - F\Psi^{a} \qquad \text{Equation 1.19}$$

Here, the acid dissociation constant (K_a) is related to the chemical potentials according to:

$$RT \ln K_a = \mu_{HA}{}^{o} - \mu_{H^+}{}^{o} - \mu_{A^-}{}^{o} \qquad \text{Equation 1.20}$$

Considering now that there is a fraction (θ) of the ionizable groups which are dissociated:

$$\theta = \frac{\Gamma_{A^-}}{\Gamma_{A^-} + \Gamma_{HA}} \qquad \text{Equation 1.21}$$

Then effectively the degree of ionization of a bound surface species is both a function of solution pH, and the applied electrochemical potential according to [55, 56, 57]:

$$\ln\left(\frac{\theta}{1-\theta}\right) = 2.3pH - 2.3pK_a - f\Psi^a \qquad \text{Equation 1.22}$$

where, $f=F/RT$.

This general concept has been further expanded in terms of the capacitance from thermodynamic equilibria [56, 57], as well as from a kinetic approach [58].

From physical capacitance measurements, which have mostly been performed at a single potential (near the OCP) while varying the solution pH, the capacitance of the charged monolayer is found to be much larger than for the uncharged species [39, 45]. This effect is greatly amplified for the short-chain SAMs and not readily distinguishable for long chain SAMs when measuring the differential capacitance at a set potential with changes in pH. Both MPA and MEA have been characterized in terms of changes in the capacitance at single potentials with changes in solution pH, yet for cys and $(cys)_2$ this data is not available. The carboxyl terminated SAMs formed from MPA are found to be in the protonated state, near the OCP, in solution pH to about 6 units [39, 49]. The amine terminated SAMs derived from MEA solutions, are also experimentally found to be in their protonated states near the OCP at solution pH near 6. Additionally, the pK_a of MEA derived SAMs, is noted to shift to more positive potentials with an increase in the solution acidity [50]. That is, the protonated state, at the surface, persists with increasing negative potentials. Cys and $(cys)_2$ contain both amino and carboxylic acid groups, and may be further stabilized by the presence of stronger hydrogen bond interactions, as

suggested by the known surface structures from STM. The characteristic desorption from gold should differ somewhat from that of either a pure carboxylate species or only amine species. In fact, it should be more difficult to ionize cys derived SAMs.

1.4 Bibliography

[1] Mendes, R. K.; Carvalhal, R. F.; Kubota, L. T. *Journal of Electroanalytical Chemistry* **2008**, *612*, 164.

[2] Shervedani, R. K.; Bagherzadeh, M.; Mozaffari, S. A. *Sensors and Actuators B* **2006**, *115*, 614.

[3] Imbayashi, S.-i.; Mita, T.; Kakiuchi, T. *Langmuir* **2005**, *21(4)*, 1470.

[4] Bonanni, B.; Bizzarri, A. R.; Cannistraro, S. *Journal of Physical Chemistry B* **2006**, *110(30)*, 14574.

[5] Andolfi, L.; Bizzarri, A. R.; Cannistraro, S. *Thin Solid Films* **2006**, *515*, 212.

[6] Zhang, J.; Welinder, A. C.; Hansen, A. G.; Christensen, H. E. M.; Ulstrup, J. *Journal of Physical Chemistry B* **2003**, *107(45)*, 12480.

[7] Zhang, J. and Ulstrup, J. *Journal of Electroanalytical Chemistry* **2007**, *599*, 213.

[8] Zhang, J.; Christensen, H. E. M.; Ooi, B. L.; Ulstrup, J. *Langmuir* **2004**, *20(23)*,10200.

[9] Tengvall, P.; Lestelius, M.; Liedberg, B.; Lundström, I. *Langmuir* **1992**, *8(5)*, 1236.

[10] Baldrich, E.; Laczka, O.; del Campo, F. J.; Munoz, F. X. *Analytical and Bioanalytical Chemistry* **2008,** *390(6)*, 1557.

[11] Ferreira, A. A. P.; Colli W.; da Costa, P. I.; Yamanaka, H. *Biosensors and Bioelectronics* **2005**, *21(1)*, 175.

[12] Shervedani, R. K.; Mehrjardi, A. H.; Zamiri, N. *Bioelectrochemistry* **2006**, *69(2)*, 201.

[13] Laredo, T.; Leitch, J.; Chen, M.; Burgess, I. J.; Dutcher, J. R.; Lipkowski, J. *Langmuir* **2007**, *23(11)*, 6205.

[14] http://www.ndt-ed.org/EducationResources/CommunityCollege/Materials/Structure/metallic_structures.htm, accessed 2008/05/20.

[15] Hamelin, A. "Double-Layer Properties at *sp* and *sd* Metal Single Crystal Electrodes." in: B.E. Conway, R.E. White and J.O.M. Bockris, Editors, Modern Aspects of Electrochemistry **Volume 16**, Plenum, New York (1985), pp. 1–101.

[16] Dakkouri, A. S. and Kolb, D. M. "Reconstruction of Gold Surfaces." in A. Wieckowski, Editor, Interfacial Electrochemistry, Marcel Dekker, New York (1999), Chapter 10, pp. 151–173.

[17] Hamelin, A; Sottomayor, M. J.; Silva, F.; Chang, Si-C.; Weaver, M. J. *Journal of Electroanalytical Chemistry* **1990**, *295*, 291.

[18] Hamelin, A. *Journal of Electroanalytical Chemistry* **1996**, *407*, 1.

[19] Arihara, K.; Ariga, T.; Takashima, N.; Arihara, K.; Okajima, T.; Kitamura, F.; Tokuda, K.; Ohsaka, T. *Physical Chemistry and Chemical Physics* **2003**, *5*, 3758.

[20] Štrbac, S.; Hamelin, A.; Adžić, R. R. *Journal of Electroanalytical Chemistry* **1993**, *362*, 47.

[21] Carvalhal, R. F.; Freire, R. S.; Kubota, L. T. *Electroanalysis* **2005**, *17(14)*, 1251.

[22] Cuesta, A.; Kleinert, M.; Kolb, D. M. *Phsyical Chemistry and Chemical Physics* **2000**, *2*, 5684

[23] Subramanian, R. and Lakshminarayanan, V. *Electrochimica Acta* **2000**, *45*, 4501.

[24] Bensebaa, F.; Voicu, R.; Huron, L.; Ellis, T. H.; Kruus, E. *Langmuir* **1997**, *13(20)*, 5335.

[25] Ma, F. and Lennox, R. B. *Langmuir* **2000**, *16(15)*, 6188.

[26] Widrig, C. A.; Chung, C.; Porter, M. D. *Journal of Electroanalytical Chemistry* **1991**, *310*, 335.

[27] Imbayashi, S.-i.; Iida, M.; Hobara, D.; Feng, Z. Q.; Niki, K.; Kakiuchi, T. *Journal of Electroanalytical Chemistry* **1997**, *428*, 33.

[28] Azzaroni, O.; Vela, M. E.; Martin, H.; Hernández Creus, A.; Andreasen, G.; Salvarezza, R. C. *Langmuir* **2001**, *17(21)*, 6647.

[29] Protsailo, L. V. and Fawcett, W. R. *Electrochimica Acta* **2000**, *45*, 3497.

[30] Kawaguchi, T.; Yasuda, H.; Shimazu, K. *Langmuir* **2000**, *16(25)*, 9830.

[31] Qian, W.; Zhuang, J.-H.; Wang, Y.-H.; Huang, Z.-X. *Journal of Electroanalytical Chemistry* **1998**, *447*, 187.

[32] Matsunaga, M.; Nakanishi, T.; Asahi, T.; Osaka, T. *Chirality* **2007**, *19*, 295.

[33] Xu, Q.-M.; Wan, L.-J.; Wang, C.; Bai, C.-L.; Wang, Z.-Y. *Langmuir* **2001**, *17(20)*, 6203.

[34] Dakkouri, A. S.; Kolb, D. M.; Edelstein-Shima, R.; Mandler, D. *Langmuir* **1996**, *12(11)*: 2849.

[35] Zhang, J.; Chi, Q.; Nielsen, J. U.; Friis, E. P.; Andersen, J. E. T.; Ulstrup, J. *Langmuir* **2000**, *16(18)*, 7229.

[36] Ron, H. and Rubinstein, I. *Journal of the American Chemical Society* **1998**, *120(51)*, 13444.

[37] Jung, C.; Dannenberger, O.; Xu, Y.; Buck, M.; Grunze, M. *Langmuir* **1998**, *14(5)*, 1103.

[38] Bain, C. D.; Biebuyck, H. A. Whitesides, G. M. *Langmuir* **1989**, *5(3)*, 723.

[39] Kakiuchi, T.; Iida, M.; Imabayashi, S-I.; Niki, K. *Langmuir* **2000**, *16(12),* 5397.

[40] Sluyters-Rehbach, M. *Pure and Applied Chemistry* **1994**, *66(9)*, 1831.

[41] Barsoukov, E. and Macdonald, J. R. Editors, Impedance Spectroscopy 2nd Edition, Wiley, New Jersey(2005), pp. 1-26.

[42] Boubour, E. and Lennox, R. B. *Langmuir* **2000**, *16(19)*, 7464.

[43] Sadkowski, A.; Motheo, A. J.; Neves, R. S. *Journal of Electroanalytical Chemistry* **1998**, *455*, 107.

[44] Bagiyan, G. A.; Koroleva, I. K.; Soroka, N. V.; Ufimtsev, A. V. *Russian Chemical Bulletin* **2003**, *52(5)*, 1135.

[45] Schweiss, R.; Werner, C.; Knoll, W. *Journal of Electroanalytical Chemistry* **2003**,*540*, 145.

[46] Chah, S.; Yi, J.; Pettit, M.; Roy, D.; Fendler, J. H. *Langmuir* **2002**, *18(2)*, 314.

[47] Fears, K. P.; Creager, S. E.; Latour, R. A. *Langmuir* **2008**, *24(3)*, 837.

[48] Kudelski, A. *Journal of Raman Spectroscopy* **2003**, *34*, 853.

[49] Imae, T. and Torii, H. *Journal of Physical Chemistry B* **2000**, *104(39)*, 9218.

[50] Nishiyama, K.; Kunbo, A.; Ueda, A.; Taniguchi, I. *Chemistry Letters* **2002**, 80-81.

[51] Bieri, M. and Bürgi, T. *Langmuir* **2005**, *21(4)*, 1354.

[52] Lee, T. R.; Carey, R. I.; Biebuyck, H. A.; Whitesides, G. M. *Langmuir* **1994**, *10(3)*, 741.

[53] Creager, S. E. and Clarke J. *Langmuir* **1994**, *10(10)*, 3675.

[54] Zhao, J.; Luo, L.; Yang, X.; Wang, E.; Dong, S. *Electroanalysis* **1999**, *11(15)*, 1108.

[55] Smith, C. P. and White, H. S. *Langmuir* **1993**, *9*, 1.

[56] Fawcett, W. R.; Fedurco, M.; Kovacova, Z. *Langmuir* **1994**, *10*, 2403.

[57] Andreu, R. and Fawcett, W. R. *Journal of Physical Chemistry* **1994,** *98(48)*, 12753.

[58] Burgess, I.; Seivewright, B.; Lennox, R. B. *Langmuir* **2006**, *22*, 4420.

Chapter 2: Adsorption/Desorption Behaviour of Cysteine and Cystine in Neutral and Basic Media: Electrochemical Evidence for Differing Thiol and Disulfide Adsorption to a Au(111) Single Crystal Electrode[†]

2.1 Introduction

Biochemically-modified surfaces are commonly employed in the electroanalytical sensing of various organic compounds. Cysteine, a small thiol-containing amino acid, has been particularly useful for electrode modifications. Cysteine-modified electrodes have been utilized for detection of cytochrome *c* [1, 2], cytochrome b_5 [1], plasma proteins [3] and vitamin B_{12} [4]. Trace copper analysis is another example of an application that employed surface-bound cysteine [5, 6]. Due to the favourable redox activity of cysteine and cystine (the oxidized dimer of cysteine), extensive electrochemical literature is available [7, 8, 9, 10, 11, 12, 13, 14, 15, 16, 17, 18, 19, 20, 21, 22, 23, 24, 25, 26, 27, 28, 29, 30, 31, 32, 33].

Cysteine behaviour under anodic conditions has been evaluated at gold [7, 8, 9, 10, 11, 12, 13, 14], mercury [15], platinum [12, 16, 17, 18], conductive diamond [19], vitreous carbon [13] and ruthenate pyrochlore modified electrodes [20]. Information regarding the behaviour of cystine at positive potentials is available in the literature for mercury [21], gold [13, 22], platinum [23] and vitreous carbon electrodes [13]. All of these studies focused on the oxidative behaviour of the amino

[†] This chapter has been reprinted in a formatted version of the original publication, "Journal of Electroanalytical Chemistry 2003, 550-551C, 291-301". Full copyright permission is maintained from Elsevier Publishing.

acids, where complications from the oxidation of the metallic substrate can be important. For example, at gold electrodes, the oxidative behaviour of cysteine can be masked by gold oxidation [24]. Monitoring the desorption of the amino acids at negative potentials (under cathodic conditions) prevents these complications. The behaviour of cysteine at negative potentials has been studied at silver [25, 26] and gold electrodes [14, 27, 28, 29]. The reductive desorption of cysteine and other thiols from gold electrodes has provided insight into the desorption kinetics, as well as the packing density on the surface [34, 35, 36, 37]. Cystine has also been reductively evaluated at mercury [30, 31, 32, 33], silver [25] and gold electrodes [27].

Thiol and disulfide containing organic molecules irreversibly bind to gold and silver substrates, thus both cysteine and cystine readily form self-assembled monolayers (SAMs) at these surfaces [38,39]. The monolayers may be formed either by spontaneous self-assembly over longer periods of time at open circuit potential (OCP) from bulk analyte solutions, or they may be induced under potential control in much shorter time frames [40].

Many studies have found that there are no apparent differences between monolayers originated from either a thiol or a disulfide species on gold surfaces, and that disulfides bind as thiolates [38, 41, 42, 43, 44, 45]. Evaluations of OCPs on gold and silver electrodes in 0.1 M $LiClO_4$ have indicated that thiol adsorption is accompanied by anodic currents (oxidative adsorption), according to:

$$RSH + M \rightleftharpoons RS - M + H^+ + e^-(M) \qquad \text{Scheme 2.1}$$

whereas disulfide adsorption is accompanied by cathodic currents (reductive adsorption) [46, 47]:

$$RSSR + M + e^{-}(M) \rightleftharpoons RS - M + RS^{-} \qquad \text{Scheme 2.2}$$

Scheme 2.2 may be followed by the subsequent anodic adsorption of the resultant thiolate according to:

$$RS^{-} + M \rightleftharpoons RS - M + e^{-}(M) \qquad \text{Scheme 2.3}$$

Further support for differences in thiol and disulfide adsorption can be found in the literature. For instance, Ron *et al* [48] have demonstrated that the level of gold oxidation influences specific sulfur adsorption at the Au(111) surface. It was found that compact monolayers for $CH_3(CH_2)_{17}SH$ were obtained, compared to very poor monolayer structures for $(CH_3(CH_2)_{17}S)_2$, suggesting that only the thiol binds to pre-oxidized surfaces [48]. Rates of adsorption to gold surfaces have also been found to vary, with disulfide functionalities binding about 40% slower than thiols, as determined from electrochemical and second harmonic generation (SHG) experiments [49]. An X-ray diffraction study for $CH_3(CH_2)_9SH$ self-assembled on Au(111) by Fenter *et al* [50] revealed a disulfide structure with a S-S spacing of 2.2 Å, contrary to an anticipated thiol structure. X-ray photoelectron spectroscopy (XPS) studies for cysteine adsorbed on a Au(111) electrode have determined that two types of sulfur signals are evident at the surface. However, assignment of the peaks was not conclusive [51]. Grönbeck *et al* [52] have performed *ab initio* calculations which indicated that binding energy differences exist between gold-thiol on Au(111), compared to gold-disulfide bonding on the same surface.

Structured SAMs are of particular interest for biological applications. These organized structures may be utilized in the micro-fabrication of biosensors. Specifically oriented metal surfaces, such as afforded by gold single-crystal electrodes, are typically

employed as the foundation of the monolayer. The lattice spacing on Au(111) is 2.88 Å, and thiolates typically occupy every sixth hollow site resulting in ($\sqrt{3}$ x $\sqrt{3}$)R30° overlayers [35, 39]. However, many of the thiol and disulfide SAMs that have been imaged from scanning tunneling microscopy (STM) indicate unique super-lattice structures for specific metal faces and conditions, not always resulting in the typical ($\sqrt{3}$ x $\sqrt{3}$)R30° adlayers [53, 42].

Monolayers of cysteine prepared in aqueous solutions at Au(111) surfaces have yielded numerous lattice structures [27, 51, 54, 55]. Indications that L-cysteine forms ($\sqrt{3}$ x $\sqrt{3}$)R30° adlayers consistent with hexagonal packing, under neutral (H_2O) [51] and slightly acidic (0.1 M $KClO_4$ + 1 mM $HClO_4$) [54] conditions have been reported. Alternatively, a ($3\sqrt{3}$ x 6)R30° network-like structure has also been suggested, as evaluated from STM data under different pH conditions (50 mM NH_4Ac, pH ~ 4.6) [27]. Still, more current STM work has shown that under very acidic conditions (0.1 M $HClO_4$) a (4 x $\sqrt{7}$)R19° structure for adsorbed L-cysteine is obtained on a Au(111) surface [55]. It has also been suggested that adsorbed cysteine follows a ($2\sqrt{3}$ x $2\sqrt{3}$)R30° structure, based on desorption charge calculations from alkaline media (0.1 M NaOH) [27].

It becomes apparent that many lattice structures are feasible, and that predefined structures could be invoked under electrochemical and pH control. The current study was initiated to gain a better understanding of surface packing and to investigate if differences between thiol and disulfide monolayers could be distinguished electrochemically. The results obtained demonstrate that, with proper control of the initial holding potentials and solution composition, the desired surface active species could be maintained. In other words, the selective adsorption of either the thiol or the disulfide could be induced.

2.2 Experimental

2.2.1 Reagents and Solutions

All solutions were prepared using ultrapure water (18.2 MΩ) from a Barnstead NANOpure Diamond water purification system. The supporting electrolyte for neutral solutions was 0.1 M $KClO_4$ (Aldrich) recrystallized twice from ultrapure water. All other chemicals were employed without further purification. The supporting electrolyte for basic solutions was 0.1 M NaOH (ACP). L-cysteine (>97% Aldrich) and D-L-cysteine (racemate, >97% Aldrich) solutions were prepared immediately prior to use, and deaerated at all times with a steady stream of pre-purified N_2 in order to prevent oxidation. L-cystine (99% Aldrich and 99% Fluka) and D-L-cystine (racemate, 99% Aldrich) solutions were deaerated thoroughly prior to use.

2.2.2 Cell and Electrodes

All experiments were performed employing either a Au(111) 3.99 mm diameter single-crystal electrode, or a Au(Poly) 3.00 mm diameter polycrystalline electrode. The geometric areas employed were 0.125 cm^2 and 0.071 cm^2 for Au(111) and Au(poly), respectively. The reference electrode was an external saturated calomel electrode (SCE) separated from the electrochemical cell by a salt bridge. A platinum mesh (Alfa Aesar) was employed as the auxiliary electrode, and flame-treated prior to use. The Au working electrode was flame-annealed prior to the experiments. The cell was purged with pre-purified N_2 for 25 minutes prior to measurements, and blanketed with a N_2 atmosphere at the solution interface at all times. All experiments were carried out at 23 ± 2°C.

2.2.3 Experimental procedures

The gold electrodes were immersed via the hanging meniscus method. A three electrode cell connected to a computer-controlled Autolab potentiostat – galvanostat (PGSTAT30) was used to obtain all electrochemical data. Cyclic voltammetric (CV) data were recorded for scan rates from 10 to 500 mV s^{-1}. Double-step chronocoulometric data were obtained using an analogue integrator module (FI20).

The values for the surface excess (Γ), given in mol cm^{-2}, were obtained from the integrated charges (Q) of the cathodic desorption peaks as follows:

$$\Gamma = \frac{Q}{n_e FA} \qquad \text{Equation 2.1}$$

where F is Faraday's constant, n_e the number of electrons transferred per molecule of redox active species and A is the area of the electrode surface). Calculations considered a one-electron process for cysteine desorption, and a two-electron process for cystine desorption. Each mole of cystine could be considered as two moles of cysteine. All integrated charges were evaluated utilizing general purpose electrochemical software available with the Autolab (GPES, EcoChemie).

2.3 Results and discussion

Cysteine (freely soluble in water) is readily oxidized in the presence of oxygen, to yield the less soluble disulfide, cystine (solubility in water at 25°C is given as 0.112 g/L, or 466 μM) [56]. The cysteine/cystine formal reduction potential is given between -0.58 and -0.63 V vs. SCE from thermal and potentiometric data [57]. Coincidentally, thiol desorption from gold in aqueous media typically occurs below –0.6 V vs. SCE [27, 28,

35, 36, 37]. Cysteine ($HSCH_2CHNH_3^+COO^-$), contains a carboxyl, amino and thiol functionality with respective pK_a values of 1.71, 8.33 and 10.78. Cystine $(SCH_2CHNH_3^+COO^-)_2$, has two carboxyl and two amino groups with respective pK_a values of 1.0, 2.1, 8.02 and 8.71 [57]. The electrochemical reduction of cystine in solution to two cysteine molecules has been shown to be electrochemically irreversible at mercury, glassy carbon, gold and silver electrodes [57].

2.3.1 0.1 M $KClO_4$ as Electrolyte

2.3.1.1 Cysteine (thiol)

Considering the pK_a values, it was expected that cysteine would be present in the zwitterionic form ($HSCH_2CHNH_3^+COO^-$) in 0.1 M $KClO_4$. CVs obtained from a Au(poly) immersed in 0.1 M $KClO_4$ solution containing 50 μM L-cysteine using various initial holding potentials indicated a cathodic peak (a) at –0.64 V vs. SCE (Figure 2.1). An anodic peak (b) on the reverse anodic scan, centered at –0.57 V, is also evident (Figure 2.1). The cathodic peak (a) was found to occur at all holding potentials, and is attributed to the desorption of the thiol. The anodic peak at –0.57 V is attributed to the thiol re-adsorption. Only the desorption peak (a) was noted when the initial potential of the Au(poly) electrode was held at values more negative than +0.25 V (Figure 2.1). A second cathodic peak (c) was induced at –0.82 V when the holding potential was more positive than +0.25 V (note that the onset of gold oxidation in 0.1 M $KClO_4$ occurs near +0.70 V). This feature can only be attributed to cystine (or dimerized cysteine), since other possible oxidation products, such as sulfoxide derivatives, are not expected to be formed at these low anodic limits. The CVs indicated that cysteine is readily oxidized to form the surface disulfide at these potentials.

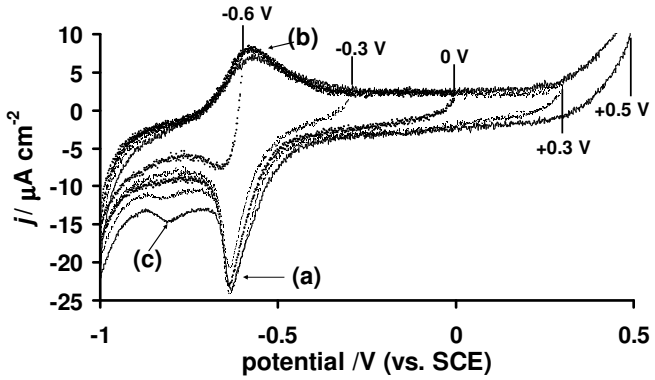

Figure 2.1: CVs obtained from Au(poly) in 0.1 M $KClO_4$ + 50 µM L-cysteine solutions. The CVs were initiated from holding potentials (indicated in the Figure) at a scan rate of 50 mV s^{-1}. Holding time was 200 s.

The same results were obtained using a Au(111) electrode, with desorption peaks (a) and (c) centered at –0.63 V and –0.82 V, respectively. The re-adsorption peak (b) was located at –0.43 V at Au(111), shifted to a potential more positive than the corresponding peak found at Au(poly). Following the findings described above (Figure 2.1), the initial holding potential for all CV experiments in 0.1 M $KClO_4$ was conveniently chosen, to ensure that the desired species was maintained at the metal-solution interface.

Figure 2.2 shows the CVs obtained from a Au(111) electrode in 0.1 M $KClO_4$ solutions with various concentrations of L-cysteine. The CVs in the presence of cysteine displayed both the typical desorption peak (a) and a distinct anodic peak (b) on the reverse scan within the potential range evaluated. The desorption peak (d), near –0.51 V, became evident at cysteine concentrations exceeding 70 µM. The potential of peak (d) coincides with previous work involving cysteine adsorption on Au(111) in acidic medium [10]. The peak was assigned to portions of the monolayer desorbing due to energetic binding differences [10]. Thiol desorption occurred at -0.63 V vs. SCE, independent of the bulk concentration. The distinct anodic peak observed between –0.42 and –0.45 V,

has been ascribed to thiol adsorption [10, 24]. Increasing the bulk cysteine concentration resulted in sharpening of this peak (b). The current of peak (b) showed a linear dependence with solution concentrations up to 70 μM. No significant change in the current was observed after the bulk cysteine concentration exceeded 70 μM. Notably, the desorption peak (a) decreased as peak (d) increased with increasing bulk concentration. At low concentrations, the monolayer would be built gradually, dependent on the diffusion of cysteine from the bulk solution to the surface. This would permit for "gap-filling" within the surface structure, leading to an improved packing density. However, at higher concentrations (>70 μM), a large number of interfacial molecules would compete for the available binding sites at the surface, and the monolayer would be constructed rapidly. This would induce a less organized adlayer, and consequently a reduced thiol desorption peak (a) (Figure 2.2).

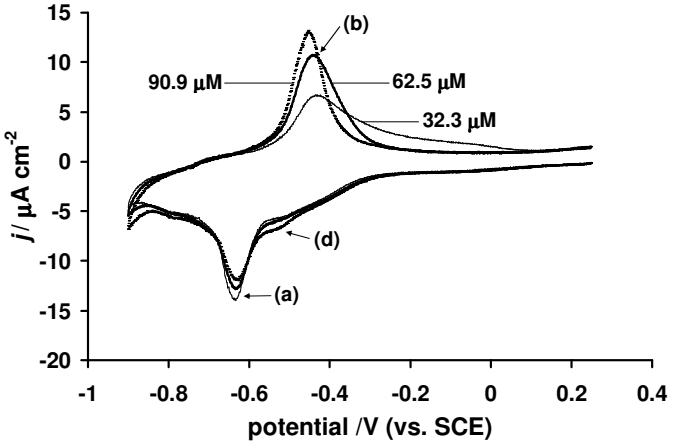

Figure 2.2: Electrochemical behaviour of a Au(111) electrode in 0.1 M $KClO_4$ containing L-cysteine at several analyte concentrations. The L-cysteine concentrations are indicated in the Figure. All scans were initiated from +0.25 V vs. SCE (holding time of 200 s), with a scan rate of 50 mV s^{-1}.

Figure 2.3 shows the variations in the CVs from a Au(111) electrode in a solution containing L-cysteine between the first and the subsequent potential sweeps. The first scan was initiated by holding the applied potential at +0.25 V for 200 seconds before scanning to more negative potentials. The holding time of 200 s was determined experimentally by obtaining the CV at various holding times for Au(poly). In fact, no change in the main features of the CV was obtained for holding times as low as 60 seconds. The 200 s holding time was therefore more than enough to ensure monolayer formation and organization. The first scan in Figure 2.3 was characterized by a sharp desorption peak (a) at –0.63 V, accompanied by a slight peak (c) at –0.82 V. The reverse anodic scan indicated the re-adsorption peak (b) at –0.43 V. Subsequent scans, performed without holding the potential at +0.25 V, indicated no change in the re-adsorption peak. However; cathodically three changes were noted:

1) A small peak (d) at –0.51 V was induced.

2) The desorption peak (a) at –0.63 V was still present but the magnitude of the current density was reduced dramatically.

3) The second cathodic desorption peak (c) was no longer evident.

Result 1 together with the fact that this peak increased with increasing bulk concentration of cysteine, seems to indicate that this feature becomes more important when little time for monolayer assembly is permitted (Figure 2.2 and Figure 2.3). Peak (d) should thus be related to defects within the adlayer, and may be due to a pre-desorption of part of the monolayer following a nucleation-growth mechanism [58]. Result 2 was anticipated for the second and subsequent scans, as the adlayer was expected to be less densely packed. At a scan rate of 50 mVs^{-1}, about 218 seconds were

allowed prior to the desorption potential (at ca -0.63 V) on the first scan (considering the 200 s holding at the initial potential). Scans where the initial potential was not held required 32 seconds from cysteine re-adsorption (-0.43 V) to desorption (-0.63 V) at 50 mV s^{-1}. The shorter time frames would increase defects in the monolayer leading to an increase of the desorption peak (d) and consequently a notable reduction in the area of the main surface desorption peak (a). The spontaneous assembly of the monolayer over shorter periods of time was clearly different than when imposing a specific potential for 200 seconds. Additionally, only about 2-5 seconds were spent in the vicinity of the surface-cysteine oxidation potential of +0.25 V at Au(111) upon cycling, whereas 200 s were allowed on the initial scan. Thus, any oxidation products on the surface would be extremely limited without holding the potential. This is supported by result 3, where the desorption peak (c) at –0.82 V, obtained upon holding, was eliminated when the potential was not held.

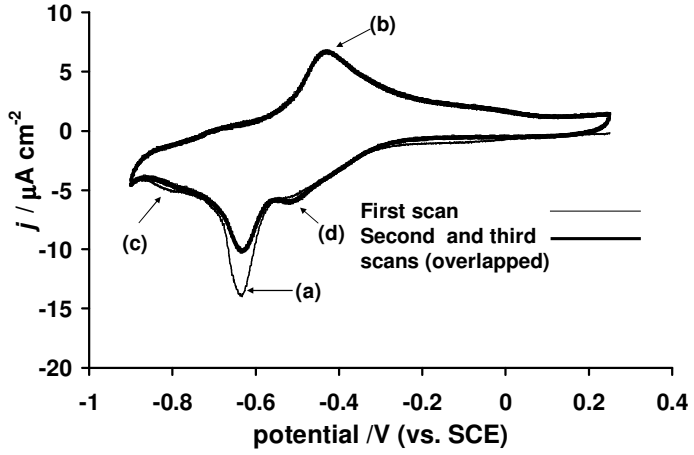

Figure 2.3: CVs from a Au(111) electrode in 0.1 M $KClO_4$ + 32.3 µM L-cysteine upon continuous cycling. Initial potential for the first scan was held at +0.25 V vs. SCE for 200 seconds. The subsequent scans were obtained without holding the potentials. The scan rate was 50 mV s^{-1}.

The integrated charges for the adsorption and desorption peaks of both L and D-L cysteine were obtained from the CVs. The values of the electric charges were used to calculate the surface excess (according to Equation 2.1) as well as the number of molecules in a monolayer. The results from these calculations are presented in Table 2.1. The monolayer charges determined from the desorption peak at 200 mV s^{-1} were found to be 29.4 ± 1.4 μC cm^{-2} for L-cysteine and 24.2 ± 1.2 μC cm^{-2} for D-L cysteine. These values correspond to surface excesses (Γ) of 3.0 ± 0.1 x 10^{-10} and 2.5 ± 0.1 x 10^{-10} mol cm^{-2}, respectively. The monolayer charges obtained by considering the adsorption peak at 20 mV s^{-1} were found to correspond to 33.1 ± 2.4 and 27.3 ± 2.6 μC cm^{-2} for L and D-L cysteine, or 3.4 ± 0.2 x 10^{-10} and 2.8 ± 0.3 x 10^{-10} mol cm^{-2}, respectively. These results are an order of magnitude smaller than the values obtained from oxidative studies in acidic media [7, 9, 10]. However, these reported studies had considered either a 4 [9, 10] or 5 [7] electron-transfer process during the cysteine oxidation to determine the monolayer charges. In addition, the gold oxidation also complicated the analysis, and the cysteine coverage was only evaluated after the charges for gold oxide formation had been subtracted [7, 9, 10]. On the other hand, the values obtained in the current study (Table 2.1), are within the range of monolayer coverages previously determined in alkaline media [27, 28].

The Γ values obtained from the adsorption peak (b) were 10% higher than the ones from the desorption peak (a). This difference suggests that defect desorption, as indicated by peak (d), is on the order of 10% for the monolayers evaluated.

Table 2.1: Monolayer Coverages for Cysteine and Cystine Species Adsorbed at Gold Electrodes from Acidic and Neutral Media: Comparison Between the Current Work and Previous Literature Values.

	Au(111) †				Au(111) ‡		Au(111)[9]	Au(poly)[10]	Au(poly)[7]
	L-cys	DL-cys	L-$(cys)_2$	DL-$(cys)_2$	L-cys	DL-cys	L-cys	L-cys	L-cys
Number of electrons	1	1	2	2	1	1	4	4	5
Monolayer Charge/ μC cm^{-2}	29.4	24.2	23.3	24.0	33.1	27.3	900	750	
Γ x 10^{9}/ mol cm^{-2}	0.30	0.25	0.12	0.12	0.34	0.28	2.3	1.95	2.7
Coverage x 10^{-15}/ molecules cm^{-2}	0.18	0.15	0.07	0.08	0.21	0.17	1.4	1.2	1.6
Area per molecule/ nm^2	0.55	0.66	1.37	1.33	0.48	0.59	0.071	0.085	0.062

cys = cysteine
$(cys)_2$ = cystine
† Obtained from the thiol desorption peak
‡ Obtained from the thiol adsorption peak

2.3.1.2 Cystine (disulfide)

Cystine is also in the zwitterionic form in the evaluated media (0.1 M $KClO_4$). It can be anticipated that the same features observed in the CVs from Figure 2.2 and Figure 2.3 (from Au(111) in solutions containing cysteine), should be obtained from a Au(111) surface in solutions containing cystine. Figure 2.4 are examples of the CVs obtained from a Au(111) electrode in solutions containing cystine at several concentrations. The main desorption spike (a) between –0.64 and –0.67 V (slightly negative of the thiol desorption peak potential for cysteine solutions at comparable concentrations) was quite evident. This peak (a), assigned to thiol desorption, was observed during the cathodic scan after the initial potential was held for 200 seconds at +0.25 V. A convoluted shoulder (e) was observed following the thiol desorption (a). This shoulder is attributed to disulfide reduction according to Scheme 2.2. The shoulder (e) was influenced by the complex kinetics of the system. The reductively adsorbed thiol is not stable at these potentials,

and desorbs as a thiolate, according to the reverse of Scheme 2.3. The immediate by-product of Scheme 2.2 is also a thiolate, thus the thiolate concentration at the interface is greatly increased. This feature was not evident in aqueous media containing cysteine, because cystine was not available in the solution (extreme care was taken during the solution preparation to prevent any unwanted cysteine oxidation).

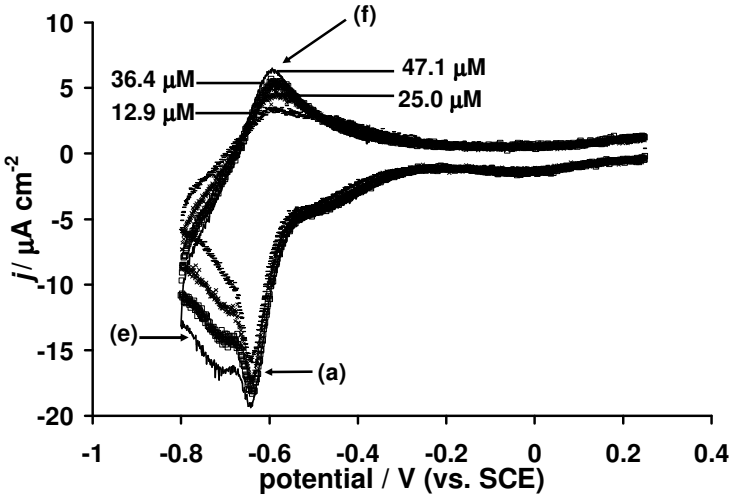

Figure 2.4: Electrochemical behaviour of a Au(111) electrode in 0.1 M $KClO_4$ containing D-L cystine at several analyte concentrations. The D-L cystine concentrations are indicated in the figure. All scans initiated from +0.25 V vs. SCE (holding time of 200 s), with a scan rate of 50 mV s^{-1}.

The reverse anodic scans in Figure 2.4 demonstrated an adsorption peak (f). Although similar to the adsorption peak (b) observed for cysteine (Figure 2.2), the peak (f) in Figure 2.4 was centered at –0.57 V, approximately 0.14 V more cathodic than the cysteine peak. Hence, the adsorption peak (f) in Figure 2.4 can be attributed to adsorption of the disulfide reduction products, as discussed above.

The breaking of the S-S bond for the bulk cystine occurs cathodically (during shoulder (e)) according to Scheme 2.2, yet the 1-electron formation of surface-bound

thiol from the resultant thiolate occurs anodically in accordance with Scheme 2.3. Cystine adsorption at Au(111) (Figure 2.4) occurred in the same potential range (-0.57 V) as cysteine adsorption on Au(poly) (Figure 2.1). Some sharpening of the peak (f) occurred with increasing the bulk cystine concentration (Figure 2.4). Nonetheless, the general shape and magnitude of the curve (peak (f) in Figure 2.4) showed more similarities to the adsorption peak (b) for cysteine at low concentrations (Figure 2.2), suggesting a gradual building of the monolayer. Gradual build-up of the monolayer would occur over a wide potential range, as disulfide molecules approached the surface and became reduced to yield the thiolate. The more complex building of the monolayer, compared to direct thiol adsorption, would agree with slower kinetics for the adsorption of a disulfide species as previously suggested [49].

At the Au(poly) electrode, the peak (f) occurred at –0.63 V, 0.06 V more cathodic than the cysteine species. Adsorption of the disulfide derived thiolate is likely to occur on different sites at the Au(111) and Au(poly) surfaces than thiol adsorption, as suggested by theoretical calculations [52] and previous electrochemical investigations [14]. The adsorption peaks from the thiol and the disulfide species were distinct at Au(poly), but at this surface the difference in the adsorption potential was only 0.06 V, compared to 0.14 V at Au(111).

The changes between the first and subsequent CVs from a Au(111) in 0.1 M $KClO_4$ solution containing 14.8 μM L-cystine are presented in Figure 2.5. The first scan is representative of the observed cystine behaviour when the initial potential was held at +0.25 V for 200 s. These scans always indicated the distorted asymmetric desorption peak (a) (with the shoulder (e)) and the re-adsorption peak (f). On occasion, at low

concentrations, these scans would also indicate the presence of the adsorption peak (b) attributed to thiol adsorption. Subsequent scans, without holding the potential, resulted in a sharp increase in the feature (d), followed by a decrease in the current of the desorption peak (a) (similar results were observed from solutions containing cysteine – Figure 2.3). On the reverse anodic scans, two adsorption peaks were always evident (Figure 2.5 - second and third scans) one at –0.57 (peak (f)) and the other at –0.43 V (peak (b)), corresponding to the adsorption from reduced disulfide and thiol re-adsorption, respectively. The adsorption peak (f) diminished during the third and subsequent cycles and the thiol peak (b) increased, as more thiols became available near the surface. The applied potential was not held at +0.25 V during the second and subsequent potential scans, thus limited time was spent at potentials positive enough to maintain the oxidized species (cystine) at the interface. Consequently, any thiol generated during the cathodic scan was not re-oxidized. The concentration of thiol at the interface increased whereas the concentration of cystine declined. These results suggest that the redox potential for the cysteine/cystine surface bound couple occurs near +0.25 V vs. SCE at gold electrodes in 0.1 M $KClO_4$, and that holding near this potential ensures that either species will be present.

Table 2.1 includes the values for surface coverage and charge densities obtained from the main desorption peak for cystine (peak (a) – Figure 2.4), yielding values comparable to those determined for cysteine. The cathodic charges under peak (a) for L and D-L cystine monolayers were calculated to be 23.3 ± 1.3 and 24.0 ± 3.2 $\mu C\ cm^{-2}$, respectively. A surface excess (Γ) of 1.2×10^{-10} mol cm^{-2} for both cystine isomers was evaluated, corresponding to 2.4×10^{-10} mol cm^{-2} in terms of cysteine units. Utilizing the

surface lattice table provided by Zhang *et al* [27], the calculated coverage would correspond to a 3 x 3 lattice.

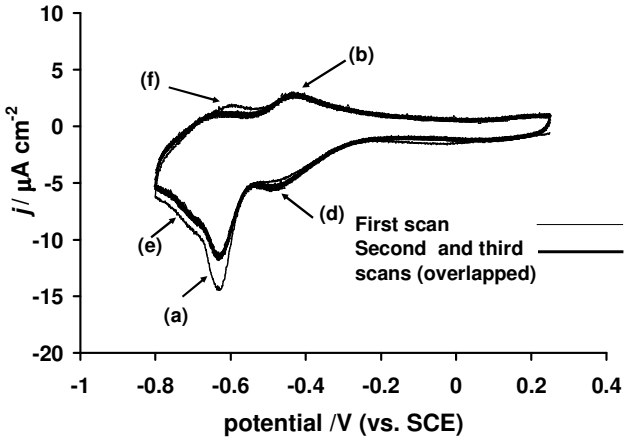

Figure 2.5: CVs from a Au(111) electrode in 0.1 M $KClO_4$ + 14.8 µM L-cystine upon continuous cycling. Initial potential for the first scan was held at +0.25 V vs. SCE for 200 seconds. The subsequent scans were obtained without holding the potentials. The scan rate was 50 mV s^{-1}.

2.3.2 0.1 M NaOH as Electrolyte

2.3.2.1 Cysteine (thiolate)

In alkaline media cysteine is present as the negatively charged thiolate ($^{-}SCH_2CHNH_2COO^{-}$), and not the same species evaluated in 0.1 M $KClO_4$ (zwitterionic form). Figure 2.6 displays a set of typical CVs obtained from a Au(111) electrode in 0.1 M NaOH solutions containing two concentrations of cysteine. Similar to the CVs obtained in the previous section (2.3.1), a suitable holding potential (–0.30 V vs. SCE) was determined and maintained for 200 seconds prior to the initial scans. Cysteine oxidative adsorption at the surface occurred at +0.25 V vs. SCE in 0.1 M $KClO_4$. Considering the Nernst equation, a shift to more negative potentials in basic media was

anticipated, since the thiolate adsorption is considered under these conditions Scheme 2.3. The desorption peak (a), centered at –0.72 V, is shown in Figure 2.6. This peak position corresponds well with the desorption peak for cysteine reported by Zhang *et al* [27] under similar conditions. The desorption peak (a) positioned at ca –0.72 V shifted negatively with increasing bulk concentrations of cysteine. This desorption peak (a) (Figure 2.6) was found to be remarkably sharp relative to the desorption peak obtained for the zwitterionic species in $KClO_4$ (Figure 2.2 and Figure 2.3), implying a more densely packed monolayer.

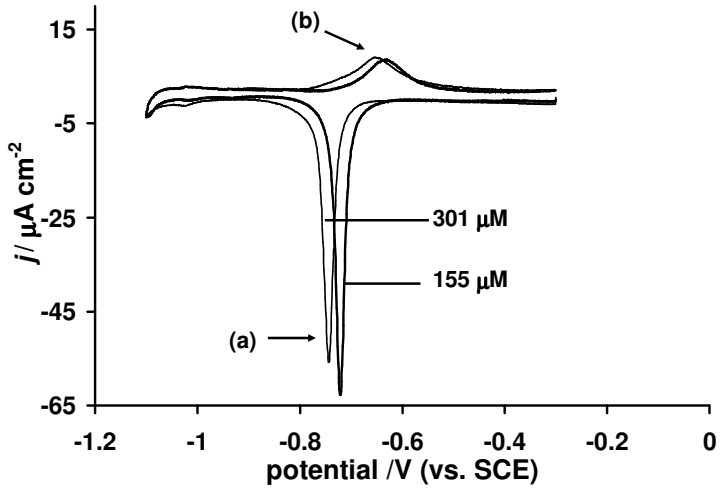

Figure 2.6: Electrochemical behaviour of a Au(111) electrode in 0.1 M NaOH containing L-cysteine at different analyte concentrations. The L-cysteine concentrations are as indicated. All scans initiated from -0.30 V vs. SCE (holding time of 200 s), with a scan rate of 50 mV s^{-1}.

The main intermolecular interaction expected within a cysteine monolayer is the hydrogen bonding between the amino and the carboxyl groups. Electrostatic contributions may also play a role for the adsorbed zwitterionic layer (as in $KClO_4$ medium). However, the positively charged electrode surface (pzc is around + 0.09 V vs. SCE for Au(111) [10]) may provide a further destabilization of the monolayer structure,

by attracting the carboxylate and repelling the protonated amino group. This contribution would have an effect on the molecular orientation, affecting the quality of the hydrogen bonding. Better hydrogen interactions could explain the higher quality of the monolayers obtained from basic medium.

The anodic re-adsorption peak (b) in Figure 2.6 was extremely broad, centered near –0.60 V, similar to the anodic adsorption peak found for the disulfide derived thiolate in 0.1 M $KClO_4$. This further supports the mechanism proposed above to explain the peak (f) in Figure 2.4 and Figure 2.5. Although reproducible upon repetitive cycling, this peak provided poor reproducibility between solutions and was not employed for monolayer coverage calculations.

The main change between the first scan (obtained after the initial potential was held at -0.30 V) and the subsequent cycles (where the initial potential was not held at -0.30 V between scans) was a positive shift of the potential for thiol desorption (not shown). The desorption peak shifted to more positive potentials during the second and subsequent scans, and no further changes were observed upon continuous cycling. The desorption peak (a) became greatly diminished and broadened during the second and subsequent scans, indicating that insufficient time was allowed for the assembly of the monolayer.

Table 2.2 summarizes the monolayer coverages calculated from the CVs in basic media containing cysteine. Previously obtained literature values are also listed in Table 2.2. The integrated charge of the desorption peak (a) obtained from the first CVs (where the initial potential was held for 200 s at –0.30 V), yielded 37.3 ± 1.8 μC cm^{-2} for L-cysteine. This value implies a monolayer coverage of 3.9 ± 0.2 x 10^{-10} mol cm^{-2},

consistent with previously obtained values of 4.0 x 10^{-10} [27] and 4.7 x 10^{-10} mol cm^{-2} [28]. This packing density has been previously suggested to follow a $(2\sqrt{3} \times 2\sqrt{3})R30°$ structure, wherein cysteine would adopt a dimerized orientation [27].

Table 2.2: Monolayer Coverages for Cysteine and Cystine Species Adsorbed at Gold Electrodes from Basic Media: Comparison Between the Current Work and Previous Literature Values.

	Au(111) †			Au(111) ‡			Au(111)	
	L-cys	DL-cys	DL-$(cys)_2$	L-$(cys)_2$	DL-$(cys)_2$	L-cys	L-cys [27]	L-$(cys)_2$ [27]
number of electrons	1	1	2	2	2	1	1	2
Monolayer Charge/ μC cm^{-2}	38.1	35.7	37.0	23.1	22.6	37.3	37	37
Γ x 10^{9}/ mol cm^{-2}	0.39	0.37	0.19	0.12	0.12	0.39	0.4	0.19
Coverage x 10^{-15}/ molecules cm^{-2}	0.24	0.22	0.12	0.07	0.07	0.23	0.24	0.11
Area per molecule/ nm^2	0.42	0.45	0.87	1.39	1.42	0.43	0.42	0.87

cys = cysteine
$(cys)_2$ = cystine
† Obtained from chronocoulometry
‡ Obtained from the thiol desorption peak

Double step chronocoulometry was employed to monitor the dependence of the cathodic charge on the initial holding potential. The coulometry data obtained for the Au(poly) electrode indicated that three distinct holding potential ranges existed. At potentials more negative than –0.40 V, the monolayer charges were on the order of 40 μC cm^{-2}, corresponding to a surface excess of 4.1 x 10^{-10} mol cm^{-2}, consistent with the current literature values [27, 28]. In this potential range, a one electron process would be associated with the desorption of the cysteine monolayer, as all molecules would be present as surface bound thiols. The potential region between –0.40 and –0.20 V indicated a gradual increase of the cathodic charge, maximizing near 80 μC cm^{-2} at –0.20 V. This region was assigned to a combination of thiol and disulfide at the interface. Similar surface coverage on the order of 4.0 x 10^{-10} mol cm^{-2} could be obtained by

considering a 1.5 electron transfer (the average electron transfer anticipated for a 50:50 mixture of thiol and disulfide species). The potential region from –0.20 to 0.0 V indicated a plateau for the surface charge near 80 μC cm^{-2} (approximately twice the value obtained when holding in the negative region at, or more negative than –0.40 V). This region was assigned to the presence of the oxidized species of cysteine, cystine, and a two electron transfer process would yield approximately 4.1 x 10^{-10} mol cm^{-2} of cysteine units. An initial two electron reduction for the conversion of disulfide to thiolate (RSSR + 2 e^- → $2RS^-$), followed by the one electron reduction for the thiol desorption was considered. Since it is easier to correlate the data in terms of cysteine units, this implies a net 2 electron acceptance per cysteine unit, or 4 electrons per cystine unit. Similar experiments utilizing the Au(111) electrode yielded 3.9 x 10^{-10} and 3.7 x 10^{-10} mol cm^{-2} for L and D-L cysteine, respectively. CV data had indicated that the oxidation of cysteine in 0.1 M NaOH started near -0.20 V, and is supported by the surface charge doubling noted with the chronocoulometric data in the same potential region.

2.3.2.2 Cystine (anionic)

Cystine is present in alkaline solutions as the anion $(SCH_2CHNH_2COO^-)_2$. Figure 2.7 depicts a set of CVs obtained from Au(111) in 0.1 M NaOH solution containing cystine. Each CV presented in Figure 2.7 was initiated from a different anodic potential. The CV obtained when the initial holding potential was at –0.20 V indicates two desorption peaks, (a) and (c), at –0.67 and –0.97 V, respectively. These peaks can be attributed to thiol desorption (peak (a)) and disulfide reduction (peak (c)). When the initial holding potential was more positive than -0.20 V, the disulfide was maintained

near and at the electrode surface, as indicated by the presence of both re-adsorption peaks (b) and (f). The adsorption peak (f) (originated from disulfide-derived species) occurred near –0.97 V, clearly coupled to the reduction peak (c), and the thiolate adsorption peak (b) occurred near –0.67 V, coupled to the thiol desorption peak (a). When the initial potentials were more negative than –0.20 V (Figure 2.7), the surface disulfide is reduced to adsorbed cysteine during the holding time. This assumption is corroborated by the single desorption peak (a), and lack of re-adsorption peak (f) observed on the reverse anodic scan. Interestingly enough, CVs obtained from basic solutions containing only cysteine can also be induced to present the reduction peak (c). This occurred when the initial holding potential was more positive than -0.20 V. Furthermore, cysteine solutions, allowed to oxygenate for 40 minutes, followed by 25 minutes of deaerating with prepurified N_2, yielded similar scans as disulfide solutions.

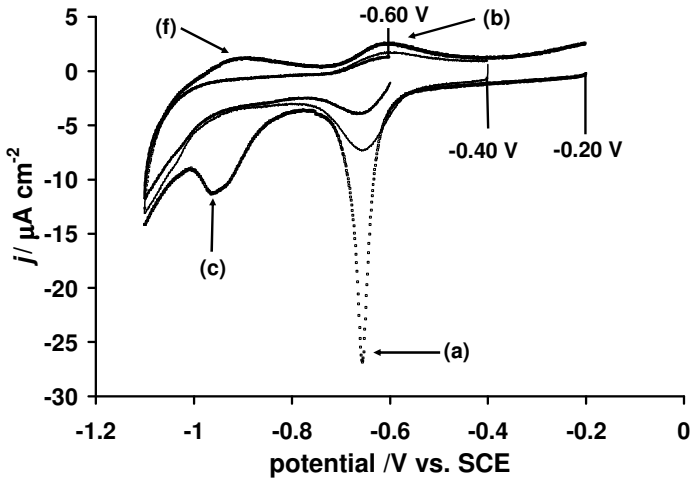

Figure 2.7: CVs obtained from Au(111) in 0.1 M NaOH + 51.8 µM L-cystine solutions. The CVs were initiated from various holding potentials (indicated in the Figure) at a scan rate of 50 mV s^{-1}. Holding time was 200 s.

Similar peaks to those reported here from the CVs obtained in cystine-containing solutions (Figure 2.7) have previously been reported for cysteine in 0.1 M KOH at a gold

disk electrode, with scans initiated from –0.20 V vs. $Ag|AgCl|Cl^-_{sat}$ [28]. The authors had immobilized cysteine onto the gold surface by immersion in 1 mM cysteine solution in phosphate buffer. As cysteine is readily oxidized in the presence of air, any transfer experiments would be subject to some oxidation. Desorption potentials for cysteine in 0.1 M KOH from gold electrodes have been reported between –0.6 and –1.4 V vs. SCE. These scans were initiated after a five-minute holding potential at +0.70 V (far beyond the initial oxidation potential of cysteine) [24]. Tüdös and Johnson also reported that the reverse scan was accompanied by slight anodic peaks between –1.4 and –0.6 V [24]. The authors ascribed the desorption and adsorption peaks to differing adsorption sites on the roughened gold electrodes [24]. We are ascribing similar peaks due to adsorption at differing sites for the thiol and disulfide, where disulfide adsorption is observed in the form of the thiolate according to Scheme 2.2 and Scheme 2.3.

Experiments employing a quartz crystal microbalance (QCM) had shown that the potential range between –0.30 and –1.5 V vs. SCE was found to be negative of the dissolution potential for gold in alkaline media [24]. Since all data in this current study had been obtained within this range, desorption due to gold dissolution did not interfere with our results.

The integrated charge densities for the thiol desorption peak (a) from Au(111) in solutions containing cystine were 23.1 ± 1.8 and 22.6 ± 2.2 μC cm^{-2} for L and D-L cystine (Table 2.2). These charges were obtained when the initial holding potential was set to -0.20 V (as in Figure 2.7). Therefore, the charge densities of the main thiol desorption peak (a) obtained from basic solution containing cystine were found to be smaller than the equivalent peaks measured from cysteine solutions (peak (a), Figure

2.6). These values are also inconsistent with the 37 μC cm^{-2} obtained by Zhang *et al* [27]. Remarkably, these values coincide with the desorption charges obtained in 0.1 M $KClO_4$, for both cysteine and cystine (Table 2.1). Once again, a calculated overlayer following a 3 x 3 structure would be obtained. It should be noted that the cystine values reported by Zhang *et al* [27] were obtained from linear sweep voltammograms initiated at –0.40 V vs. SCE, a potential we have shown to facilitate disulfide reduction at the surface and the formation of a thiol adlayer. It is then suggested that under our experimental conditions (potential held at -0.20 V prior to scan), only approximately 2/3 of the monolayer had been converted to adsorbed thiol.

Double step chronocoulometry was used to estimate the total cathodic charge at different initial potentials from Au(111) in basic solutions containing cystine. The maximum charge density was found to be 37.0 μC cm^{-2} or 3.8 x 10^{-10} mol cm^{-2} of cysteine units. This suggests that the same full coverage was measured regardless which species (cysteine or cystine) were initially present in the solution. In principle, this value for the maximum cathodic charge density obtained from chronocoulometry does not seem to agree with the equivalent quantities evaluated from CV. The cathodic charges under the peak (a) were obtained from CVs when the initial potential was held at –0.20 V. It can be seen from Figure 2.7, that another cathodic peak (c) was present under these conditions. When the charge of the peak (c) was also considered the total cathodic charge obtained by CV coincided (within the experimental uncertainties) with the chronocoulometric data.

2.3.3 Summary

The large thiol desorption spike, between –0.63 and –0.74 V vs. SCE, was observed in the CVs from solutions containing all species evaluated on Au(111) regardless of pH. This peak is consistent for thiol desorption [14, 27, 28]. Integrated charges obtained for this peak in 0.1 M $KClO_4$ for solutions containing cysteine at Au(111) are comparable at 29.4 ± 1.4 and 24.2 ± 1.2 μC cm^{-2} for the L and D-L species, respectively (Table 2.1). Slightly higher values were obtained for the L isomer, suggesting that a more densely packed monolayer is attained when reducing the number of phase boundaries. The racemic solution would contain two different species, and may present a different structure at the surface than presented by a single isomer. Also, the possibility for improved hydrogen bonding within the monolayer formed by the single isomer should not be excluded. Due to steric considerations, hydrogen bonding is much more feasible for monolayers derived from L-cysteine solutions compared to monolayers formed from racemate or disulfide solutions. It is important to stress that this difference is statistically significant. For instance, considering two separate populations, the calculated t was found to be 5.14, compared to t_5 at 4.03 for 99% confidence. These differences between the packing densities of the cysteine isomer and the racemate are currently being further investigated in our laboratory. Integration of the corresponding adsorption peaks resulted in slightly higher values of 33.1 ± 2.4 and 27.3 ± 2.6 μC cm^{-2} for L and D-L cysteine. The L- isomer also provided marginally higher charges when the anodic process was evaluated. Again, statistically the calculated t value was 3.50, compared to t_9 of 3.25 at 99 % confidence, suggesting a significant difference.

Surface charge determination for the desorption peak from solutions containing cystine in 0.1 M $KClO_4$ yielded 23.3 ± 1.3 and 24.0 ± 3.2 μC cm^{-2} for the L and D-L species, slightly lower than the charges obtained from solutions containing L-cysteine. The charges, however; were almost the same as found for the cysteine racemate. No significant differences between the two disulfide species were noted. In all cases, coverage could be calculated to approximate a 3 x 3 structure.

The CVs obtained in 0.1 M $KClO_4$ for cysteine and cystine solutions indicated some differences in the adsorption behaviour for thiol and disulfide species. Adsorption from disulfide-derived thiolate occurs at the Au(111) surface near a potential of –0.57 vs. SCE, 0.14 V more cathodic than adsorption of the thiol species at –0.43 V. This observation may indicate that the disulfide and thiol species do not bind to the same sites of the Au(111) surface. Moreover, according to Scheme 2.3, the adsorption of the disulfide involves both a cathodic and an anodic process, of which the anodic thiolate adsorption is observed at peak (f). Adsorption from $KClO_4$ to a Au(poly) electrode also indicated binding differences for the thiol and disulfide-originated species. The thiol, cysteine, re-adsorbed to the polycrystalline surface at –0.57 V vs. SCE. The disulfide, in the form of the thiolate, re-adsorbed to the Au(poly) surface at –0.63 V, 0.06 V more cathodic than the thiol.

The integrated charge density obtained for the thiol desorption peak in the CVs from a Au(111) electrode in 0.1 M NaOH solution in the presence of L-cysteine was comparable, at 37.3 ± 1.8 μC cm^{-2}, with previously reported values of 37 μC cm^{-2} [27] under similar conditions. Considering that cysteine could be dimerized, a ($2\sqrt{3}$ x $2\sqrt{3}$)R30° structure has previously been proposed for the obtained packing density [27].

Surface charges, obtained from the thiol desorption peak in the CVs from cystine solutions in 0.1 M NaOH, were 23.1 ± 1.8 and 22.6 ± 2.2 μC cm^{-2} for the L and D-L species. The thiol charges measured from solutions containing cystine by CV were significantly lower than the charges obtained from cysteine solutions. Experiments utilizing disulfide solutions again suggest either that the monolayer adsorption was incomplete, or that the packing density of the monolayer was reduced.

Theoretical calculations employing local density approximation (LDA) [52], have indicated that two separate binding mechanisms exist for thiols and disulfides. It is suggested that different surface sites are required for thiol and disulfide moieties, and that these can be experimentally monitored using electrochemical techniques. Differences in thiol and disulfide adsorption behaviour have also been observed electrochemically [46, 47, 48, 49] and from X-ray diffraction studies [50]. Previous XPS work with cysteine has also indicated two types of sulfur peaks evident on the gold surface [51]. It is suggested that some oxidation had occurred and the presence of two sulfur peaks may have been indicative of a surface disulfide species [51]. A surface bound disulfide, formed from the oxidation of cysteine, has been proposed on silver surfaces based on surface-enhanced Raman scattering (SERS) measurements [25].

CVs from Au (111) in 0.1 M NaOH solutions containing cystine presented two distinct reduction peaks. The first reduction peak observed at –0.67 V was ascribed to the thiol desorption, and the second peak, at more negative potentials (–0.97 V) was assigned as being due to the reduction of disulfide (R-S-S-R). In 0.1 M $KClO_4$, the thiol desorption peak measured from cystine solutions did not appear as a single peak, rather, there was a large post-wave shoulder, indicating bulk disulfide reduction. It was evident

that the reduction potential for the disulfide overlaps with the desorption potential for the thiol, at lower pH values on Au(111). This overlap did not occur for CV experiments performed in basic media.

2.4 Conclusions

The thiol/disulfide redox couple, cysteine/cystine, were shown to adsorb at different potentials at a Au(111) surface. The adsorption peak from solutions containing cystine was centered at –0.57 V vs. SCE while cysteine adsorption occurred at –0.43 V in 0.1 M $KClO_4$ solution. A similar separation between the adsorption potentials was observed from experiments performed in basic media. This demonstrated clearly an observable difference in the adsorption of thiols and disulfides from bulk solution to the Au(111) surface. We have also demonstrated that specific species (thiol or disulfide) can be maintained at the interface by proper control of the applied potential. The disulfide (cystine) was present at the surface when the applied potential was held at values more positive than +0.25 V in $KClO_4$ and -0.20 V in NaOH. The corresponding thiol (cysteine) was the only species maintained at the surface when the applied potentials were more cathodic than +0.25 V and -0.20 V and in $KClO_4$ and NaOH, respectively. The measured desorption charges indicate that thiol monolayers present a higher packing density than their disulfide counterparts. Preliminary results also indicated small (but statistically significant) differences in the surface coverage of L-cysteine and D-L cysteine monolayers.

2.5 Bibliography

[1] Qian, W.; Zhuang, J.-H.; Wang, Y.-H.; Huang, Z.-H. *Journal of Electroanalytical Chemistry* **1998**, *447*, 187.

[2] Di Gleria, K.; Hill, H. A. O.; Lowe, V. J.; Page. D. J. *Journal of Electroanalytical Chemistry* **1986**, *213*, 333.

[3] Tengvall, P.; Lestelius, M.; Liedberg, B.; Lundström, I. *Langmuir* **1992**, *8(5)*, 1236.

[4] Zagal, J. H.; Aguirre, M. J.; Parodi, C. G.; Sturm, J. *Journal of Electroanalytical Chemistry* **1994**,*374*, 215.

[5] Liu, A.-C.; Chen, D.-C.; Lin, C.-C.; Chou, H.-H.; Chen, C.-H. *Analytical Chemistry* **1999**, *71(8)*, 1549.

[6] Stewart, S. and Fredericks, P. M. *Spectrochimica Acta Part A* **1999**, *55*, 1641.

[7] Arrigan, D. W. M. and Le Bihan, L. *Analyst* **1999***, 124*, 1645.

[8] Fawcett, W. R.; Fedurco, M.; Kováčová, K.; Borkowska, Z. *Journal of Electroanalytical Chemistry* **1994***, 368*, 265.

[9] Fawcett, W. R.; Fedurco, M.; K. Kováčová, K.; Borkowska, Z. *Journal of Electroanalytical Chemistry* **1994***, 368*, 275.

[10] Fawcett, W. R.; Fedurco, M.; Kováčová, K.; Borkowska, Z. *Langmuir* **1994***, 10(3)*, 912.

[11] Koryta, J. and Pradáč, J. *Journal of Electroanalytical Chemistry* **1968**, *17*, 177.

[12] Koryta, J. and Pradáč, J. *Journal of Electroanalytical Chemistry* **1968**, *17*, 185.

[13] Reynaud, J. A.; Malfoy, B.; Canesson, P. *Journal of Electroanalytical Chemistry* **1980**, *114*, 195.

[14] Tüdös, A. J. and Johnson, D. C. *Analytical Chemistry* **1995**, *67(3)*, 552.

[15] Heyrovský, M. and Vavřička, S. *Bioelectrochemistry and Bioenergetics* **1999**, *48*, 43.

[16] Davis, D. G. and Bianco, E. *Journal of Electroanalytical Chemistry* **1966**, *12*, 254.

[17] Johll, M. E.; Williams, D. G.; Johnson, D. C. *Electroanalysis* **1997**, *9(18)*, 1397.

[18] Dixon, M. and Quastel, J. H. *Journal of the Chemical Society* **1923**, *23B*, 2943.

[19] Spãtaru, N.; Sarada, B. V.; Popa, E.; Tryk, D. A.; Fujishima, A. *Analytical Chemistry* **2001**, *73*, 514.

[20] Zen, J. M.; Kumar, A. S.; Chen, J.-C. *Analytical Chemistry* **2001**, *73*, 1169.

[21] Heyrovský, M.; Mader, P.; Veselá, V.; Fedurco, M. *Journal of Electroanalytical Chemistry* **1994**, *369*, 53.

[22] Johll, M. E.; Wong, S.-S.; Johnson, D. C. *Electroanalysis* **1999**, *11(14)*, 1049.

[23] Koryta, J. and Pradáč, J. *Journal of Electroanalytical Chemistry* **1968**, *17*, 167.

[24] Tüdös, A. J. and Johnson, D. C. *Analytical Chemistry* **1995**, *67(3)*, 557.

[25] Watanabe, T. and Maeda, H. *Journal of Physical Chem*istry **1989**, *93*, 3258.

[26] Brolo, A. G.; Germain, P.; Hager, G. *Journal of Physical Chemistry B* **2002**, *106(23)*, 5982.

[27] Zhang, J.; Chi, Q.; Nielsen, J. U.; Friis, E. P.; Andersen, J. E. T.; Ulstrup, J. *Langmuir* **2000**, *16(18)*, 7229.

[28] Yang, W.; Gooding, J. J.; Hibbert, D. B. *Journal of Electroanalytical Chemistry* **2001**, *516*, 10.

[29] Yang, D.-F.; Wilde, C. P.; Morin, M. *Langmuir* **1996**, *12(26)*, 6570.

[30] Çakir, S.; Biçer, E.; Çakir, O. *Electrochemistry Communications* **1999**, *1*, 257.

[31] Kolthoff, I. M. and Barnum, C. *Journal of the American Chemical Society* **1941**, *63*, 520.

[32] Kolthoff, I. M.; Stricks, W.; Tanaka, N. *Journal of the American Chemical Society* **1955**, *77*, 5215.

[33] Vavřička, S. and Heyrovský, M. *Journal of Electroanalytical Chemistry* **1994**, *375*, 371.

[34] Mulder, W. H.; Calvente, J. J.; Andreu, R. *Langmuir* **2001**, *17*, 3273.

[35] Zhong, C.-J.; Zak, J.; Porter, M. D. *Journal of Electroanalytical Chemistry* **1997**, *421*, 9.

[36] Martin, H.; Vericat, C.; Andreasen, G.; Hernández Creus, A.; Vela, M. E.; Salvarezza, R. C. *Langmuir* **2001**, *17(8)*, 2334.

[37] Azzaroni, O.; Vela, M. E. ; Martin, H. ; Hernández Creus, A.; Andreasen, G.; Salvarezza, R. C. *Langmuir* **2001**, *17(21)*, 6647.

[38] Bain, C. D.; Biebuyck, H. A.; Whitesides, G. M. *Langmuir* **1989**, *5(3)*, 723.

[39] Ulman, A. *Chemistry Reviews* **1996**, *96(4)*, 1533.

[40] Ma, F. and Lennox, B. R. *Langmuir* **2000**, *16(15)*, 6188.

[41] Szafranski, C. A.; Tanner, W.; Laibinis, P. E.; Garrell, R. L. *Langmuir* **1998**, *14(13)*, 3570.

[42] Nelles, G.; Schönherr, H.; Jaschke, M.; Wolf, H.; Schaub, M.; Küther, J.; Tremel, W.; Bamberg, E.; Ringsdorf, H.; Butt, H.-J. *Langmuir* **1998**, *14(4)*, 808.

[43] Sawaguchi, T.; Mizutani, F.; Taniguchi, I. *Langmuir* **1998**, *14(13)*, 3565.

[44] Noh, J.; Murase, T.; Nakajima, K.; Lee, H.; Hara, M. *Journal of Physical Chemistry B* **2000**, *104(31)*, (2000), 7411.

[45] Noh, J. and Hara, M. *Langmuir* **2000**, *16(5)*, 2045.

[46] Paik, W.-K.; Eu, S.; Lee, K.; Chon, S.; Kim, M. *Langmuir* **2000**, *16(26)*, 10198.

[47] Chon, S. and Paik, W.-K. *Physical Chemistry and Chemical Phys*ics **2001**, *3*, 3405.

[48] Ron, H. and Rubinstein, I. *Journal of the American Chemical Society* **1998**, *120(51)*, 13444.

[49] Jung, C.; Dannenberger, O.; Xu, Y.; Buck, M. ; Grunze, M. *Langmuir* **1998**, *14(5)*, 1103.

[50] Fenter, P.; Eberhardt, A.; Eisenberger, P. *Science* **1994**, *266*, 1216.

[51] Dodero, G.; De Michieli, L.; Cavalleri, O.; Rolandi, R.; Oliveri, L.; Daccà, A.; Parodi, R. *Colloids and Surfaces A: Physiochemical and Engineering Aspects* 2000, *175*, 121.

[52] Grönbeck, H.; Curioni, A.; Andreoni, W. *Journal of the American Chemical Society* **2000**, *122*, 3839.

[53] Strong, L. and Whitesides, G. M. *Langmuir* **1988**, *4(3)*, 546.

[54] Dakkouri, A. S.; Kolb, D. M.; Edelstein-Shima, R.; Mandler, D. *Langmuir* **1996**, *12(11)*, 2849.

[55] Xu, Q.-M.; Wan, L.-J.; Wang, C.; Bai, C.-L.; Wang, Z.-Y.; Nozawa, T. *Langmuir* **2001***, 17*, 6203.

[56] Budavari, S. Merck Index, 12th ed., Merck & Co. Inc., Whitehouse Station, NJ, 1996.

[57] Ralph, T. R.; Hitchman, M. L.; Millington, J. P.; Walsh, F. C.; *Journal of Electroanalytical Chemistry* **1994**, *375*, 1.

[58] Vinokurov, I. A.; Morin, M.; Kankare, J. *Journal of Physical Chemistry B* **2000**, *104*, 5790.

Chapter 3: Deprotonation and Protonation of Cysteine and Cystine Monolayers Probed by Impedance Spectroscopy

3.1 Introduction

The behaviour of self-assembled monolayers (SAMs) is of interest as these surfaces are quite often employed in the development of chemical sensors for medical and environmental applications [1, 2, 3, 4, 5]. Previously, we had used cyclic voltammetry (CV) to evaluate the desorption of SAMs formed from the small chain amino acids, cysteine (cys = $HSCH_2CHNH_3^+COO^-$) and cystine ($(cys)_2$ = $(SCH_2CHNH_3^+COO^-)_2$), onto a Au(111) surface in 0.1 M NaOH and 0.1 M $KClO_4$ solutions [6]. We had found that, for cys monolayers, the surface charge densities in basic conditions (37 μC cm^{-2}) were consistently higher than equivalent experimental charge densities obtained when the monolayers were reduced (desorbed) in $KClO_4$ solutions (23 - 33 μC cm^{-2}). The general findings in basic media (Chapters 2 and 4) were consistent with those reported by others [7, 8], and additional processes such as ionization (protonation/deprotonation) were not considered due to the strong basicity of the medium (0.1 M NaOH). It was also found that electrochemically-formed self-assembled monolayers (SAMs) derived from cys in $KClO_4$ yielded a higher packing density than those obtained from the complementary disulfide $(cys)_2$. It should also be noted that these surface coverages are significantly lower than what is generally determined for long-chain alkane thiols. For instance, the surface coverage for cys in basic medium was approximately 3-4 x 10^{-10} mol cm^{-2} as compared to nearly 7-8 x 10^{-10} mol cm^{-2} for mercaptoundecanoic acid (MUA) monolayers in similar conditions. In

perchlorate medium, the coverage is even less dense at 2.5 – 3.0 x 10^{-10} mol cm^{-2}, almost 1/3 the coverage of long chain alkane thiol SAMs.

The surface charges from monolayers desorbed in 0.1 M NaOH were evaluated at 20 mV s^{-1} whereas those desorbed in 0.1 M $KClO_4$ were evaluated at 200 mV s^{-1} or faster. In the $KClO_4$ medium, scan rates of 200 mVs^{-1} and faster, resulted in maximum, constant charge values. Linear scan voltammograms for the desorption of cys monolayers are shown in Figure 3.1.

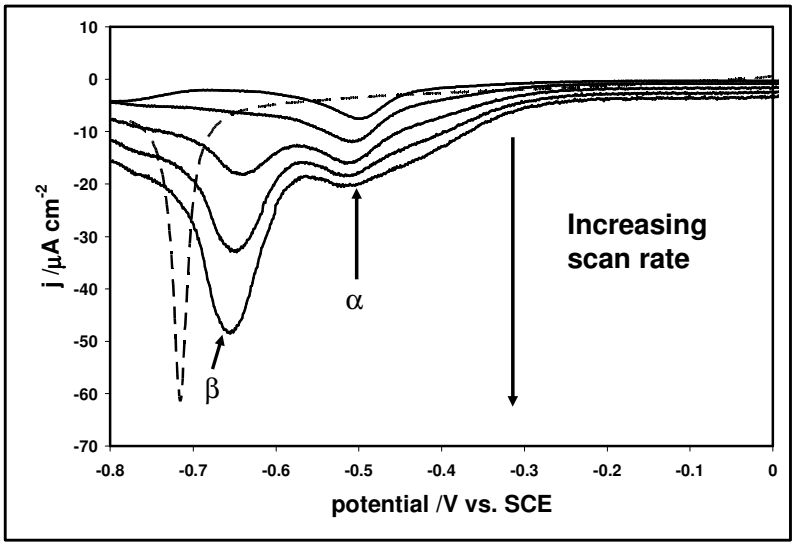

Figure 3.1: Linear Sweep voltammograms for cysteine at various scan rates in 0.1 M $KClO_4$ (solid lines) indicating α, the pre-desorption feature as well as the monolayer desorption peak, β. For contrast, the typical desorption wave obtained in 0.1 M NaOH at 20 mV s^{-1} is also presented (dashed line).

Under basic conditions (0.1 M NaOH), the desorption process was found to proceed according to a simple one electron reduction, and a single sharp desorption peak was observed at all scan rates (dashed line in Figure 3.1). However, the voltammograms from cys in 0.1 M $KClO_4$ electrolyte (solid lines in Figure 3.1) indicated a strong pre-desorption wave which obscured the desorption wave at slower scan rates (< 200 mV s^{-1}).

In Figure 3.1, this pre-desorption wave is indicated as "α" and the desorption peak is labeled "β". Between 50 mV s^{-1} and 75 mV s^{-1}, the wave "β" begins to emerge. In contrast to the desorption process in NaOH (dashed line), the desorption from perchlorate medium (solid lines) clearly indicates two very distinct processes (α and β) of different kinetics, separated by approximately 150 mV. Other researchers have also found that scan rates greater than 200 mV s^{-1} were required to evaluate the desorption charges of short chain alkanethiols in neutral media by voltammetry [9].

Peak "β" occurs when the potential is swept rapidly towards negative potentials, whereby the slower process "α", is given insufficient time to complete. The assumption of a single electron reduction for cys SAMs appears to hold for hydroxide media (where only "β" is present [7, 8]), and for the $KClO_4$ medium at high scan rates. However, recent work has shown that SAMs undergo a complex solvent substitution reaction and not a one electron reduction at the gold surface [10]. This is reflected in the formal charge number per adsorbed molecule evaluated over a wide potential range (for $C_{18}SH$ this value approximates 0.9 at negative potentials, and decreases in value towards more positive potentials [10]). The decrease of the formal charge is noted more in the presence of OH^-, as the adsorption of hydroxide influences the formal charge to a greater extend.

There are a few plausible explanations for the observations of two cathodic peaks in the voltammogram from perchlorate medium shown in Figure 3.1. One possibility is the existence of two adsorbed geometries, as has been noted for cysteamine (MEA, mercaptoethylamine) [11, 12]. MEA is quite similar to cys, but with a hydrogen replacing the carboxylate group. MEA binds as both *trans* and *gauche* conformers at a gold surface due to the amine group. For two differently bound surface species, one

would expect reasonable peak separations for the two species undergoing analogous reactions (in another words: two desorption peaks would be expected).

Another alternative is the protonation/de-protonation (or ionization) of the surface species prior to the desorption. Ionization at metal-solution electrified interfaces has been evaluated theoretically and experimentally, for both carboxylic acid-terminated as well as amino-terminated SAMs [13, 14, 15, 16, 17, 18, 19, 20, 21, 22]. General trends for both the pK_a values of the adsorbed species and the double layer capacitance in relation to the solution pH are well established. In general, for amine-containing species, the surface pK_a of the adsorbate shifts to higher values relative to the solution pK_a [18, 19, 20]. For carboxylic acid-containing species, a similar pK_a shift of about 2 - 3.5 units is observed towards higher values than noted for solution species [18, 19, 20, 21]. In these cases, the pK_a values were evaluated at potentials slightly more negative than the potential of zero charge (pzc). In addition, the surface pK_a values have also been shown to be a function of the applied potential, shifting towards lower values with the application of more positive potentials as demonstrated for MEA [19].

The double layer capacitance is found to be greater for charged species (Au-S-$RCOO^-$ or Au-S-RNH_3^+) than it is for the neutral species (Au-S-RCOOH or Au-S-RNH_2) [15, 18, 20]. This effect is greatly amplified for smaller molecules. Since changes in the ionization of a surface species directly affect the dielectric environment, the state of protonation can also be determined with non-electrochemical techniques such as surface plasmon resonance (SPR) [23, 24]. The most recent study on the surface pK_a values incorporated the comparison of carboxylic and amine terminated alkane thiol SAMs, both structurally long-chain (HS-$(CH_2)_{11}$-R). This work compared the solution pH to the

surface pK_a using SPR and calculated theoretical absolute surface values. The authors clearly demonstrated that the variations of surface pK_a values found in the literature can be ascribed to differences in the measurement techniques [24].

In the particular case of monolayers derived from either cys or $(cys)_2$ solutions, where both carboxylic and amino functionalities are present, the interactions of the adsorbed species are quite different than observed from similar molecules containing just one of these moieties. For instance, STM studies of cysteine adsorbed on Au(111) report the formation of dimerized sub-units within the monolayer lattice [8, 25, 26, 27] supported by hydrogen interactions between adjacent carboxylic and amino groups. Such an interaction would provide an increased stability over similar species containing lone carboxylic or lone amino terminating groups. Thus, it is expected that the deprotonation process from cys-derived monolayers (surface pK_a) would be shifted to more negative potentials.

Here we report new insights into the mechanism of cys and $(cys)_2$ monolayer desorption in 0.1 M $KClO_4$ using electrochemical impedance spectroscopy (EIS). Under neutral conditions, the amino group of cys is protonated, and hence a two step mechanism for desorption, incorporating deprotonation of the monolayer is possible, and explains our previous findings, including the presence of a pre-desorption peak that dominates at low scan rates in CV scans.

3.2 Experimental

A gold (111) single crystal electrode was flame annealed and transferred with a drop of Nanopure water (18 MΩ cm) to a N_2 purged and blanketed three electrode

cell.[28] A Pt wire mesh auxiliary electrode (Alfa Aesar, 52 mesh, 99.9%), separated by a glass frit from the main cell compartment, and a saturated calomel electrode (SCE) as reference (used with a Luggin capillary) were employed. The gold (111) crystal was connected with a stainless steel clip modified with a copper wire. Impedance measurements were recorded employing either a reversible hydrogen electrode (RHE) with a constant H_2 flow rate, or a SCE. All experimental data are referenced against SCE for simplicity.

Admittance and impedance measurements were recorded using an Autolab potentiostat/galvanostat (EcoChemie PGSTAT10) equipped with a frequency response analyzer (FRA) and general purpose electrochemical software (GPES). A rms amplitude of either 5 mV or 10 mV of the AC component was applied, in the frequency range of 0.1 Hz to 1 kHz. Fitting routines were executed using multiple electrochemical impedance spectroscopy parameterization (MEISP) and ZSimpWin software for both circuits considered (Figure 3.2).

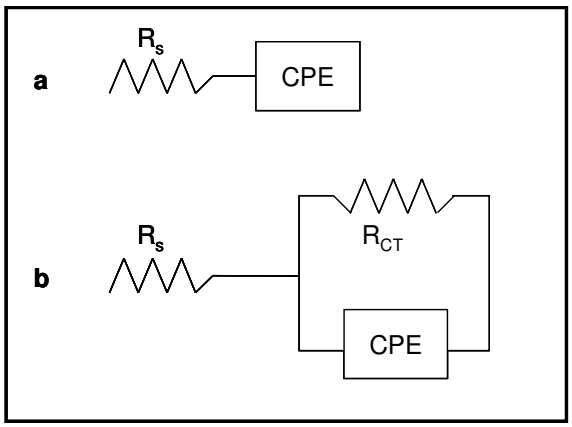

Figure 3.2: Equivalent circuits used to evaluate the cysteine and cystine monolayers on Au(111) in 0.1 M $KClO_4$. a) Constant phase element in series with the solution resistance and b) Constant phase element parallel to a charge transfer resistance.

Aqueous solutions were prepared from recrystallized 99.9 % $KClO_4$ to provide concentrations of 0.1 M. The cell solution volume was 60 mL. Acidification to pH values between 2.5 and 4 was achieved by addition of diluted ultrapure H_2SO_4 (Baseline). This reagent was readily available with confirmed purity level of 99.998%. Experiments were performed by addition of approximately 2 mL of concentrated cysteine (DL cysteine, Sigma) or cystine (L cystine, Fluka) solutions to bring the cell concentration between 100 and 200 μM,, sufficient to ensure full monolayer coverage. Addition of analyte led to a final pH of solution between 5 and 6. Analyte addition was performed at OCP while monitoring either the total capacitance or potential. Prior to each scan, the potential was held at -0.15 V in $KClO_4$ solutions for 200 seconds. The functionalized thiol and disulfide investigated adsorb at this potential and the holding time was sufficient for full coverage. Between experiments, the Au(111) electrode was treated with piranha solution (3 H_2SO_4:1 H_2O_2) and cycled in ultrapure H_2SO_4 (Baseline) to ensure that a clean surface was evident. Additional impedance scans were performed where either analyte was injected at applied potentials negative of the known desorption potentials.

3.3 Results

3.3.1 Addition of the amino-acids at open circuit

Addition of either cys or $(cys)_2$ to 0.1 M $KClO_4$ solutions was performed at the open circuit potential (OCP) and the corresponding changes in potential were monitored by open circuit chrono-potentiometry. When cys solutions were employed, a “sharp” (between 30 to 50 s after the addition) potential shift of -300 mV was observed, indicating rapid adsorption as shown in Figure 3.3. The OCP potential then settled at -70

mV, which is 100 mV more negative than the one for a bare Au(111) surface in 0.1 M $KClO_4$. These findings are congruent with those of Chon and Paik [29], and support the widely accepted idea that thiol adsorption is a simple one electron oxidative process, as shown in Scheme 3.1.

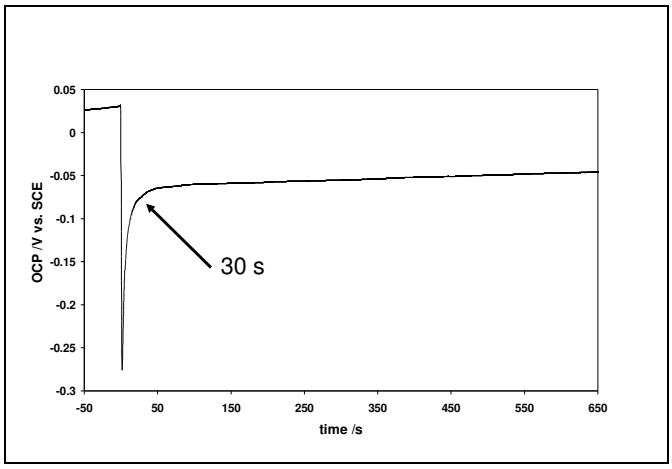

Figure 3.3: The potential shift due to oxidative adsorption of cys. Cys was added at the OCP to 0.1 M $KClO_4$ to bring analyte concentration to 100 µM.

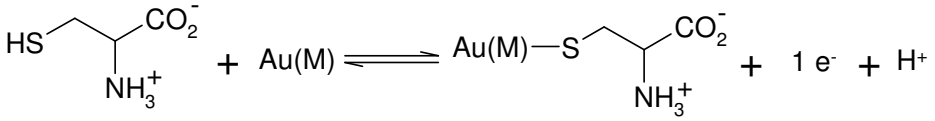

Scheme 3.1

However, addition of $(cys)_2$ to 0.1 M $KClO_4$ solutions resulted in irreproducible profiles, with no recognizable trend in either the direction or the magnitude of the OCP shift. Open circuit chrono-potentiometry curves were also irreproducible for $(cys)_2$ addition experiments to electrolyte solution acidified to pH values of less than 5 with H_2SO_4. Chon and Paik [29] had noted that particularly in neutral solutions, there was only a marginal shift in the OCP upon addition of disulfide species which was attributed

to an adsorption process that involves both oxidative and reductive steps according to Scheme 3.2.

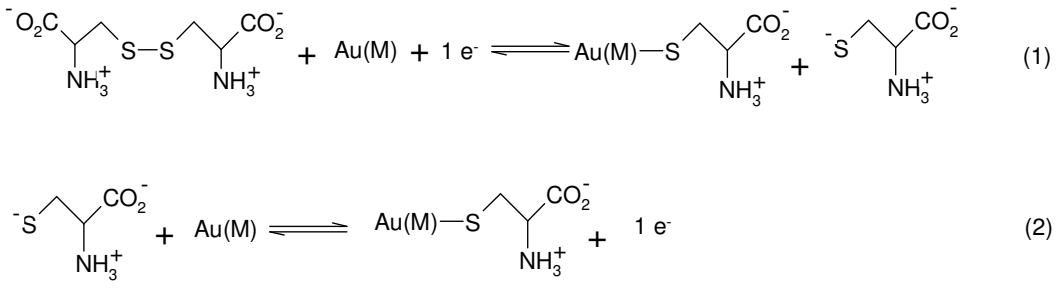

Scheme 3.2

3.3.2 Impedance Measurements

The impedance experiments were restricted to 4 hours or less, as the system became unstable with time resulting in increased kinetic dispersion. Similar complications were noted by Brevnov *et al* [30] when evaluating the electrochemical behaviour of short chain alkane thiols by AC measurements. The impedance scans were performed by holding the working electrode at an initial positive DC potential near or more negative than the OCP, followed by a potential scan to negative values (these will be denoted "negative scans" in the following text). After a preset end potential was reached, the DC scan was reversed back to more positive values up to the initial potential (these will be called "positive scans"). The DC step increments were 5 or 10 mV.

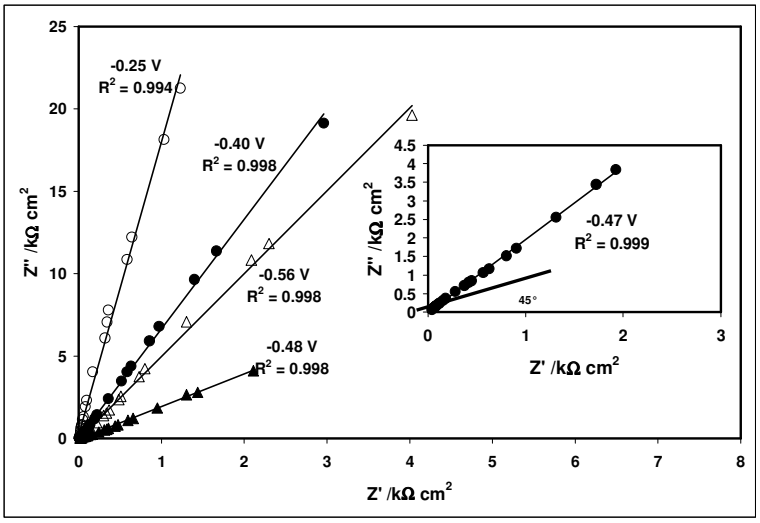

Figure 3.4: Nyquist plot for select potentials during a negative scan. Cys concentration was 100 μM in 0.1 M $KClO_4$. The linear plots indicate strict CPE behaviour. Inset shows that the same linearity is observed during the positive scan.

Figure 3.4 shows the Nyquist plot for cys containing solutions at four separate potentials, prior to the desorption of the monolayer (potential range between -0.15 to -0.60 V). The circuit presented in Figure 3.2a, considering essentially the solution resistance (R_S) in series with a constant phase element (CPE), was used to generate the fits. This type of circuit is commonly accepted for double layer processes at Au(111) electrodes. The double layer in the presence of cys or $(cys)_2$ may be considered as inhomogenous, due to the general low packing density. The fitting of a straight line in the Nyquist plane is excellent at all potentials, consistent with strict CPE behaviour, expected for a distribution of time constants.

Table 3.1 indicates the slope values as well as the relative errors of the slopes at 95% for the data presented in Figure 3.4. Much larger errors were noted in the intercept values. The R_S values, determined both from background scans and from cys containing solutions, were found to average 21 ± 8 Ω cm^2. This is on the order of 27 ± 8.1 Ω cm^2

reported by Janek *et al* [31]. A strong potential dependence of the phase angle prior to the desorption is evident from the changing slopes in Figure 3.4.

Table 3.1: Slope values for selected potentials during the reduction of a cys SAM at Au(111).

E /V vs. SCE	slope	%RSD	R^2
-0.25	17.7	1.8	0.994
-0.40	6.7	0.9	0.998
-0.48	2.0	1.0	0.998
-0.56	5.0	1.0	0.998

Impedance data obtained during the positive scans show that the same linear response is obtained in the same potential region with a minimum near -0.47 V (Nyquist plot shown in the inset of Figure 3.4), and the position of this minimum coincides with the pre-desorption feature observed in the voltammetric measurements (process α in Figure 3.1).

The charge transfer associated with the monolayer desorption (process β), depicted as the reverse reaction of Scheme 3.1 (or the reverse of Scheme 3.2, reaction 2), is clearly demonstrated in Figure 3.5. The desorption, which initiates near -0.60 V, is evident as a depressed semi-circle in the Nyquist plane. Figure 3.5 depicts five separate potentials during the desorption step with the associated fits obtained using the circuit shown in Figure 3.2b. The response of the cys monolayers at -0.15 V, prior to any surface changes, is also shown.

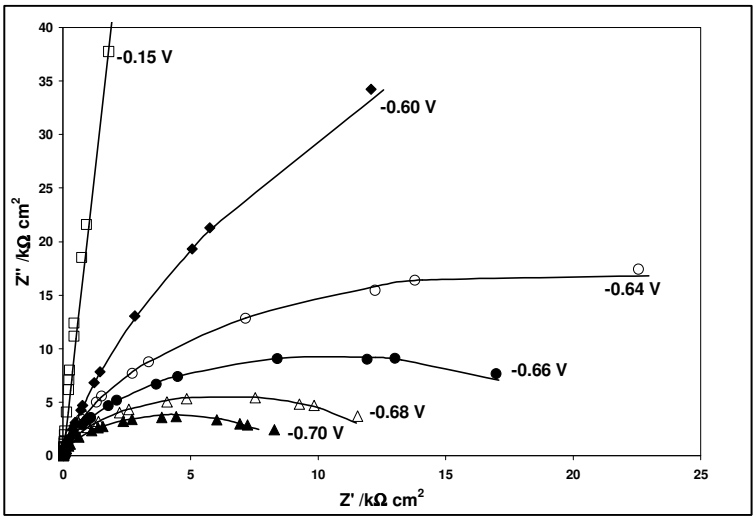

Figure 3.5: Nyquist plot for the charge transfer process β at six different DC potentials during a reduction scan of cysteine in 0.1 M $KClO_4$. Solid lines indicate the fit parameters obtained using circuit 2b (except -0.15 V, circuit 2a).

The goodness of fit for the data from Figure 3.4 and Figure 3.5 was assessed from the χ^2 values. Figure 3.6 shows that circuit 2a (open circles, o) provided relative low χ^2 values in the potential region positive to any surface reaction. The fit errors begin to increase as reaction α initiates. It is of interest to note that the χ^2 values are higher just prior to and past the potential related to the process α, at about -0.47 V. As the desorption potential is approached, the χ^2 values for fittings using the circuit a (Figure 3.2) increase again around -600 mV due to the onset of the monolayer desorption (process β). At this potential (-600 mV), the curvature associated with a charge transfer process warrants the use of circuit b (Figure 3.2).

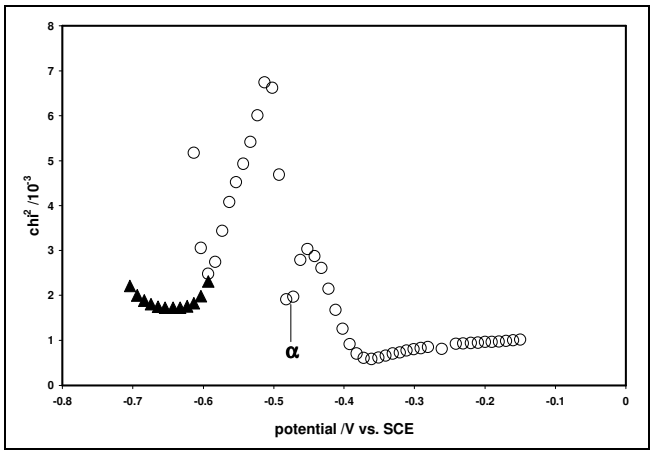

Figure 3.6: χ^2 values obtained by fitting the Nyquist plots during a negative scan. Open circles (o) represent χ^2 values employing circuit 2a, and closed triangles (▲) represent fit parameters when circuit 2b was required.

The monolayer desorption occurs as the potential becomes more negative than -600 mV, leading to an increase in the rate of the charge transfer. This is further highlighted in Figure 3.7, which represents the Tafel plot calculated from the charge-transfer resistance (R_{CT}) obtained from the fitting of the curves from Figure 3.5 using circuit 3-2b. A slope of 33.6 mV/decade is obtained (closed circles, •) which correlates to a transfer coefficient (α) of approximately 0.85 (slope = αF/RT for one electron transfer). An estimated i_o value of 4.4 μA cm^{-2} is obtained using -0.59 V as an approximate value for the initiation of the charge transfer process. The open circles (○) in Figure 3.7 represent the R_{CT} values obtained at potentials more negative than -0.67 V. Since these measurements are made at steady-state conditions, the charge transfer post desorption most likely contains contributions related to the reduction of solution cys.

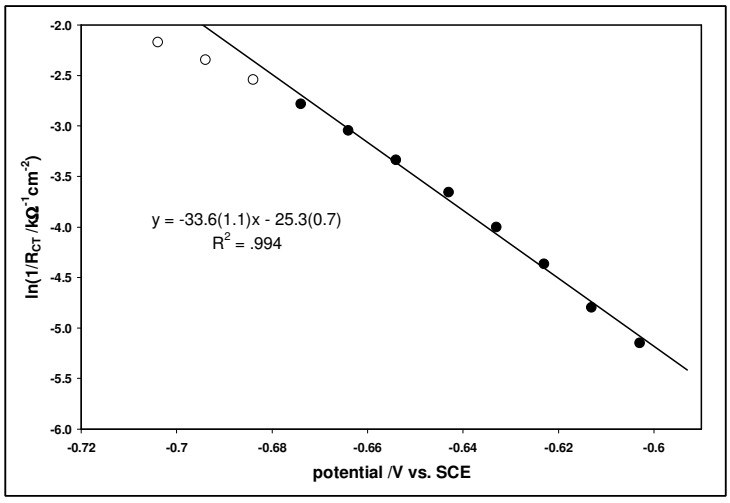

Figure 3.7: Tafel plot for the desorption process, β, obtained from the charge transfer resistance as determined by fitting the Nyquist plots to circuit b (Figure 3.2).

The admittance (Y_C) for a CPE element is given by:

$$Y_C(\omega) = Q(i\omega)^{\alpha_f} \qquad \text{Equation 3.1}$$

Where Q is the CPE parameter and α_f is the CPE exponent.

Table 3.2: Fitting parameters obtained for the desorption process β, for cysteine containing solutions in 0.1 M $KClO_4$.

E /V vs. SCE	Q /μS cm^{-2} s$^{\alpha f}$	α_f	R_{CT} /kΩ cm^2
-0.60	41	0.91	172
-0.61	37	0.91	121
-0.62	35	0.92	79
-0.63	33	0.92	55
-0.64	32	0.92	39
-0.65	32	0.92	28
-0.66	32	0.92	21
-0.67	32	0.92	16
-0.68	33	0.92	13
-0.69	35	0.91	10
-0.70	37	0.91	9

The Q-values for the actual desorption step, β, determined from fitting using circuit b (Figure 3.2) are summarized in Table 3.2. Table 3.2 provides the fit parameters for select potentials during the charge transfer process (β) due to desorption. The CPE exponent (α_f) does not significantly approach 1, hence Q approximates, but does not equal C_{DL}.

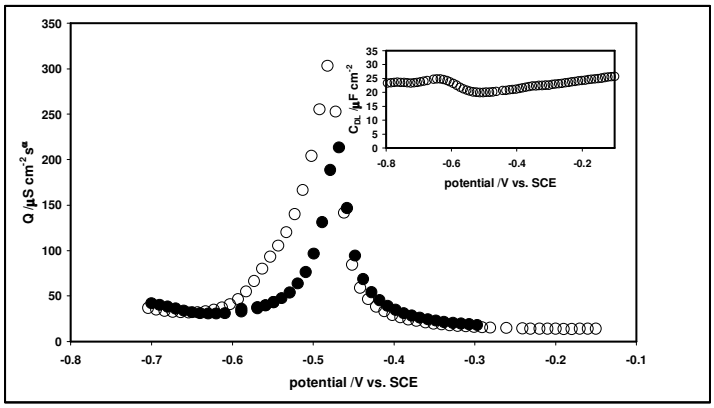

Figure 3.8: Q values vs. DC potential for cys on Au(111) in 0.1 M $KClO_4$. Open circles represent measurements during a reduction cycle for cys monolayers. Closed circles represent analogous measurements during the re-adsorption scan. Inset indicates the double layer capacitance obtained during an AC voltammetry scan at 128 Hz, in the absence of cysteine.

Figure 3.8 demonstrates the value of Q obtained from the fits as a function of applied DC potential. The Q values for potentials more positive than -0.60 V were determined employing circuit a and circuit b was used for the remaining negative potentials (Figure 3.2). This is in accordance to the χ^2 values shown in Figure 3.6. The open circles (o) in Figure 3.8 correspond to a negative scan (initiated at- 0.15 V and terminated at – 0.70 V). The Q values calculated for the impedance curves obtained during the positive scan are shown as closed circles (•). The sharp peaks in Figure 3.8 are due to the process α. In the absence of the monolayer, there are no peaks evident in the double layer region, as can be seen from the inset of Figure 3.8. The inset shows the

double layer capacitance obtained during an AC scan of the clean Au(111) electrode at 200 Hz. The C_{DL} at bare Au(111) is maintained between 20 and 25 μF cm^{-2}.

For values of α_f approximating 1, *Q* may be considered analogous to the double layer capacitance. In our experiments, this only holds true for DC potentials positive of process α and the capacitance values in this range, measured from Figure 3.8, are on the order of 15 μF cm^{-2} (α_f approximates 0.97). This value is close to the values found for $HSCH_2CH_2NH_2$ (20.6 μF cm^{-2}) and $HSCH_2CH_2COOH$ (10.0 μF cm^{-2}) determined in 0.1 M H_2SO_4 [32]. The peak observed in Figure 3.8 is not present when the experiments are realized in 0.1 M NaOH. The large value of *Q* at the peak (during the process α) suggests a large structural change at the interface.

Figure 3.9a and Figure 3.9b show the phase angle and frequency response for cysteine in respect to the applied DC potential for both negative and positive scans. One immediately notes the very well defined peak in the phase plot near -0.47 V, which is evident for both scan directions at all frequencies investigated. The peak minima are assigned to the process α, and are found to occur at a single potential. The position of this peak agrees with the pre-desorption feature previously observed from our CV measurements (Figure 3.1). The process β in Figure 3.9 is related to the desorption of the monolayer, depicted in the reverse reaction of Scheme 3.1. In CV experiments, the process β dominates at high scan rates (≥ 200 mV s^{-1}), which is a consequence of the slow kinetics of process α. However, the impedance scans are measured at steady state conditions, and process α is expected to be fully completed prior to the more negative desorption potential associated with process β. In this case, partial gradual desorption

prior to β should occur, and at peak β there would be an equilibrium between solution cys and adsorbed cys.

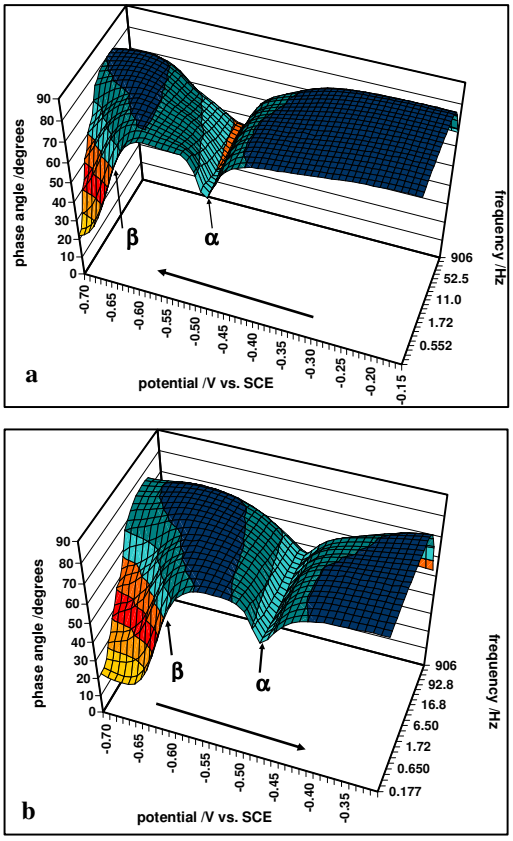

Figure 3.9: The phase angle response as a function of frequency and applied DC potential for cys on Au(111) in 0.1 M $KClO_4$ indicating both processes α and the desorption (β) a) negative scan. b) positive scan.

As observed in Figure 3.9, at potentials positive of the process α the phase angle approximates 90°, consistent with the interphase behaving as a capacitor. Following the process α, the phase angle again approximates a capacitor. At the peak centre, the phase angle reaches a minimum of 0.63 (α^f on the CPE reaches 0.71), suggesting that the process α is intermediate between capacitive and diffusion controlled processes. Due to the apparent slow kinetics, a discrete charge transfer is not evident, even at frequencies as low as 0.1 Hz. The sharpness of the peak is also suggestive of a phase transition,

which may occur due to structural changes in the adsorbed species and extending double layer.

For a reversible surface process involving only adsorbed species, one would expect that the peaks observed in the negative and positive going scans would overlap. This is not completely the case for the peaks assigned to the process α shown in Figure 3.8 and Figure 3.9. The process α is then noted to be quasi-reversible ($\Delta E \approx 5$ - 15 mV). However, in experiments where the $KClO_4$ solution was acidified with H_2SO_4, the peaks came close to reversibility ($\Delta E < 5$ mV). Moreover, the peak α is not observed in basic media in either scan direction. The pH-dependence of the peak is a good indication that process α could be related to a protonation/deprotonation process. The separation of the peak potential, ΔE, is more important to neutral than to acidic media, since it should be related to the rate of diffusion of protons involved in an ionization process. As no buffer system was employed, the absolute pH of solutions could not be rigorously regulated. However, a general peak shift to more positive values as the solution pH is acidified was observed for the process α in both the phase angle and *Q* curves, which is expected from theory and other experimental data involving monolayer ionization [13, 14, 20, 21]. We note that this peak shift is on the order of 40 mV per pH unit for α, much less than the 67 mV per pH unit reported for MUA ionization [21].

Ionization of SAMs, from both a short-chain amino-thiol (MEA) and a long chain carboxylic acid-thiol (MUA), has been shown to occur in the potential region between -0.20 V to -0.40 V vs. SCE at Au(111), prior to the monolayer desorption which occurs at more negative potentials [12, 21]. The peak observed in our studies initiates near -0.40 V vs. SCE, and could be considered associated with the amino group undergoing de-

protonation/deprotonation, similar to a mechanistic scheme proposed by Zhang *et al* 12] for cysteamine (MEA). The mechanism suggested for MEA considered a full electron transfer to generate molecular hydrogen, yet in our studies there does not appear to be a measurable charge transfer associated with this process α. If a charge transfer is occurring, it would be considered as a very slow process, and may be noted at frequencies below 0.1 Hz. Alternatively this process can be considered according to Scheme 3.3, where at slow scan rates both α and β are observed. At faster scan rates, only β would be observed, and the protonated amino state would be desorbed. The more negative protonation/deprotonation potential than observed for MEA is expected, due to the stabilization effect by the formation of dimers in the case of cys. It has frequently been shown by *in situ* imaging that cysteine, regardless of solvent conditions, assembles in dimeric-subunits at single crystal gold electrodes [8, 25, 27].

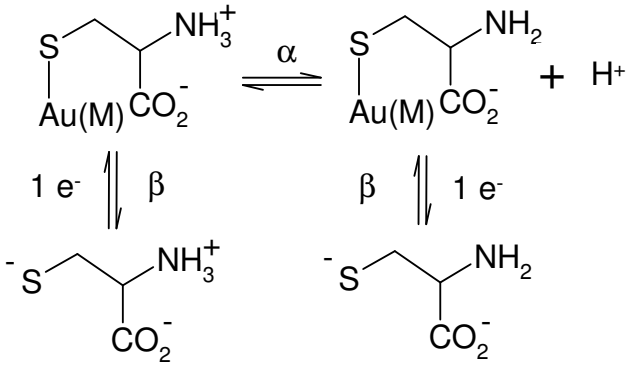

Scheme 3.3

The ionization of surface species in SAMs has been theoretically modeled considering the thermodynamic equilibria (without incorporation of a Stern layer [13]), and including the expansion to a Stern layer [14]. The original treatment proposed by

Smith and White [13] was successful in predicting the pH dependant shift of the ionization (protonation/de-protonation) process, whereas Fawcett *et al* [14] further optimized this model, which resulted in an increased calculated magnitude of the capacitance peak observed at the potential of maximum ionization. More recently, Burgess *et al* [21] approached this ionization process from a strictly kinetic stand point. The model they developed was found to represent their experimental data quite well. All of these studies, however, considered a monolayer comprised of longer chain acid-terminated head-groups, at full coverage (7-8 x 10^{-10} mol cm^{-2}). For short-chain species, such as cys, $(cys)_2$ and MEA, considering that the one electron reduction is not always valid [10], and that solvent substitution reactions become more pronounced due to the low density packing, such systems are bound to be much more complex to evaluate.

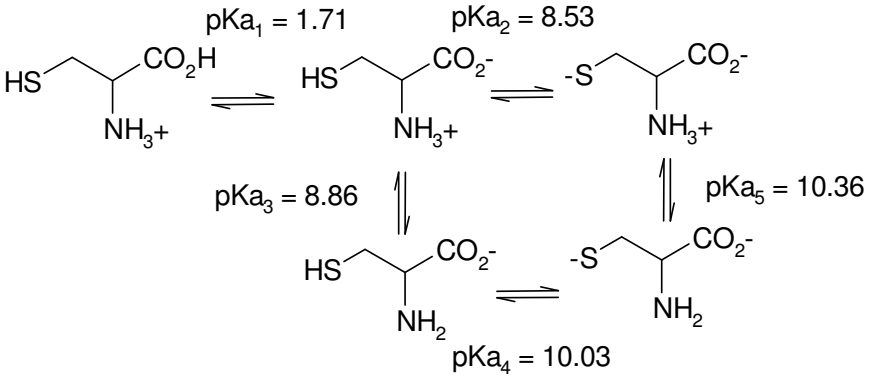

Scheme 3.4

Due to its small molecular size and the close proximity of the thiol and amino functional groups, cys may well exist as a collection of four subspecies in neutral media, which further complicates the equilibria existing at the metal solution interphase. Cys has three basic moieties, including the thiolate, the amino and the carboxylate groups.

Benesh and Benesh [33] calculated the dissociation equilibrium constants for aqueous cys according to Scheme 3.4. Since pK_{a2} and pK_{a3} are almost of the same value, the intermediate species ($^{-}SCH_2CHNH_3^{+}CO_2^{-}$ and $HSCH_2CHNH_2CO_2^{-}$) are indistinguishable.

It is reasonable to suggest, that at an electrified interphase, cys may exist in a number of protonated or partially protonated states. Moreover, a potential-induced reorientation of adsorbed cys has been observed by *in-situ* spectroelectrochemical measurements using a silver electrode [34, 35]. The spectroelectrochemical data indicate that, in the range between -300 and – 600 mV (vs. SCE), cys in 0.1 M KCl adsorbs on silver by the sulphur group with the protonated amino moiety pointing towards the surface. A clear transition is observed at -650 mV and it has been assigned to a potential-induced reorientation, where a rotation in the C - C bond of the cys skeleton would bring the carboxylate group towards the surface and the amino group facing the solution. It is possible that similar re-orientation may also be present for cys at gold surfaces, since such transitions have been noted for MEA [11, 12].

Considering the discussion above, we assign the process α to the protonation/deprotonation of cysteine monolayers. This process may also inherently be coupled with a phase change (due to re-orientation of some or all adsorbed species), since it is likely that the protonated amino group is partially interacting with the gold surface.

At potentials more negative than the surface reaction α the double layer capacitance is almost twice the pre-peak value (30-35 $\mu F\ cm^{-2}$ and α_f approximates 0.92). This suggests that the de-protonation of the monolayer leads to a more weakly adsorbed species, the majority of which will only become completely desorbed at more negative

potentials during the process β. The capacitance due to the blank electrolyte is on the order of 22 ± 3 μF cm^{-2}, consistent with others [31]. In other works employing 0.01 M $HClO_4$, it was inferred from CV data that approximately 40% of the cysteine monolayer may be desorbed in the process α potential region [36]. Based on that report, we had previously attributed this feature to pin-hole desorption in our earlier CV work [6]. Figure 3.9, however, seems to imply that many of the cys species are still adsorbed during the process α, supporting the idea that a deprotonation step is a dominant effect in this potential region. This does not however, exclude that small portions of the monolayer may be desorbing due the deprotonation, which would most likely destabilize the dimer-subunits or monolayer in general. In fact, in very acidic media, it has been shown with STM imaging that at very low cysteine concentrations (3.3 μM), the monolayer desorption occurs beginning at -0.40 V vs. SCE [37]. We note that we found it necessary to employ concentrations on the order of 70 μM or greater to ensure full coverage.

One also notes from Figure 3.8 that during the negative scan (open circles) there appears to be an inherent asymmetry to the observed peak. This could be attributed to partial desorption of the deprotonated species. Another possible explanation is related to a concentration gradient created by proton diffusion. When scans are reversed from the most negative potentials (closed circles in Figure 3.9), the calculated *Q* values demonstrate complete symmetry about the peak centre. This symmetry is found for both scan directions in acidified media.

Similar experiments in $KClO_4$ were conducted for $(cys)_2$, and Figure 3.10 shows the phase angle and frequency response during the DC scans. It is immediately apparent that process α is not well defined when the disulfide was employed for either scan

direction. Further, the capacitive nature of the monolayers derived from $(cys)_2$ was poor relative to cys. One also notes that process β is not well defined. This is due to contributions from the bulk cystine reduction, as discussed in our previous paper [6]. During the scan to positive potentials (Figure 3.10b), reduction of the bulk disulfide leads to huge kinetic distortion and data could not be fitted to appropriate equivalent circuits.

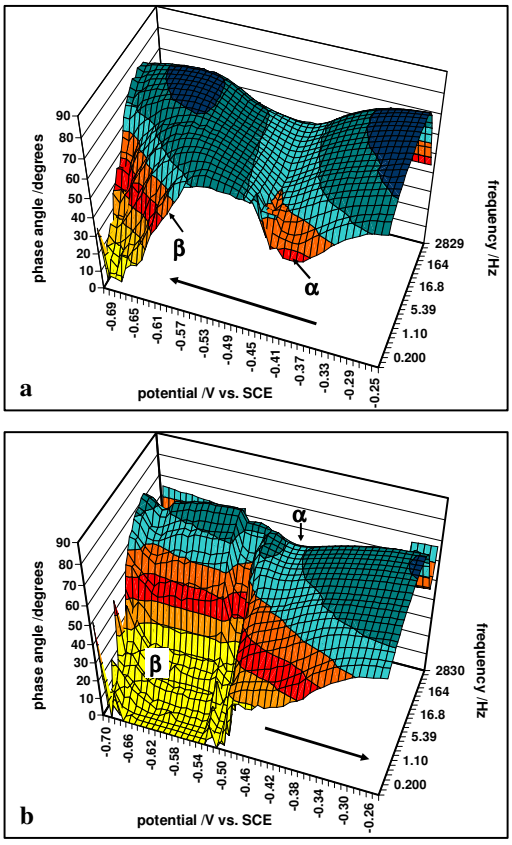

Figure 3.10: The phase angle response as a function of frequency and applied DC potential for $(cys)_2$ in 0.1 M $KClO_4$ indicating both processes α and β. a) negative scan b) positive scan.

3.4 Summary and Conclusion

In 0.1 M $KClO_4$, the adsorption of cys proceeds rapidly at OCP and the resultant monolayers are well formed. Experiments employing $(cys)_2$ yield monolayers which are comparatively less organized. Since ClO_4^- is a weakly adsorbing anion, no kinetic complications are observed. The poor quality of the $(cys)_2$ monolayers may be attributed to differential binding sites, as well as slower arrangement kinetics. The behaviour of adsorbed cys can be modeled using equivalent circuits that employ a CPE. A process α was observed prior to the monolayer desorption (process β), and it was assigned to the deprotonation of the monolayer (amino group) at the surface.

At potentials more positive than the process α the capacitance values approximate 15 $\mu F\ cm^{-2}$ and the system follows apparent strict CPE behaviour. It is most likely that prior to deprotonation, due to the zwitterionic species, a second layer of cysteine molecules (hydrogen bonded) may exist at the more positive potentials. Such a structure has previously been proposed from XPS spectra analysis [38, 39, 40]. The deprotonation of the amino groups of the monolayer may lead to a re-orientation of the 1^{st} adsorbed layer, resulting in a decrease of packing density and subsequently an increase in the capacitance. Due to the apparent large magnitude of the capacitance (actually Q) observed at the peak centre, large structural changes at the interphase must be occurring.

During previous CV experiments, high scan rates were used and insufficient time was provided for the kinetically slow step. Consequently, only thiolate desorption, according to Scheme 3.1 was observed. Further, when the potential was reversed after desorption, little time was permitted at the most negative potentials, and the re-adsorption of the bulk thiol was observed near -0.45 V. During the AC voltammetry measurements,

scans initiated at negative potentials would have led to the adsorption of the thiolate observed near -0.65 V. What is noted during the positive scan is the adsorption and protonation of the amino functionality, possibly coupled with a re-orientation of the monolayer. This process occurs at discrete DC potentials. Protonation would facilitate intermolecular hydrogen bonding between the carboxylic and amino termini, and increase the monolayer stability, as supported by the lower capacitance values. During the gradual reduction imposed by the step-wise applied DC potentials, it is possible that the deprotonation also results in partial desorption of the monolayer.

For experiments where the disulfide was employed, poor monolayer formation is noted. These results contradict findings where disulfides provide equivalent coverage to the thiol species [41, 42]. However, for such studies the typical 24 hour incubation was used, and is recommended when adsorbing cystine. This explains why electrochemically formed monolayers from the disulfide $(cys)_2$ provided lower coverage values than when cysteine was employed. These findings, indicating a protonation/deprotonation and several possible surface species for adsorbed cys, should help explain why numerous lattice structures for cysteine at Au(111) are observed. In 0.1 M $KClO_4$ acidified with $HClO_4$ the standard $(\sqrt{3} \times \sqrt{3})R30^o$ structure common to alkane thiols at applied positive potentials is observed for cysteine [37]. This is also the structure observed when gold electrodes had been immersed in aqueous solutions of cysteine [25].

In 0.1 M $HClO_4$, when conditions are more acidic, a $(4 \times \sqrt{7})$ structure is reported for cysteine, indicating decreased packing of the monolayer [27].

In 0.1 M NaOH, the process α is not observed during impedance measurements, and cyclic voltammetry only indicates one desorption peak. Since protonation/deprotonation should not be evident, these results are expected.

3.5 Bibliography

[1] Di Gleria, K.; Hill, H. A. O.; Lowe, V. J.; Page, D. J. *Journal of Electroanalytical Chemistry* **1986,** *213*, 333.

[2] Maree, S. and Nyokong, T. *Journal of Electroanalytical Chemistry* **2000,** *492*, 120.

[3] Qian, W.; Zhuang, J.-H.; Wang, Y.-J.; Huang, Z.-X. *Journal of Electroanalytical Chemistry* **1998,** *447*, 187.

[4] Tengvall, P.; Lestelius, M.; Liedberg, B.; Lundstroem, I. *Langmuir* **1992,** *8(5)*, 1236.

[5] Yang, N.; Wang, X.; Wan, Q. *Electrochimica Acta* **2006,** *51*, 2050.

[6] Hager, G. and Brolo, A. G. *Journal of Electroanalytical Chemistry* **2003**, *550-551C*, 291.

[7] Zhang, J.; Chi, Q.; Nielsen, J. U.; Friis, E. P.; Andersen, J. E. T.; Ulstrup, J. *Langmuir* **2000**, *16*, 7229.

[8] Arihara, K.; Ariga, T.; Takashima, N.; Arihara, K.; Okajima, T.; Kitamura, F.; Tokuda, K.; Ohsaka, T. *Physical Chemistry and Chemical Physics* **2003**, *5*, 3758.

[9] Munakata, H.; Oyamatsu, D.; Kuwabata, S. *Langmuir* **2004**, *20*, 10123.

[10] Laredo, T.; Leitch, J.; Chen, M.; Burgess, I. J.; Dutcher, J. R.; Lipkowski, J. *Langmuir* **2007**, *23(11)*, 6205.

[11] Michota, A.; Kudelski, A., Bukowska, J. *Surface Science* **2002**. *502-503*, 214.

[12] Zhang, J. D.; Bilic, A.; Reimers, J. R.; Hush, N. S.; Ulstrup, J. *Journal of Physical Chemistry B* **2005**, *109*, 15355.

[13] Smith, C. P. and White, H. S. *Langmuir* **1993**, *9*, 1.

[14] Fawcett, W. R.; Fedurco, M.; Kovacova, Z. *Langmuir* **1994**, *10*, 2403.

[15] Andreu, R. and Fawcett, W. R. *Journal of Physical Chemistry* **1994,** *98(48)*, 12753.

[16] Hu, K. and Bard, A. J. *Langmuir* **1997**, *13*, 5114.

[17] Zhao, J.; Luo, L.; Yang, X.; Wang, E.; Dong, S. *Electroanalysis* **1999**, *11(15)*, 1108.

[18] Kakiuchi, T.; Iida, M.; Imabayashi, S-I.; Niki, K. *Langmuir,* **2000**, *16(12),* 5397.

[19] Nishiyama, K.; Kubo, A.; Ueda, A.; Taniguchi, I. *Chemical Letters* **2002**, 80.

[20] Schweiss, R.; Werner, C.; Knoll, W. *Journal of Electroanalytical Chemistry* **2003**, *540*, 145.

[21] Burgess, I.; Seivewright, B.; Lennox, R. B. *Langmuir* **2006**, *22*, 4420.

[22] Zhang, J.; Demetriou, A.; Welinder, A. C.; Albrecht, T.; Nichols, R.; Ulstrup, J., *Chemical Physics* **2005,** *319(1-3)*, 210.

[23] Chah, S.; Yi, J.; Pettit, C. M.; Roy, D.; Fendler, J. H. *Langmuir* **2002** *18(2)*, 314.

[24] Fears, K. P.; Creager, S. E.; Latour, R. A. *Langmuir* **2008***, 24(3)*, 837.

[25] Dodero, G.; De Michieli, L.; Cavalleri, O.; Rolandi, R.; Oliveri, L.; Dacca, A.; Parodi, R. *Colloids and Surfaces A: Physiochemical and Engineering Aspects* **2000**, *175*, 121.

[26] Kuehnle, A.; Linderoth T. R.; Schunack, M.; Besenbacher, F. *Nature,* **2002**,*415*, 891.

[27] Xu, Q.-M.; Wan, L.-J.; Wang, C.; Bai, C.-L.; Wang, Z.-Y. *Langmuir* **2001**, *17*, 6203.

[28] Hamelin, A. "Double-Layer Properties at *sp* and *sd* Metal Single Crystal Electrodes." in: B.E. Conway, R.E. White and J.O.M. Bockris, Editors, Modern Aspects of Electrochemistry **Volume 16**, Plenum, New York (1985), pp. 1–101.

[29] Chon, S.; Paik, W.-k. *Physical Chemistry and Chemical Physics* **2001**, *3*, 3405.

[30] Brevnov, D. A.; Finklea, H. O.; Van Ryswyk, H. *Journal of Electroanalytical Chemistry* **2001**, *500*, 100.

[31] Janek, R. P.; Fawcett, W. R.; Ulman, A. *Journal of Physical Chemistry B* **1997**, *101*, 8550.

[32] Esplandiu, M. J.; Hagenstroem, H.; Kolb, D. M. *Langmuir* **2001**, *17*, 828.

[33] Benesch, R. E. and Benesch, R. *Journal of the American Cheical. So*ciety **1955**, 5877.

[34] Brolo, A. G.; Patrick, G.; Hager, G. *Journal of Physical Chemistry B* **2002**, *106*, 5982.

[35] Graff, M. and Bukowska, J, *Journal of Physical Chemistry B*, **2005**, *109*, 9567.

[36] Fawcett, W. R.; Fedurco, M.; Kovacova, Z.; Borkowska, Z. *Langmuir* **1994**, *10*, 912.

[37] Dakkouri, A. S.; Kolb, D. M.; Edelstein-Shima, R.; Mandler, D. *Langmuir* **1996**, *12*, 2849.

[38] Cavalleri, O.; Oliveri, L.; Dacca, A.; Parodi, R.; Rolandi, R. *Applied Surface Sciience* **2001**, *175-176*, 357.

[39] Cavalleri, O.; Gonella, G.; Terreni, S.; Vignolo, M.; Floreano, L.; Morgante, A.; Canepa, M.; Rolandi, R. *Physical Chemistry and Chemical Physics* **2004**, *6*, 4042.

[40] Uvdal, K.; Bodoe, P.; Liedberg, B. *Journal of Colloid and Interface Science* **1991**, *149*, 162.

[41] Jung, C.; Dannenberger, O.; Xu, Y.; Buck, M.; Grunze, M. *Langmuir* **1998**, *14*, 1103.

[42] Zhong, C.-J.; Brush, R. C.; Porter, M. D. *Langmuir* **1999**, *15*, 518.

Chapter 4: Impedance Spectroscopy of the Reductive Desorption of Cysteine and Cystine Monolayers in 0.1 M NaOH

4.1 Introduction

The reductive desorption of alkane thiols from Au(111) in alkaline or ethanolic-alkaline solutions has been broadly investigated [1, 2, 3, 4, 5, 6, 7, 8, 9, 10, 11]. In particular, cyclic voltammetry (CV) has been most commonly employed to determine surface monolayer coverage and desorption rates for self-assembled monolayers (SAMs) formed from alkane and functionalized-alkane thiols [1, 2, 5, 6, 7, 8, 9, 10, 11]. Use of CV has also established that the desorption peak potential is a linear function of carbon chain-length for longer chain alkane thiols [2, 5, 9]. That is, the longer the chain-length, the more stable or well-organized the monolayer is; in other words, as the chain-length decreases, less negative potentials are required for the desorption process. For SAMs formed from short-chain thiols, the weaker inter-molecular interactions lead to a low density packing at the surface, and linearity as a function of desorption potential is not apparent [2, 7, 11].

For the relatively small amino acid cysteine ($^{-}SCH_2CHNH_2COO^{-}$ in basic medium), it has been shown that the desorption peak potential is a function of the gold surface crystallographic orientation [8]. Desorption of cysteine (cys) monolayers in basic media is found to occur near -0.70 V vs. SCE at Au(111) [7, 8, 11, 12]. On the other hand, the desorption of cys occurs at -0.99 and -1.0 V vs. Ag/AgCl at Au(100) and Au(110) surfaces, respectively [8]. The typical desorption charge density for a monolayer of cys at Au(111) in basic media is 37 $\mu C\ cm^{-2}$, which is equivalent to a

surface excess (Γ) of 3.8 x 10^{-10} mol cm^{-2} [7, 11, 12]. The surface coverage is obtained when one electron per surface molecule reduced is considered. The coverage is substantially less than what is found for longer chain alkane thiols ($4 \leq n \leq 16$, here n is the number of methylene ($-CH_2-$) units), where the surface charge density for a monolayer is approximately 85 – 100 μC cm^{-2} (Γ~8.8 – 1.0 x 10^{-10} mol cm^{-2}) [1, 3, 5]. It must be stressed that the majority of the literature surface densities are obtained based on:

$$\Gamma = \frac{Q}{nFA} \qquad \text{Equation 4.1}$$

Recent work on the evaluation of octadecanethiol ($C_{18}SH$) by Laredo *et al* [13] demonstrates that the assumption of a simple one electron reduction is not always valid. The cathodic desorption is a substitution reaction at the electrode surface, and the formal charge number (n), is a function of applied potential as well as dependant on the nature of the supporting electrolyte [13]. However, since the majority of published values do not account for the charging currents inherent in Q, and assume the transfer of one electron, the inflation of the values partially cancel out.

One may consider that small chain functionalized thiols, such as MEA (structurally similar to cysteine, but lacking the carboxylic group), bind to the gold surface as both gauche and trans isomers [14, 15, 16]. This type of binding is in total contrast to the upright tilted configuration of tightly packed long chain alkanethiols [17]. In fact, cysteamine ($^-SCH_2CH_2NH_2$) at roughened gold electrodes yields a trans to gauche ratio of 0.8, as determined from SERS [14]. The amino functionality indicates a preference to bind to gold and thus other amino-containing species such as cys, may indicate similar adsorption characteristics [15, 16].

For experiments in basic media, one must consider that OH^- has a higher adsorption strength than electrolytes used in more neutral pH conditions (such as ClO_4^- and $H_2PO_4^-$). The OH^- anions are considered to be adsorbed at the electrode surface to about -0.40 V vs. SCE. At potentials more negative to -0.40 V hydroxide ions are not considered surface-bound [18]. Although strongly adsorbing, the Au - OH^- interaction is weaker than the thiol-gold interaction. Due to the low packing density of cys monolayers, the double-layer region between -0.40 and -0.75 V vs. SCE may have the two species (amino acid and hydroxide ion) co-adsorbed, and the double layer structure should be significantly different than for long-chain thiol SAMs.

Previously, we had focused on the comparative surface coverages of cys and cystine $(cys)_2$ considering zwitterionic species in a neutral medium (0.1 M $KClO_4$) as well as the fully deprotonated species in 0.1 M NaOH [11]. In this paper, we investigated the desorption kinetics of cys and $(cys)_2$-derived monolayers using CV and electrochemical impedance spectroscopy (EIS). Unlike CV, EIS has not been widely used to investigate the desorption of thiol monolayers. Here, further insights into the electrochemical desorption of the amino acids is obtained by modeling the resultant impedance spectra with appropriate equivalent circuits.

4.2 Experimental

A Au(111) single crystal electrode was flame annealed and transferred with a drop of nanopure water to a N_2 purged and blanketed cell, including a Pt wire mesh auxiliary electrode and SCE reference electrode. Impedance measurements were recorded employing either a reversible hydrogen electrode (RHE) or saturated calomel

electrode (SCE). All experimental data are referenced against SCE for simplicity. Prior to data collection the Au(111) electrode was treated with piranha solution (3 H_2SO_4:1 H_2O_2) and cycled in ultrapure H_2SO_4 (Baseline) to ensure that a clean surface was evident.

Admittance and impedance measurements were recorded using an Autolab potentiostat/galvanostat (EcoChemie) equipped with a frequency response analyzer (FRA) and General Purpose Electrochemical Software (GPES). A rms amplitude of either 5 mV or 10 mV of the ac component in the frequency range of 0.1 Hz to 1 kHz was applied. Frequencies were set as a logarithmic function with highest weighting at the low frequency end, where the most notable changes in the spectra were observed. Fitting routines were executed using Multiple Electrochemical Impedance Spectroscopy Parameterization (MEISP) software as well as ZSimpWin, for all circuits considered.

Aqueous solutions were prepared from 99.998 % NaOH (Aldrich) to provide concentrations of 0.1 M. Experiments were performed by addition of concentrated cys (DL-cysteine, Sigma) or $(cys)_2$ (L-cystine, Fluka) solutions to bring the cell concentration between 100 and 200 μM of analyte, sufficient to ensure full monolayer coverage. Analyte addition was performed at OCP while monitoring the potential response. Prior to each scan, the potential was held at -0.35 V in NaOH solutions for 200 seconds, sufficient time for full coverage. After each desorption scan the potential was held at the most negative applied potential and the scan was reversed to terminate at the initial applied potential.

4.3 Results and Discussion

4.3.1 Addition of the amino acids at open circuit potential (OCP)

Addition of either cys or $(cys)_2$ to 0.1 M NaOH solutions at OCP was followed by open circuit chronopotentiometry. Very similar adsorption profiles were obtained from both amino acids, as indicated in Figure 4.1.

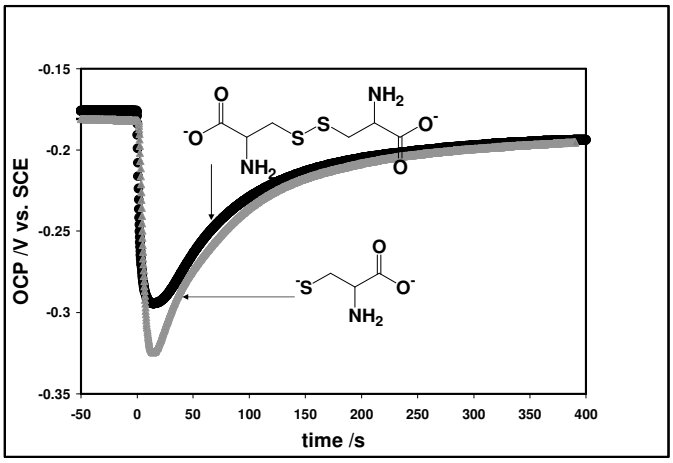

Figure 4.1: Addition of cys and $(cys)_2$ to 0.1 M NaOH solutions at open circuit potential indicating the net negative shift of the measured potential.

The open circuit chronopotentiometry profiles show an initial negative shift of 100 to 150 mV. The potential then stabilized at around -200 mV, which is ~25 mV more negative than the potential before the addition. The profiles of the two species indicate that approximately the same time is required for adsorption. Addition of cys results in a sharper profile than adsorption of $(cys)_2$, as the latter is considered to undergo a combination of reductive and oxidative adsorption [19]. However, this does not preclude that longer times are required for monolayer organization for the disulfide relative to the thiol species. From surface coverage charges, it has been calculated that cys is more densely packed than $(cys)_2$, with intermolecular distances between surface species of 6.9 Å and 9.4 Å, respectively [12]. It is widely accepted that the resulting

monolayers on Au(111) from cys and $(cys)_2$ are structurally equivalent. However, some experiments have shown that the cys-derived monolayer is in fact more stable and equivalent packing qualities are only obtained when a long incubation time, required for extra organization of the adsorbed $(cys)_2$, is employed.

4.3.2 Cyclic Voltammetry (CV) Results

Considering the case of an adsorbed thiol species undergoing a simple one electron reduction (desorption from gold surface), the reaction in basic medium generates a thiolate species:

$$RS - Au(m) + 1e^- \longrightarrow RS^-_{(aq)} + Au_{(m)} \qquad \text{Scheme 4.1}$$

In the case of an irreversible reaction, the peak current density values (j_p) from the CVs should be linear with the scan rate (υ), according to Equation 4.2 [20]:

$$j_p = \frac{\alpha F^2 \upsilon \Gamma^*_O}{2.718RT} \qquad \text{Equation 4.2}$$

Thus, if the surface coverage of the monolayer (Γ^*_o) is known (obtained from the integrated charge density under the voltammetric peak), one may readily determine the transfer coefficient (α) from the slope of the j_p vs. υ plots. These assumptions should hold as long as the region being investigated is at net negative potentials and complications from the hydroxide co-adsorption are not evident. Figure 4.2a shows the cathodic portion of the CV scan for the desorption of cys from a Au(111) electrode. Peak current density in relation to scan rate, υ, for a sample set of $(cys)_2$ CV scans is shown in Figure 4.2b. The current density was found to be linear with the scan rate from 0.01 V s^{-1} to 0.25 V s^{-1} for both cys and $(cys)_2$, Figure 4.2b, but linearity was lost at higher scan

rates. From these measurements, α was determined to be 0.90 ± 0.07 for cys and 0.78 ± 0.12 $(cys)_2$.

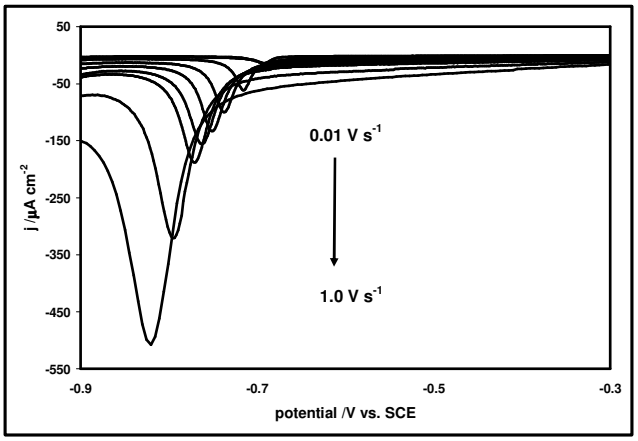

a)

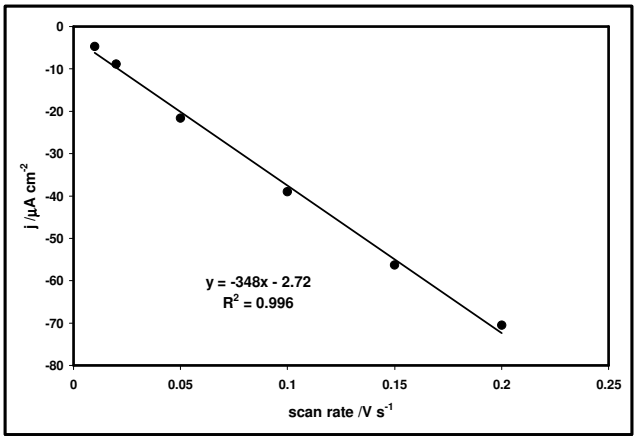

b)

Figure 4.2: a) Cyclic voltammograms for cys at various scan rates. b) Peak current density of the desorption peak as a function of scan rate for $(cys)_2$.

Under the same conditions of an irreversible one electron process, the desorption peak potential (E_p) should be linear as a function of $\ln(1/\upsilon)$, according to Equation 4.3 [20].

$$E_p = E^{o'} + \frac{RT}{\alpha F}\ln\left(\frac{RTk^o}{\alpha F \upsilon}\right) \qquad \text{Equation 4.3}$$

Thus, two methods were available to obtain the transfer coefficient, employing the same data set. Figure 4.3 shows the E_p versus υ plots for both cys and $(cys)_2$. The data points in Figure 4.3 correspond to the average values of E_p from multiple data sets, with the associated error bars, and the lines correspond to the fits to Equation 4.3. For both cys and $(cys)_2$, the correlation coefficients of the linear fits exceeded 0.99 for the desorption peak potential plots in all data sets. Cys and $(cys)_2$ yielded almost identical values for the transfer coefficient, averaging 0.82 ± 0.02 for a total of 20 data sets. These values are consistent with α determined from j_p versus υ plots.

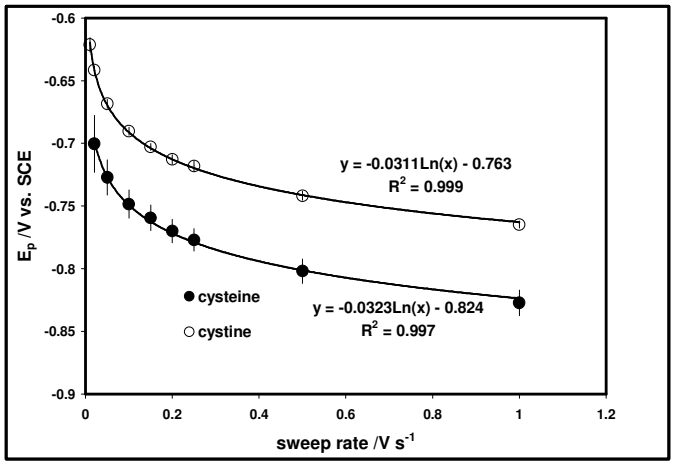

Figure 4.3: Cyclic voltammetry desorption peak potentials as a function of changing sweep rate for cys (•) and $(cys)_2$ (○) in 0.1 M NaOH.

An additional point to note from Figure 4.3 is the fact that the two species appear to have approximately a 100 mV peak separation between their desorption potentials. This potential difference is also evident in the linear sweep voltammograms presented by Matsunaga *et al* [12], but was not noted by Zhang *et al* [7]. This feature strongly

suggests that the cys monolayer is more stable than the $(cys)_2$; hence, a more negative potential for desorption is required.

The rate constant (k_d) may also be determined from Equation 4.3. However, $E^{o'}$ must be obtained from extrapolation of E_p. Since the linearity is lost as υ approaches 0 mV s^{-1}, systematic errors are inherent to the technique. Using this method, a k_d value approximating 0.34 ± 0.03 s^{-1} was obtained for both cys and $(cys)_2$.

As Figure 4.3 illustrates, the data obtained from cys and $(cys)_2$ in 0.1 M NaOH adhere well to Equation 4.3, as supported by the small error in the α and k_d values. It is clear that the assumption for a simple one step irreversible reduction of an adsorbed species is valid in basic media for cys and $(cys)_2$. As there is a consensus in the literature, desorption for the monolayers should yield an aqueous thiolate. Whether the monolayer was derived from thiol or disulfide species in 0.1 M NaOH would seem to be inconsequential, as the average rate constant values of 0.34 s^{-1} are the same within the error of measurement. For the basic system evaluated, k_d is in agreement to the values obtained for long chain alkanes in ethanolic KOH solution. For instance, decanethiol desorption from gold was evaluated with a rate constant of 0.24 s^{-1}, and the higher value of 0.34 s^{-1} obtained for the cysteine thiolate is reasonable considering the smaller size of the analyte [5].

4.3.3 Impedance Analysis

Figure 4.4 shows Nyquist plots for cystine on Au(111) at two separate potentials. At -0.36 V (•), where the double layer capacitance is at a minimum, and at -0.60 V (○) where $(cys)_2$ is desorbing. The plots in the absence of the amino acid are shown in the inset. The solution background data clearly show that little change occurs in the Nyquist

plot when only the hydroxide is present. Curvature of the data at all evaluated DC potentials is observed both in the presence and in the absence of cys or $(cys)_2$.

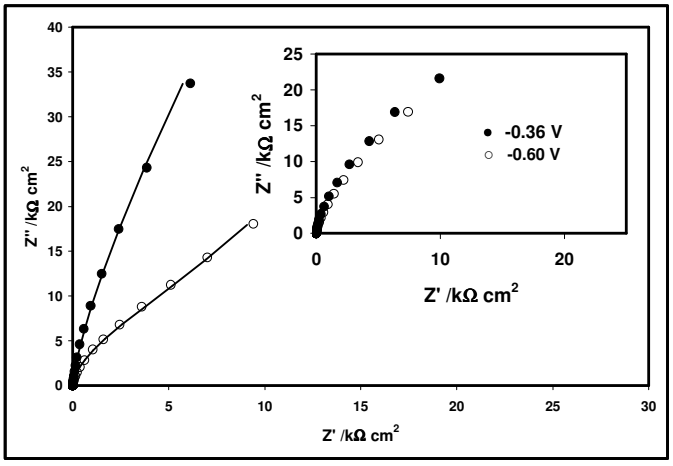

Figure 4.4: Nyquist plot for cystine monolayers in 0.1 M NaOH at -0.36 V (•) and at -0.60 V (○). Inset shows the Nyquist plot for the same potentials when analyte is not present in 0.1 M NaOH.

The Au(111) surface in aqueous solution has been modeled with the incorporation of a constant phase element (CPE) [21]. A CPE was also required in a study of 1,8-octandithiol on Au(111) in KOH solutions [1]. In this work, the data from the Nyquist plots as the one presented in Figure 4.4, were fit using the circuits represented in Figure 4.5.

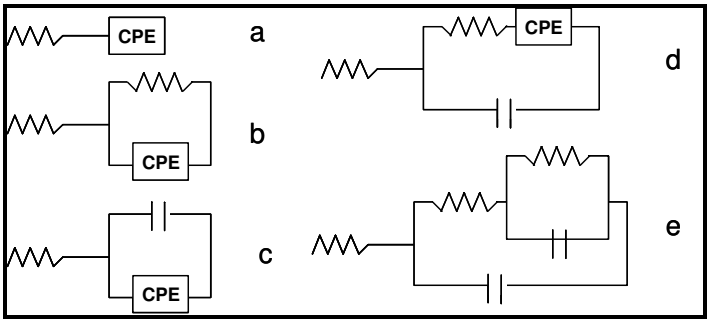

Figure 4.5: Equivalent circuits used for impedance analysis: a) YARC, b) ZARC, c) only the double layer capacitance and adsorption pseudocapacitance in series with the solution resistance, d) same as c, but incorporating the charge transfer associated with reduction of the monolayer and e) regular circuit for adsorption pseudocapacitance.

4.3.3.1 Au(111) in NaOH

Background impedance scans for Au(111) in 0.1 M NaOH were performed over the potential range from -0.35 V to -1.00 V, as well as from -1.00 V to -0.35 V. This potential range is equivalent to those in which voltammetric measurements were made (Figure 4.2). *Q*-values were calculated employing both circuits a and b from Figure 4.5. Circuit 4-5a would represent a non-ideal capacitance in series with the solution resistance, whereas circuit 4-5b would account for any dissipation of charge parallel to the double layer capacitance. Both circuits yielded almost identical values for the interfacial electrical parameters (*Q* and α_f) up to about -0.80 V; however, the Nyquist plot obtained even in the absence of the amino acids presented a slight curvature (see inset in Figure 4.4). To account for the small charge transfer that was evident (due to the curvature) fitting parameters were obtained when the circuit in Figure 4.5b was employed. Figure 4.6 presents the resultant *Q* versus applied potential profiles obtained when scans were initiated from -0.35 V and proceeding towards the more negative potentials (called thereafter "negative scan"). The *Q*-profiles were always featureless and the same *Q*-values were obtained whether circuit a or b (Figure 4.5) was used. The capacitance of the Au(111) electrode in the double layer region of -0.50 V to -0.80 V vs. SCE was found to approximate 30 $\mu S\ cm^{-2}\ s^{\alpha_f}$ in the negative scans. The CPE exponent, α_f, was found to be greater than 0.96; hence, the *Q*-values may be considered as approaching capacitance in that potential region. Hydroxide ions have been shown to be completely desorbed from a Au(111) surface at about -0.40 V vs. SCE [18] using cyclic voltammetry and the corresponding charge density plots. However, no indication of this process was evident in Figure 4.6, and the double layer capacitance indicated minimum

values between -0.50 and -0.80 V. The use of circuit b (Figure 4.5) provided charge transfer resistance (R_{CT}) values, and a surface process was always evident as a broadened peak in the potential profile (inset in Figure 4.6). This feature was found to span the potential range between -0.50 V and -0.80 V vs. SCE, where the double layer capacitance was at a minimum. This would also be the potential region immediately after the reported potential of -0.40 V for hydroxide desorption [18].

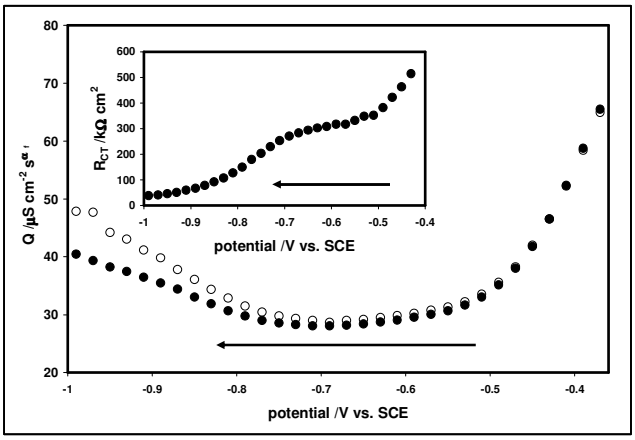

Figure 4.6: Double layer capacitance profiles (indicating measured Q values) in 0.1 M NaOH solutions at Au(111) when impedance scans are initiated from relative positive potentials towards more negative potentials. Data obtained using circuit a (○) and circuit b (•) (Figure 4.5). Inset indicates the charge transfer resistance (R_{CT}) calculated from circuit b.

It is conceivable that partial hydroxide desorption is still occurring in this potential range, and that the difference in the measurement techniques indicates the process. It should also be noted that Chen *et al* [18] employed a potential of -0.75 V vs. SCE for "complete" desorption in subsequent FTIR studies. A slight broad peak in the same potential region was also observed for the plot of the CPE parameter (α_f) versus the applied potential. The α_f values corresponding to the Q values shown in Figure 4.6, were 0.96 in the potential region of -0.35 V to -0.73 V (circuit 4-5a) and the range of -0.35 V

to -0.79 V (circuit 4-5b). At potentials more negative, α_f declined to 0.89 (circuit 4-5a) and 0.93 (circuit 4-5b) at the most negative limit.

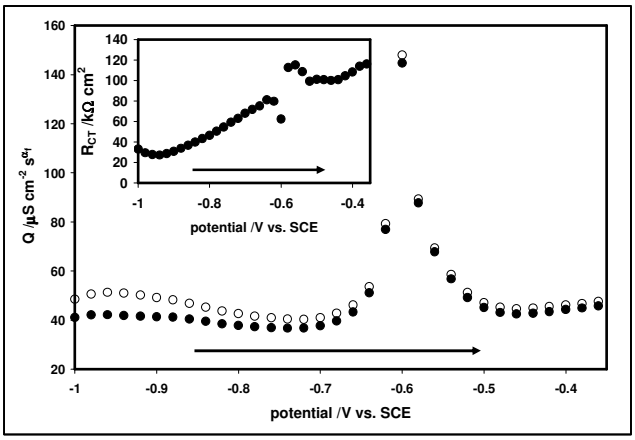

Figure 4.7: Double layer capacitance profiles (indicating measured Q values) in 0.1 M NaOH when scans are initiated from potentials negative to -0.80 V vs. SCE proceeding to positive potentials. Data obtained using circuit a (○) and circuit b (•) (Figure 4.5). Inset indicates the charge transfer resistance (R_{CT}) calculated from circuit 5b.

In contrast, scans initiated at -1.00 V and proceeding to more positive potentials (thereafter named "positive scans") always revealed a peak in the capacitance profile near -0.60 V vs. SCE (Figure 4.7). This peak was evident for both circuits 4-5a and 4-5b. The origin of this peak is most likely related to hydroxide ions, although the adsorbtion process has been reported at -0.60 V vs. NHE, [22] and -0.40 V vs. SCE [18]. We are not aware of any impedance work for Au surfaces in 0.1 M NaOH (or KOH) that present double layer capacitance values for positive-going scans initiated at potentials more negative than -0.80 V vs. SCE. When positive scans were initiated from potentials more positive than -0.80 V, this feature was not apparent and the capacitance profiles were consistent with those reported by others [4, 18, 23]. Rigorous cleaning treatments of the electrode and the electrochemical cell did not eliminate the observation of this feature, which was never apparent in the complementary CV profiles. The Au(111) electrode was

conditioned in 0.1 M H_2SO_4 until the appropriate profile for a clean electrode, indicated by the un-obstructed sulphate adlayer peaks in the CV, was obtained. This procedure was completed between respective impedance data collection. Further, the feature was also noted when KOH was used as an electrolyte..

The analysis of the impedance measurements for experiments initiated at potentials more negative than -0.80 V, indicated minimal charge transfer. The inset of Figure 4.7 shows the typical R_{CT} values obtained from circuit b (Figure 4.5). One may note that a distinct baseline is present, showing a gradual increase of the resistance as the scan proceeds to more positive potentials. Near -0.60 V, where the pronounced peak of the capacitance profile is located, the charge transfer resistance undergoes a small drop, followed by a rapid increase, and return to normal values. Therefore, the peak observed in Figure 4.7 is considered mainly capacitive in nature. Further, this capacitive process occurs at the same potential for all frequencies investigated, as seen in the phase angle diagram for all measured frequencies presented in Figure 4.8a.

Similar phase angle plots for scans initiated from -0.80 V vs. SCE do not indicate this feature at any of the measured frequencies (Figure 4.8b). The nature of the peak observed in the positive scans in hydroxide media cannot be inferred directly from the impedance data. However, we suggest the following explanation: when the positive scans are initiated from -0.80 V vs. SCE, the potential was held at that value promoting the formation of a well-organized structure of hydroxide in the double-layer. On the other hand, when the potential is held more negative than -0.80 V the hydroxide is fully desorbed and the hydroxide re-arrangement in the double layer is revealed upon scanning to positive potentials as a capacitance peak around -0.80 V.

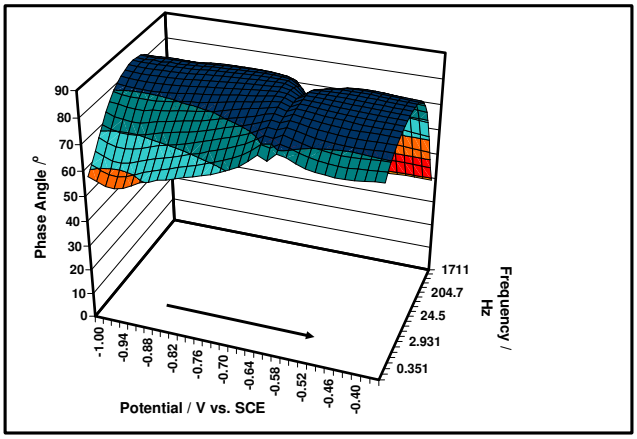

a)

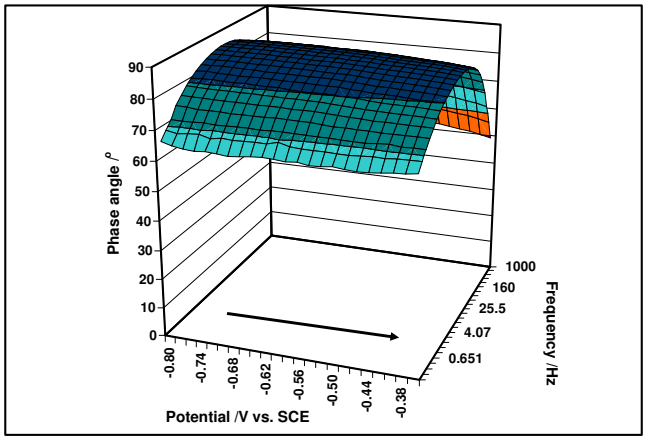

b)

Figure 4.8: a) Phase angle diagram for Au(111) in 0.1 M NaOH when potential scans are initiated from -1.0 V vs. SCE towards more positive potentials. b) Phase angle diagram under same conditions as a), but initiated from -0.80 V.

4.3.3.2 Au(111) in NaOH in the presence of cys or $(cys)_2$

Various factors were considered to generate the impedance parameters obtained by fitting the data from Au(111) in 0.1 M NaOH in the presence of cys and $(cys)_2$. The circuit presented in Figure 4.5b was employed for $(cys)_2$ within the full potential range,

including the desorption region. For this circuit, the errors on the *Q* values were on the order of 3%, and the calculated CPE exponents (α_f) had errors below 1%. This circuit has also been used for monolayers of longer functionalized alkane thiols which have surface defects at negative applied potentials in K_2HPO_4 (desorbing from polycrystalline gold) [24]. The same circuit has also been applied to monitor the desorption of various long chain alkanethiols from gold evaporated films on silicon wafers in phosphate buffered saline solutions [25]. Since $(cys)_2$ under electrochemical conditions yields a very low packing density, one may view the surface as having a large number of defects. In the case of cys the circuits in Figure 4.5c and Figure 4.5d, which represents the double layer capacitance and the adsorption pseudocapacitance, were used in the double-layer region. Although circuit e (Figure 4.5) is the basic representation of adsorption pseudocapacitance [26], the cys data were found to yield much lower errors when circuit d (Figure 4.5) was employed (suggesting a wide range of time constants for the rate of desorption). Presence of the cys species in the bulk solution leads to much better organization, and may also affect the hydroxide contributions in the double layer, as blocking of the electro-active surface is much more effective. Sporadically, the circuit in Figure 4.5b fit some of the cys data sets, and one may conclude that these had not been as well organized (or having defects) as may be expected. The fact the cys data were better fit by the circuits in Figure 4.5c (double layer region) and Figure 4.5d (during desorption), while the circuit in Figure 4.5b was used for $(cys)_2$ in all potential ranges can be rationalized considering the differences in the packing of the monolayers derived from cys and $(cys)_2$. The adsorption equilibrium of OH^- combined with a poorly packed monolayer may introduce the resistance present in Figure 4.5b. It is important to notice

that the circuit in Figure 4.5b fit well the impedance data obtained in the absence of the monolayers. A better packed monolayer would decrease the OH^- interaction, blocking any ion permeation and both the double layer capacitance, and the adsorption capacitance can be realized as in Figure 4.5c. A charge transfer resistance was required during the desorption process for all monolayers (Figure 4.5b or Figure 4.5d).

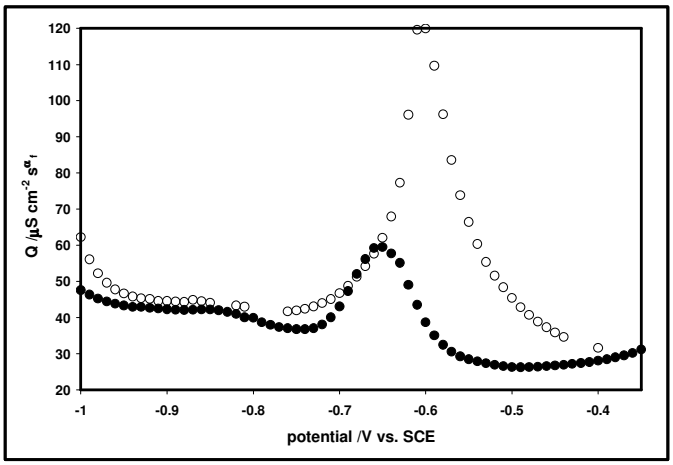

Figure 4.9: Double layer capacitance profile during the reduction (positive to negative potential scan) of a $(cys)_2$ monolayer in 0.1 M NaOH when utilizing circuit 5b (●) and the re-adsorption scan (○) from -1.0 V towards more positive potentials.

A typical capacitance profile obtained for a Au(111) in 0.1 M NaOH in the presence of $(cys)_2$ during the negative scan (●) is shown in Figure 4.9. The profile presents a peak near -0.65 V which corresponds to the desorption of the monolayer. The pseudocapacitance, which was determined as the CPE in all cases, reaches a peak maximum on the order of 100 – 200 µS cm^{-2} s^{α}. The positive scan profile (○) of Figure 4.9, measured in the presence of $(cys)_2$, is virtually indistinguishable from the profile obtained when the analyte is not present (Figure 4.7). It must also be stated that upon completion of the positive scan, following re-adsorption, the pseudocapacitance returned to the original values once the potential became more positive than -0.40 V. This

strongly suggests that any defects on the surface, induced by the desorption process, are insignificant in affecting the double layer region capacitance. The same profile as in Figure 4.9 was also observed from cys-derived monolayers.

The *Q*-values for the Au(111) electrode in the presence of $(cys)_2$ prior to the onset of the desorption peak, shown in Figure 4.9, are slightly lower than what is observed when only the electrolyte is evaluated (Figure 4.6). However, the same *Q*-values in the presence and absence of $(cys)_2$ are obtained after the desorption. The approximated values for the double-layer capacitance at potentials between -0.35 to -0.5 V (where α_f is greater than 0.97) for Au(111) in the presence of the amino acids were determined to lie in the range of 20 – 26 $\mu F\ cm^{-2}$, which is quite large compared to values below 3 $\mu F\ cm^{-2}$ which are typical for long-chain alkane thiols [1, 24, 27, 28]. This again accentuates that the monolayers derived from cys and $(cys)_2$ are quite diffuse when compared to long chain alkane thiols.

The peak in Figure 4.9 occurs within the same potential region as the observed feature from the capacitance curves obtained without the amino acid shown in Figure 4.7. However, even though the desorption/re-adsorption of cys and $(cys)_2$ occurs at the same potential as the feature observed in the hydroxide only scans, the resultant phase diagrams are diagnostically different. For instance, Figure 4.10a and Figure 4.10b show the phase angle versus potential diagrams for a Au(111) in 0.1 M NaOH in the presence of cys (similar diagrams were obtained for $(cys)_2$). Figure 4.10a (which was obtained from a negative scan) shows a clear peak in the phase angle during the desorption at all frequencies. The width of this peak is around 100 mV. A notable feature in Figure 4.10a is the diagonal shift of the peak as a function of the frequency and applied DC potential.

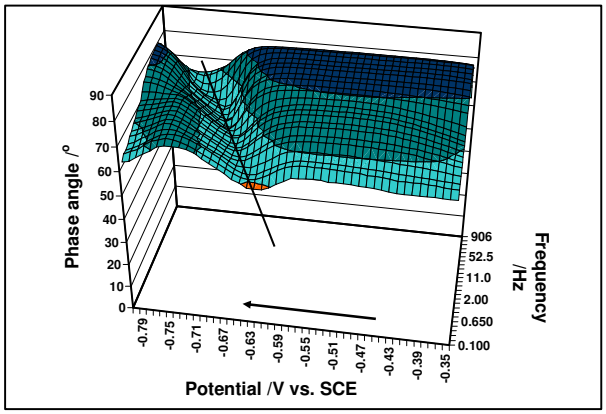

a)

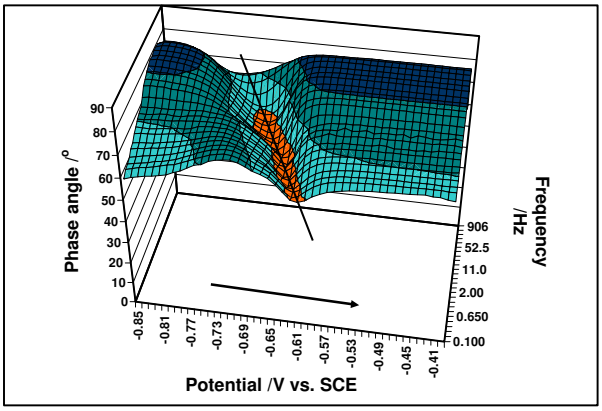

b)

Figure 4.10: a) Phase angle response during the reduction of a cys monolayer in 0.1 M NaOH. b) the phase angle diagram for the re-adsorption of cys onto Au(111) in 0.1 M NaOH.

The shift is expected, since the rate of the desorption process increases with the applied potential. The re-adsorption scans are qualitatively the same, spanning the same potential range and indicating the reverse change in rate, as shown in Figure 4.10b. In contrast, the feature in the phase angle profile shown in Figure 4.8b due only to the electrolyte does not shift with either the applied potential or frequency. Therefore, when the thiol or disulfide are present, the sharp, discrete feature noted in the electrolyte scans

is not evident, but is replaced by the diagonal, frequency dependant profile associated with the adsorption of the amino acid. A stronger interaction with the gold surface is evident for cys and $(cys)_2$, but this adsorption does not appear to be much greater than that of the hydroxide ions based on the capacitance values. The difference in the phase plots however, suggests that the amino acid re-adsorbtion disrupts the hydroxide structure in the double layer.

Sahalov *et al* [25] monitored the desorption of octanedecanethiol, nonanethiol and tetradecanethiol from gold using a similar method in phosphate buffered saline solution and noted that the charge transfer resistance decreased exponentially during the desorption. The inverse slopes were shown to increase as a function of carbon chain length from 206 to 257 mV per decade from $C_9H_{19}SH$ to $C_{18}H_{37}SH$ respectively [25]. Hence, Tafel slopes for cys and $(cys)_2$ derived monolayers are expected to indicate inverse slope values below 200 mV per decade. The results are presented as Tafel plots in Figure 4.11a and Figure 4.11b for cys and $(cys)_2$, respectively.

The slopes from the Tafel plots for both cys and $(cys)_2$ were quite similar and fell between 22 to 39 V^{-1}. In all cases the linearity had a correlation greater than 0.99 for the fit, but reproducibility of the slopes between data sets was poor. This suggests that the rate of cys desorption may be influenced by the presence of hydroxide ions during the steady state measurements. Taking only the inverse slopes of the charge transfer resistance we obtain a range of 59 to 106 mV per decade, consistent with expected lower values for shorter chain thiols [25]. One electrochemical parameter that can be readily gained from the Tafel slope is α, the transfer coefficient (slope = $\alpha F/RT$). Employing the slope values, α was determined to fall between 0.55 and 0.99. These values were

generally lower than obtained from the dynamic measurements, as discussed for Figure 4.2 and Figure 4.3.

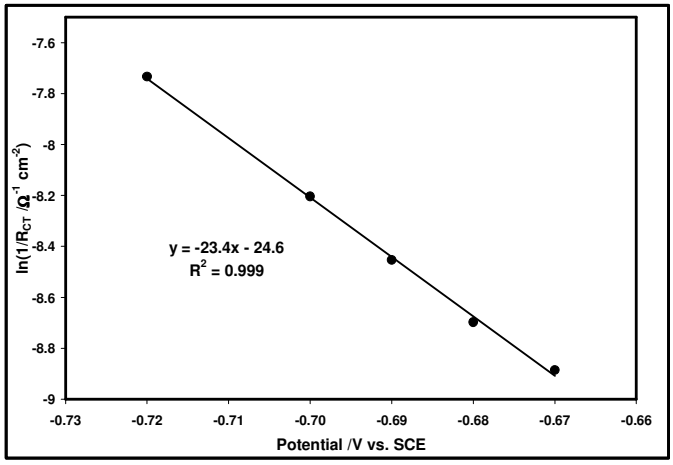

a)

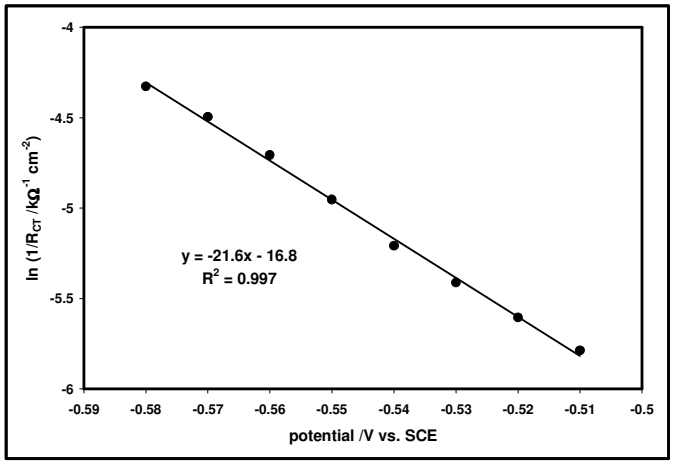

b)

Figure 4.11: a) Tafel slope determined for cys employing the charge transfer resistance from circuit d (Figure 4.5), and b) for $(cys)_2$ using circuit b (Figure 4.5).

When discussing Figure 4.3, we noticed a separation in the peak potentials of desorption from cys and $(cys)_2$ solutions of the order of 100 mV. This peak separation is also evident from the Tafel plots in Figure 4.11. For instance, in Figure 4.11a, the

reductive desorption of the monolayer from Au(111) in cys solutions initiated near -0.67 V and peaks at ca -0.72 V. On the other hand, Figure 4.11b, obtained for the desorption of the monolayer from Au(111) in $(cys)_2$ solution, shows that the processes starts at near -0.51 V and maximizes at -0.58 V. This peak difference between cys and $(cys)_2$ solutions was also very reproducible. This further substantiates that layers formed from $(cys)_2$ solutions under the electrochemical conditions investigated in this work are less stable than the corresponding cys-derived monolayers. There was no correlation found between the potential of the initiation of the desorption process and the Tafel slope values, which could have been expected were the desorption rate a function of the stability of the monolayer. As the inverse slope of the charge transfer resistance [25] and the desorption potential[2, 5, 9] are dependent on chain length, higher inverse Tafel slopes thus correlate with more negative potentials. Since the linearity of these trends is much less evident at shorter chain SAMs [2, 7, 11], we could not correlate the 100 mV change in desorption potential between cys and $(cys)_2$ with the Tafel slope values.

4.4 Conclusion

Based on the CV data, the assumption of a one electron reduction appears to hold in the potential region evaluated. The peak potential data, which has no dependence on the formal charge transferred, yields the same transfer co-efficient values as evaluated from current data.

The monolayers formed from cys or $(cys)_2$ are clearly not as well packed as those derived from long-chain alkane thiols where the capacitance reaches values below 3 μF

cm^{-2}. This is readily implied by the low surface coverage values obtained in hydroxide solutions for cys species by CV [7, 11, 12]. Our impedance results also demonstrate this by providing values for the double layer capacitance between 20 and 26 μF cm^{-2}. Hydroxide is a strongly adsorbing electrolyte and is considered to co-adsorb in the double-layer region. Without the presence of cys or $(cys)_2$ in solution, a sharp, discrete peak is evident in the impedance data initiated from potentials negative of -0.80 V vs. SCE. .

It is clear that the monolayers of the amino acids are not of the same character as those of long-chain alkane thiols, being less effective insulators as demonstrated by the high double layer capacitance. It is found that when $(cys)_2$ was employed, the data were always fit using circuit b given in Figure 4.5. In cases where cys solutions were present, greater variability of the monolayer structure was evident, as numerous circuits were required. The separation of the capacitance into the double layer contribution and adsorption pseudocapacitance indicates the greater intermolecular interactions from cys compared to $(cys)_2$. This is also evident by the peak separations noted from both CV and EIS data, as greater applied negative potentials were required for cys derived monolayers.

4.5 Bibliography

[1] Carot, M. L.; Esplandiu, M. J.; Cometto, F. P.; Patrito, E. M.; Macagno, V. A. *Journal of Electroanalytical Chemistry* **2005**, *579*, 13.

[2] Imabayashi, S.-I.; Iida, M.; Hobara, D.; Feng, Z. Q.; Niki, K.; Kakiuchi, T. *Journal of Electroanalytical Chemistry* **1997**, *428*, 33.

[3] Kawaguchi, T.; Yasuda, H.; Shimazu, K.; Porter, M. D. *Langmuir* **2000**, *16*, 9830.

[4] Madueño, R.; Pineda, T.; Sevilla, J. M.; Blázquez, M. *Langmuir* **2002**, *18*, 3903.

[5] Sumi, T.and Uosaki, K. *Journal of Physical Chemistry B* **2004**, *108*, 6422.

[6] El-Deab, M. S. and Oshaka, T. *Electrochemistry Communications* **2003**, *5*, 214.

[7] Zhang, J.; Chi, Q.; Nielsen, J. U.; Friis, E. P.; Andersen, J. E. T.; Ulstrup, J. *Langmuir* **2000**, *16*, 7229.

[8] Arihara, K.; Ariga, T.; Takashima, N.; Arihara, K.; Okajima, T.; Kitamura, F.; Tokuda, K.; Ohsaka, T. *Physical Chemistry and Chemical Physics* **2003**, *5*, 3758.

[9] Azzaroni, O.; Vela, M. E.; Martin, H.; Hernandez Creus, A.; Andreasen, G.; Salvarezza, R. C. *Langmuir* **2001**, *17*, 6647.

[10] Wano, H. and Uosaki, K. *Langmuir* **2005**, *21*, 4024.

[11] Hager, G. and Brolo, A. G. *Journal of Electroanalytical Chemistry* **2003**, *550-551C*, 291.

[12] Matsunaga, M.; Nakanishi, T.; Asahi, T; Osaka, T. *Chirality* **2007**, *19*, 295.

[13] Laredo, T.; Leitch, J.; Chen, M.; Burgess, I. J.; Dutcher, J. R.; Lipkowski, J. *Langmuir* **2007**, *23(11)*, 6205.

[14] Kudelski, A. *Journal of Raman Spectroscopy* **2003**, *34*, 853.

[15] Zhang, J. D.; Bilic, A.; Reimers, J. R.; Hush, N. S.; Ulstrup, J. *Journal of Physical Chemistry B* **2005**, *109*, 15355.

[16] Michota, A.; Kudelski, A.; Bukowska, J. *Surface Science* **2002**, *502-503*, 214.

[17] Love, J. C.; Estroff, L. A.; Kriebel, J. K.; Nuzzo, R. G.; Whitesides, G. M. *Chemistry Reviews* **2005**, *105*, 1103.

[18] Chen, A. and Lipkowski, J. *Journal of Physical Chemistry B* **1999**, *103*, 682.

[19] Chon, S. and Paik, W.-k. *Physical Chemistry and Chemical Physics* **2001**, *3*, 3405.

[20] Bard, A. J. and Faulkner, L. R. Electrochemical Methods: Fundamentals and Applications; 2nd ed.; John Wiley: New York, 2001.

[21] Sadkowski A, Motheo AJ, Neves RS, *Journal of Electroanalytical Chemistry* **1998**, *455*, 107.

[22] Rogozhnikov, N. A. *Russian Journal of Electrochemistry* **1996**, *32*, 1191.

[23] Štrbac, S.; Hamelin, A.; Adžić, R. R. *Journal of Electroanalytical Chemistry* **1993**, *362*, 47.

[24] Boubour, E. and Lennox, R. B. *Langmuir* **2000**, *16*, 7464.

[25] Sahalov, H.; O'Brian, B.; Stebe, K. J.; Hristova, K.; Searson, P. C. *Langmuir* **2007**, *23*, 9681.

[26] Gileadi, E.; Kirowa-Eisner, E.; Penciner, J. Interfacial Electrochemistry : an Experimental Approach; Addison-Wesley Publishing: Don Mills, Ontario, 1975.

[27] Campuzano, S.; Pedero, M.; Concepcion, M.; Fatas, E.; Pingarron, J. M. *Journal of Electroanalytical Chemistry* **2006**, *586*, 112.

[28] Mendes, R. K.; Freire, R. S.; Fonseca, C. P.; Neves, S.; Kubota, L. T. *Journal of the Brazilian Chemical Society* **2004**, *15*, 849.

Chapter 5: Cyclic and AC Voltammetry of the Reductive Desorption of Mercaptopropionic Acid (MPA) and Cysteamine (MEA) Monolayers from Au(111)

5.1 Introduction

The electrochemical behaviour of thiol-coated gold surfaces is currently a widely explored area in surface science. Much of the research in this area is on long chain alkanethiols. However, a fair number of studies have been based on short chain functionalized alkanethiols, which are commonly used for biological nano-sensor development [1, 2, 3, 4, 5, 6]. These types of self-assembled monolayers (SAMs), are also utilized in the exploration of ternary SAMs and metal deposition [7, 8, 9]. We have previously contributed to this field by reporting the electrochemical behaviour of the amino acids cysteine (cys) and cystine ($(cys)_2$), in both near-neutral and basic media [10]. Both cys and $(cys)_2$ were found to bind to gold through their sulfur group, leaving their terminal carboxyl and amino groups pointing towards the solution. These terminal groups undergo protonation prior to the electrochemical desorption of the monolayer in 0.1 M $KClO_4$, but this process is not observed in 0.1 M NaOH. In order to gain further insights into the understanding of electrochemical surface processes involving small chain thiols, we have evaluated the electrochemical responses of mercaptopropionic acid (MPA, $HSCH_2CH_2CO_2^-$) and cysteamine ($HSCH_2CH_2NH_2$, or mercaptoethylamine, MEA) adsorbed on a Au(111) electrode. The chemical structure of both MPA and MEA is very similar to cys, however, each molecule has just one of the amino-acid functionalities; i.e., MPA is cys without the amino group and MEA is cys without the carboxylate group. By evaluating the single functionalized states under the same

experimental conditions, new insights into the behaviour of the bi-functional species may be attained. Therefore, the comparison of the electrochemical responses of these three species should provide a better understanding of the role of each functionality on their surface chemistry.

The orientation of an adsorbed short-chain functionalized thiol is a function of applied potential, which consequently affects: the pH of the local environment (and thus the protonation state of any functional groups) [11, 12, 13, 14, 15, 16, 17, 18, 19, 20]; the local anion concentration; and the ratio of gauche and trans isomers of the adsorbed species [21, 22, 23]. In addition, different surface packing geometries are noted for small chain functionalized alkanethiols, depending on the nature of the accompanying electrolyte and pH. For instance, MPA displays a 3 x 3 lattice structure on Au(111) when evaluated in 0.05 M $HClO_4$ [24]. A surface structure of $(2\sqrt{3} \times 5)R30^{\circ}$ has been reported in phosphate buffer when the applied potentials is near the open circuit potential [25]. Since such different structures are realized, the maximum surface excess, Γ, has been estimated near 7.6×10^{-10} mol cm^{-2}, which corresponds to a charge density, Q, of approximately 73 $\mu C\ cm^{-2}$ [25, 26, 27]. At this molecular scale, MPA, MEA and cys should yield similar coverage values due to their relative similar sizes and functional groups. Large variations between species could then be attributed to differences in the intermolecular interactions of the CO_2^- and NH_3^+ functional groups.

As in our previous work with cys, we have focused on evaluating MPA and MEA in $KClO_4$ (a weakly adsorbing electrolyte, providing a pH between 5 - 6) and NaOH (a strongly binding electrolyte affording basic conditions). The electrochemical desorption process of MPA and MEA from Au(111) was followed using cyclic voltammetry and

impedance spectroscopy. The results are compared to our findings for cys and $(cys)_2$ under the same experimental conditions.

..

5.2 Experimental

A gold (111) single crystal electrode was flame annealed and transferred with a drop of nanopure water to a N_2 purged and blanketed cell, including a Pt wire mesh auxiliary electrode and SCE reference electrode. All electrochemical measurements were recorded employing either a reversible hydrogen electrode (RHE) or saturated calomel electrode (SCE). All experimental data are referenced against SCE for simplicity. Between experiments, the Au(111) electrode was treated with piranha solution (3 H_2SO_4:1 H_2O_2) and cycled in ultrapure H_2SO_4 (Baseline) to ensure a clean surface.

Admittance and impedance measurements were recorded using an Autolab potentiostat/galvanostat (EcoChemie) equipped with a frequency response analyzer (FRA) and General Purpose Electrochemical Software (GPES). A rms amplitude of either 5 mV or 10 mV of the ac component in the frequency range of 0.1 Hz to 1 kHz was applied. Frequencies were set as a logarithmic function with highest weighting at the low frequency end. Fitting routines were executed using Multiple Electrochemical Impedance Spectroscopy Parameterization (MEISP) software for all circuits considered.

Aqueous solutions were prepared from either double recrystallized $KClO_4$ (99.9%, Aldrich) or 99.998 % NaOH (Aldrich) to provide concentrations of 0.1 M. Experiments were performed by addition of concentrated MPA (>99%, Aldrich) or MEA (>98%, Fluka) solutions to bring the cell concentration to approximately 200 μM of analyte, sufficient to ensure full monolayer coverage. Analyte addition was performed at

OCP while monitoring the potential response. Prior to each scan, the potential was held at -0.35 V in NaOH solutions for 200 seconds, sufficient time for full coverage, for desorption experiments. After each desorption scan the potential was held at the most negative applied potential and the scan was reversed to terminate at the initial applied positive potential. Additional admittance scans were performed where either analyte was injected at negative applied potentials to the known desorption potentials. Measurements of the final solution pH were made at the completion of all experiments, to ensure that the electrochemical cell was not contaminated.

5.3 Experiments in 0.1 M $KClO_4$

For each species (MPA and MEA), cyclic voltammograms were recorded over the range of scan rates from 0.02 V s^{-1} to 1.0 V s^{-1}. Prior to each initial scan, the potential was held at or slightly more negative than the open circuit potential, OCP (0.0 to -0.1 V vs. SCE) for 200 s. This was sufficient time to permit full adsorption of the thiol species. Monitoring the current during injection of analyte indicated that the current began to stabilize 2 - 5 s after the addition of MPA or 20 – 25 s after the addition of MEA. After 150 s, no further notable changes in current occurred for either MPA or MEA. *In-situ* monitoring of the adsorption of MPA in ethanol solution also indicated that adsorption was complete prior to 200 s [28]. It should be noted that the monolayers, although self-assembled, are not necessarily as well packed and organized as those which are induced by incubation over a 24 hour period. Although adsorption under these time frames appears to be complete, monolayer organization may require longer time [29]. However, some of the charge values attained from the electrochemical desorption of SAMs formed

from extended periods of incubation also exceed the theoretical coverages assessed from STM surface structures, which is approximately 70-76 μC cm^{-2}. It is widely suggested that contributions from the charging current inflate the actual surface coverage values obtained from CV experiments, although most reported values are attained without double-layer correction [30].

The desorption of the monolayers of functionalized thiols from Au surfaces can be induced by sweeping the applied potential towards the negative direction. A potential is then reached, where the reduction of the adsorbed thiol group to thiolate results in the desorption from the surface of the gold substrate. This monolayer desorption may be considered an irreversible one-electron process, and the peak current values should be found to be linear with the scan rate according to Equation 5.1 for CV data [31]:

$$i_p = \frac{\alpha F^2 A \upsilon \Gamma_O^*}{2.718RT} \qquad \text{Equation 5.1}$$

The desorption peak potentials, for the same irreversible one-electron process should plot as a linear function of ln υ,

$$E_p = E^{0'} + \frac{RT}{\alpha F}\ln\left(\frac{RT}{\alpha F}\frac{k_d}{\nu}\right) \qquad \text{Equation 5.2}$$

Hence, if the reduction of the monolayer is a simple one-electron process, then Equations 5.1 and 5.2 should hold for both MPA and MEA. However, although the reduction model is widely used, recent work by Laredo *et al* [30] has demonstrated that the reduction is much more complicated (a solvent replacement mechanism), and that the assumption of a one electron transfer per molecule is not always valid.

5.3.1 MPA

In 0.1 M $KClO_4$ the pH is in the range of 5 – 6 pH units, and bulk MPA would have a deprotonated carboxylic group, because pK_{a1} is 4.16 and pK_{a2} is 10.1 [25]. However, measuring the solution pH at the end of each experiment indicated that the final solution pH was in the range of 3.3 to 4 units in the electrochemical cell, which would influence the state of the adsorbed carboxylic group. The surface pK_a for MPA adsorbed on Au surfaces near the OCP has been determined as 5.6 [15], 5.8 [32], 6.0 [33] and 6.62 [18] for different methods and electrolytes. This indicates that the functional carboxylate group on the adsorbed species in 0.1 M $KClO_4$ should be mostly protonated, since addition of MPA shifts the solution pH towards acidic values. At a pH below 5, the hydrogen bonding which has been shown to be quite dominant for MPA monolayers [28], may be less prevalent, and the packing density could be slightly less than full theoretical coverage, since insufficient time for arrangement was permitted.

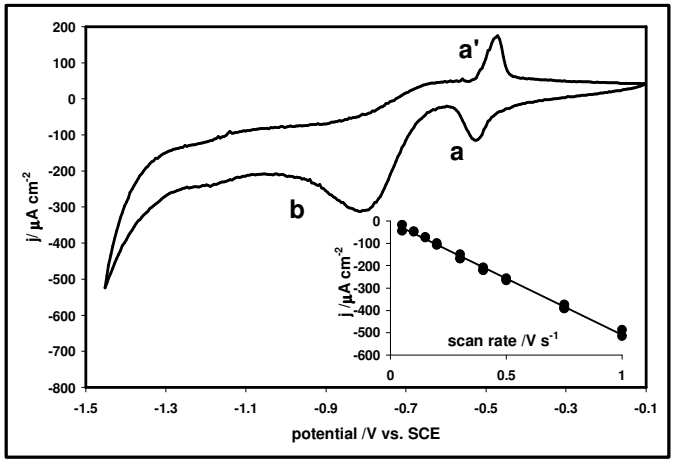

Figure 5.1: Cyclic voltammogram of MPA in 0.1 M $KClO_4$ recorded at 200 mV s^{-1} (after initial potential was held at -0.10 V for 200 seconds) indicating: a) the monolayer desorption, b) electrode passivation reaction and a') the re-adsorption of MPA. The inset indicates the linearity of the peak current density for the desorption peak (a) of MPA in 0.1 M $KClO_4$ as a function of scan rate.

Figure 5.1 is a typical CV, recorded at 200 mV s^{-1}, for a Au(111) electrode in 0.1 M $KClO_4$ and 200 μM MPA solution. A quasi-reversible reaction is identified in Figure 5.1 as peaks *a* and *a*'. Additionally, the electrode surface is passivated after a cathodic process labeled in Figure 5.1 as peak *b*.

Table 5.1: Surface coverage evaluations and/or desorption peak potentials for MPA and MEA under various electrolyte conditions.

SAM	Conditions	Surface	E /V	Q /μC cm^{-2}	Γ /x 10^{-10} mol cm^{-2}
MPA	0.05 M $HClO_4$[27]	Au(111)	-0.015 (RHE)	49.4	5.1
	0.1 M H_2SO_4[9]	Au(111)	-0.35 (SCE)		
	0.1 M H_2SO_4[34]	Au(111)		78	8.1
	0.1 M $KClO_4$	**Au(111)**	**-0.52 (SCE)**	**47 ± 6**	**4.9**
	phosphate buffer[25,a]	Au(111)		67	6.9
	0.1 M NaOH*	**Au(111)**	**-0.71 (SCE)**	**39 ± 4**	**4.1**
	0.1 M NaOH**	**Au(111)**		**49 ± 3**	**5.1**
	0.1 M NaOH[27]	Au(111)		65-76	6.7-7.9
	0.1 M NaOH[24]	Au(111)	-0.789 (Ag/AgCl)	65.8	6.82
	0.1 M KOH[40,b]	Au(poly)	-1.058 (SCE)	67	70
	0.5 M KOH[33]	Au(film)		66	6.8
	0.5 M KOH[33]	Au(film)		78	8.1
	0.5 M KOH[3]	Au(111)	-0.74 (Ag/AgCl)	102	10.6
	0.5 M KOH[43]	Au(poly)	-0.80 (Ag/AgCl)	39	4.0
MEA	0.1 M H_2SO_4[34]	Au(111)		70	7.3
	0.1 M $KClO_4$[c]	**Au(111)**	**-0.70 (SCE)**	**67 ± 5**	**6.9**
	phosphate buffer[29,d]	Au(film)		1	0.1
	phosphate buffer[29,d]			58	6
	phosphate buffer[29,d]			87	9
	0.1 M NaOH	**Au(111)**	**-0.76 (SCE)**	**45 ± 3**	**4.6**
	0.1 M NaOH[44]	Au(111)	-0.705 (SCE)	55	5.7
	0.1 M KOH[40,b]	Au(poly)	-1.159 (SCE)	67	70
	0.5 M KOH[36]	Au(111)		80	8.3

All values obtained from CV data except: a) STM coverage estimation, b) differential pulse voltammetry, c) double-step chrono-coulometry. d) variation in surface coverage for immersion times of 5 min, 1 hr. and 24 hrs. *coverage evaluated at numerous scan rates and **evaluated at 20 mV s^{-1}. Data represented in bold corresponds to current findings.

The redox couple (*a*/*a*') is present at all scan rates evaluated, and both their peak current ratio $i_{pa}/i_{pa'}$ and their charge ratio $Q_a/Q_{a'}$ were generally close to one. The average charge under peaks *a*/*a*' was approximated at 47 ± 6 μC cm^{-2} (Γ of 4.9 x 10^{-10} for a one electron process). The reduction charge is listed in Table 5.1, and compares well to the values determined for MPA reduction in 0.05 M $HClO_4$ of 49 μC cm^{-2} (Γ of 5.1 x 10^{-10} mol cm^{-2}) [24]. The foregoing study had incubated MPA for 10 minutes, and the values we obtained at 200 seconds are the same within experimental error. However, these surface charges are quite lower than the charge of 78 μC cm^{-2} reported by Esplandiu *et al* [34] under acidic conditions, where the electrode had been immersed in MPA solutions for 12 - 16 hours (Table 5.1). This suggests that, when longer incubation times are permitted, incorporation of additional MPA molecules occurs. SERS measurements have also indicated that, under aqueous conditions, MPA on gold reveals a trans to gauche ratio of 1.0 [21]. This implies that the coverage should be much lower than those observed for long chain functionalized SAMs, which typically correspond to surface charges of 85 – 100 μC cm^{-2} (Γ~8.8 – 10 x 10^{-10} mol cm^{-2}).

The current density for both the reduction (peak *a*) and the oxidation (peak *a*') are found to be linear with the scan rate, as expected from Equation 5.1. This linearity for the cathodic peak (*a*) and the scan rate can be observed from the inset of Figure 5.1. The inset in Figure 5.1 represents the data from 22 CVs, obtained while randomly changing the scan rates and repositioning the electrode numerous times. Employing the surface coverage (Γ) of MPA (obtained from the charge under the peaks *a* and *a*'), the transfer coefficients (α) were found to be 0.81 ± 0.04 and 0.68 ± 0.03 for desorption and adsorption, respectively. The desorption potentials of peak *a* also followed Equation 5.2,

providing an α value of 0.94 ± 0.09, which is close to the value determined using Equation 5.1. The peak separation (ΔEp) was generally linear with scan rate, with an intercept at 0 V s^{-1} between 30 and 40 mV. The α values determined for the monolayer reduction approximate the values determined for cys and $(cys)_2$ in 0.1 M NaOH (Chapter 4), and the model for a one electron reaction appears to hold.

The charge under peak *b* is much larger than expected from a monolayer desorption, and this peak should be assigned to the decomposition of bulk MPA. At a very slow scan rate (10 mV s^{-1}), the negative scan (from positive to negative potentials) indicates almost continual reduction. Interestingly, the hydrogen evolution seems to be blocked by the bulk MPA reduction. Since, the solution pH was typically below 4, a strong hydrogen wave was expected much earlier than the negative limit (-1.4 V) of Figure 5.1. As most desorption studies are performed in the absence of bulk MPA, this passive effect has not been noted before.

The Nyquist plot of a Au(111) electrode in 0.1 M $KClO_4$ in the presence of MPA is presented in Figure 5.2, at several DC potentials. In the region of adsorbed MPA (•, -0.13 V), a slight arc is evident, and data fit equally well employing either a YARC or ZARC circuit (the curvature was only evident at the first 2-3 positive DC potentials, hence the YARC was utilized over the entire potential range). Schweiss *et al* [18] also employed a YARC when evaluating the double layer capacitance of MPA in 0.3 mM KCl. The average double layer capacitance in the potential region of -0.10 to -0.20 V was determined at 15 ± 2 μF cm^{-2} (α_f on the CPE >0.96). Errors in this potential region were on the order of 3% for *Q* and α_f. Compared to the literature values listed in Table 5.2, the capacitance determined in this work is slightly higher than the expected

capacitance for a protonated layer. However, in accordance with the acidic pH measured after the reduction experiments, and the lower surface coverages, this value is quite reasonable.

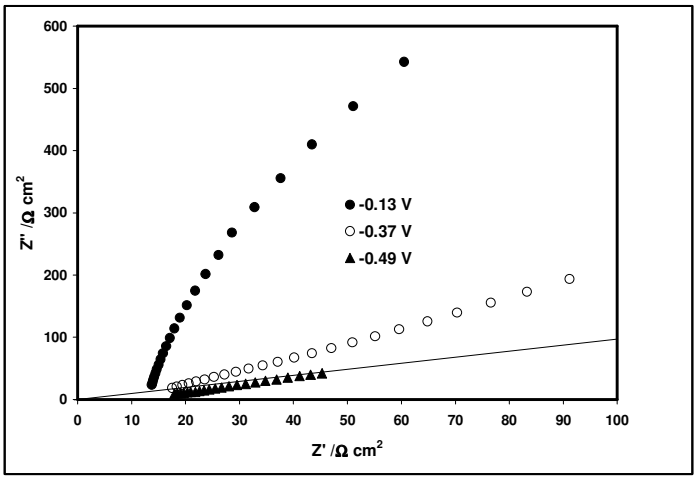

Figure 5.2: Nyquist plot for MPA in 0.1 M $KClO_4$ at various applied DC potentials: (•) at -0.13 V where the double layer capacitance is at a minimum, (○) at -0.37 V where the onset of reduction is occurring, and (▲) at -0.49 V which corresponds to the maximum of peak a.

Table 5.2: Surface pK_a and double layer capacitance values for MPA and MEA monolayers at gold.

SAM	Conditions	Surface	pKa	E /V	C_{DL} /μF cm^{-2}	
					charged	uncharged
MPA	**0.1 M $KClO_4$**	**Au(111)**		**-0.10 - -0.20 (SCE)**		**15 ± 2**
	0.1 M NaOH	**Au(111)**		**-0.40 - -0.48 (SCE)**	**14.5 ± 0.5**	
	$NaClO_4$ + $HClO_4$ or NaOH[16]	Au(111)	8	0.0 (Ag/AgCl)	15	8-10
	0.1 M ionic[33]	Au(film)	5.2/6	-0.21 (MSE)		
	0.1 M NaCl + HCl or NaOH[32]	Au(film)	5.8			
	0.1 M H_2SO_4[34]	Au(111)				10.0
	contact angle titration[15]	Au(poly)	5.6			
	KCl + HCl or NaOH[18]	Au(film)	6.62	0.0 (Ag/AgCl)	10	7.5
MEA	**0.1 M $KClO_4$**	**Au(111)**		**-0.10 - -0.34 (SCE)**		**15.5 ± 1.0**
	0.1 M NaOH	**Au(111)**		**-0.39 - -0.49 (SCE)**		**23.0 ± 0.1**
	$NaClO_4$ + $HClO_4$ or NaOH[16]	Au(111)	5.3	0.0 (Ag/AgCl)	20	15
	0.1 M H_2SO_4[34]	Au(111)			20.6	
	0.1 M PBS + $NaClO_4$[35]	Au(poly)	7.6			

Data represented in bold corresponds to currents findings.

As the scan progressed to more negative potentials, it is seen in Figure 5.2 that the response in the Nyquist plane became more linear: (○,-0.37) in the region of desorption initiation, and (▲,-0.49) at the maximum of peak *a*. Figure 5.3 indicates the Q-values vs. potential obtained by fitting Nyquist plots obtained during a negative scan. The CPE parameter (α_f) at the peak maxima approximated 0.50 ± 0.05, which suggests that mass transport is occurring at this potential, a result of the surface being available to solution species.

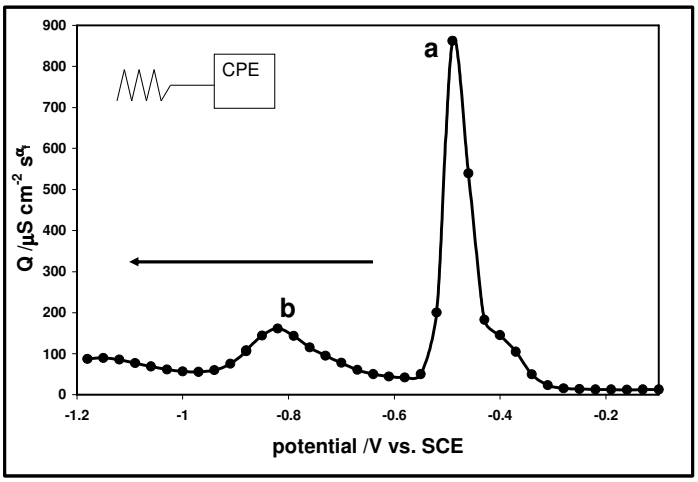

Figure 5.3: The approximation of the double layer capacitance in terms of *Q* for MPA desorption in 0.1 M $KClO_4$. Values obtained using YARC circuit.

5.3.2 MEA

Under near neutral conditions the amino group of bulk MEA should be mostly protonated (pK_{a1} = 8.35, pK_{a2} = 10.81). Surface pK_a values for the amino group of MEA have been reported as 5.3 [16] and 7.6 [35]. The surface pK_a for MEA in 0.25 M $NaClO_4$ has also indicated a dependence on the applied potential with values of: 5.0 at 0 V, 4.1 at 0.1 V and 3.4 at 0.2 V vs. Ag/AgCl [17]. Since our measured pH was between 7.6 and 8 pH units, this suggests that at our initial potentials near OCP (circa 0.0 to 0.1 V), the

amino group should not be protonated. It has also been shown from spectroscopic analysis that both trans and gauche isomers are present at gold in an aqueous environment at a ratio of 0.8 (trans to gauche) [21]. As with MPA, surface coverage is expected to be lower for MEA than what is typical for long-chain thiol species.

Figure 5.4 shows the CV of a Au(111) electrode in the presence of MEA in 0.1 M $KClO_4$ at 0.5 V s^{-1}. Two cathodic waves, labeled *a* and *b* in Figure 5.4, were observed and only one broad anodic peak, *b*', is evident. The two cathodic peaks have been previously observed in experiments realized in other media [36]. The peaks have been assigned to the desorption of the trans and gauche forms of the adsorbed amine. This assignment has been confirmed by spectroscopic data [21, 22, 23]. Peak *b*' should be related to the adsorption of the thiol group from bulk MEA, since both trans and gauche species anchor via the S-Au bond.

Over a wide range of scan rates evaluated, the cathodic peaks could not be resolved in the presence of large charging currents, and surface coverage for MEA could not be determined from CV.

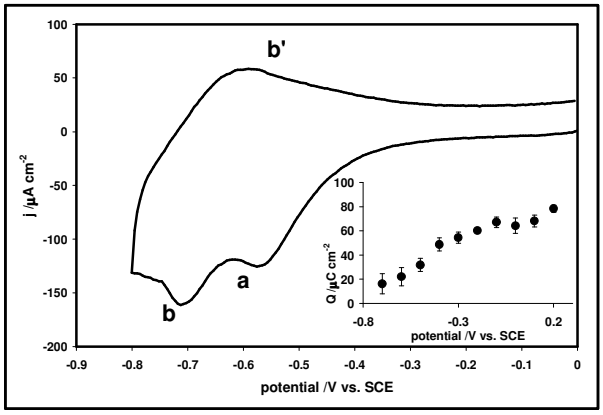

Figure 5.4: CV for MEA in 0.1 M $KClO_4$ at 0.5 V s^{-1} indicating: the cathodic desorption peaks (a and b), and the broad re-adsorption peak b'. The inset shows the charge density for the MEA monolayer with associated error bars obtained from double-step chrono-coulometry.

However, use of double step chrono-coulometry provided surface coverage charges in agreement with values determined in phosphate buffer as listed in Table 5.1 [29]. Stepping the potential from values more negative than the desorption peak (-0.8 V vs. SCE), to more positive potentials and back to the initial potential, resulted in surface charges with steady values in the potential range of -0.1 V to 0.1 V (near the OCP). This is seen in the inset of Figure 5.4, and an average surface charge of 67 ± 5 μC cm^{-2} (Γ of 6.9 x 10^{-10} mol cm^{-2}) was obtained. This coverage compares well to the 70 μC cm^{-2} (Γ of 7.3 x 10^{-10} mol cm^{-2}) reported by Esplandiu *et al* [34]. Stepping to potentials greater than 0.1 V, indicated that the charge was increasing, likely due to the onset of an oxidation current, as this potential region was more positive than the pzc. Larger fluctuations in the formal charge transferred (*n*) to a SAM at applied positive potentials has been demonstrated [30].

Since the terminal amine may be considered to be deprotonated in the range of our potential scans, any mechanism associated with the acid/base group should not be evident. Hence, under steady-state AC perturbations the desorption of the two species (trans and gauche) only should be observed.

Figure 5.5 shows the Nyquist plots for MEA in 0.1 M $KClO_4$ at selected potentials: in the double layer region (• -0.20 V), during peak *a* reduction (○ -0.58 V), and during peak *b* reduction (Δ -0.66 V). The angle of 45º is shown to highlight that the response is not diffusion limited, but appears to be more capacitive in nature. It is evident in Figure 5.5 that the response of peak *a* and peak *b* are virtually the same. This suggests that in 0.1 M $KClO_4$ the trans and gauche species desorb in the same manner.

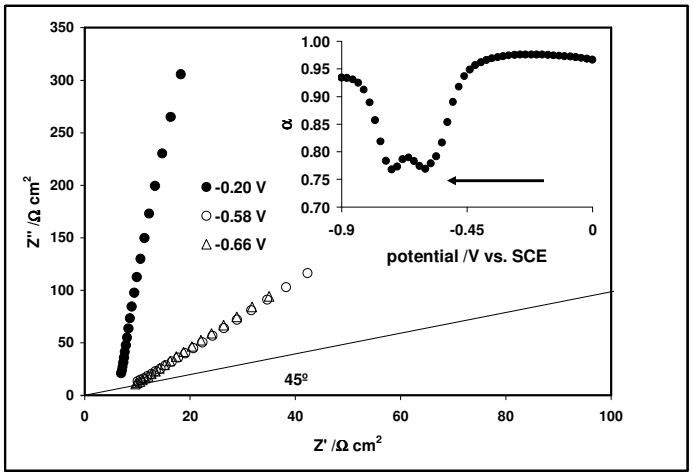

Figure 5.5: The Nyquist plot for MEA in 0.1 M $KClO_4$ at selected potentials: (• -0.20 V) in the double layer region, (○ -0.58 V) during peak a reduction, and (Δ -0.66 V) during peak b reduction. The inset indicates the CPE parameter variation as a function of potential during a negative scan.

The data were fitted using a simple YARC circuit, and the inset of Figure 5.5 shows the CPE parameter during a negative scan. Use of the Randles equivalent circuit for the redox activity of parabenzoquinone at MEA modified electrodes was found to also model well when a CPE was incorporated instead of a capacitor [6]. In the potential region of -0.10 to -0.34 V, the double layer capacitance was at a minimum, and resulted in a value of 15.5 ± 1.0 μF cm^{-2} (α_f on the CPE > 0.96), in accordance with the value obtained by Kakiuchi *et al* [16].

The *Q*-values of the CPE were evaluated from the Nyquist data and are plotted against the potential in Figure 5.6. The desorption of both conformers is shown by the two peaks in Figure 5.6. The desorption occurs over a fairly broad range (~300 mV). The broad range is due to the gradual desorption of the two species. The capacitance measured at the maxima of the two peaks are found to be almost the same. At the peak

potentials, α_f approximates 0.75 ± 0.05, and the desorption process is mostly capacitive in nature.

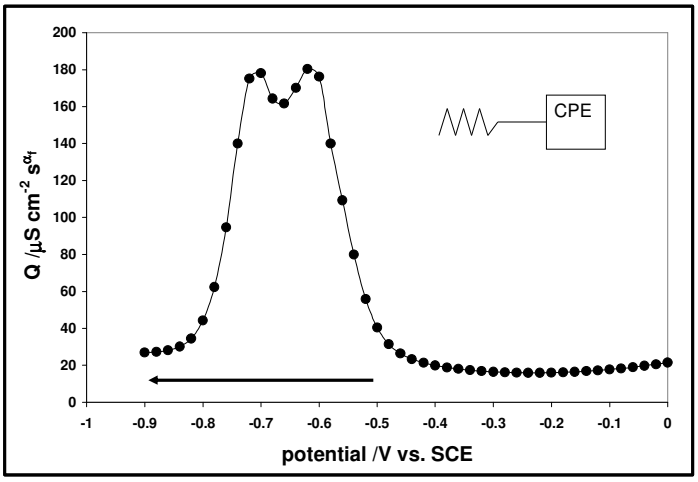

Figure 5.6: The approximation of the double layer capacitance for MEA as a function of potential in 0.1 M $KClO_4$. *Q* values were obtained using YARC circuit.

5.3.3 Summary for 0.1 M $KClO_4$

The desorption of MPA occurs at more positive potentials than the desorption noted for MEA. This is partially due to the pH shift of the bulk solution to more acidic values (3.3 – 4) during MPA addition, and more basic values (pH 7.6 to 8) with MEA addition. Table 5.1 clearly indicates that the desorption potential is a function of solution pH for MPA, and that this effect is less prominent for MEA. Imbayashi *et al* [26] had also noted the sensitivity of the desorption potential of MPA to the solution pH, and attributed this shift to electrostatic repulsion. Cysteine, having both functional groups, desorbs in 0.1 M $KClO_4$ between -0.63 V and -0.68 V. The order for the desorption potential is thus MPA<cys<MEA, a result of contribution of the surface interactions of the amine group, which binds well to gold.

The surface coverage of MPA was significantly lower than the coverage determined for MEA by approximately 30%, yet both species indicated a higher surface coverage than 29 – 33 μC cm^{-2}, which we previously reported for cys [10]. Cys is expected to show a lower coverage, as the molecule itself is larger than either MPA or MEA. The decrease of the monolayer coverage for MPA relative to MEA, cannot be explained at this point, since the reported trans to gauche ratio is higher for MPA than MEA. This would suggest that the coverage for MEA should be lower. However, one may consider that MPA requires longer times for monolayer organization than MEA.

The double layer capacitance in either case was approximately 15 μF cm^{-2}, which is notably higher than values less than 3 μF cm^{-2} that are typical for a well formed SAM from long-chain alkane thiols [37, 38]. However, these values are on the order of reported values for MPA and MEA, and coincide with the value of 15 μF cm^{-2} we had obtained for cys monolayers [Chapter 3]. The value for MEA is in accordance to reported values for an uncharged monolayer, and the value for MPA is higher than expected. Since an increase in the capacitance is a result of a less insulating SAM, this further supports that MPA organization requires longer time frames than the organization of the amine terminated species.

5.4 Experiments in 0.1 M NaOH

Cyclic voltammograms were recorded for scan rates from 0.02 V s^{-1} to 1.0 V s^{-1}. Prior to each initial scan, the potential was held at or slightly more negative than the OCP for 200 s. This was sufficient time to permit full coverage, as monitoring the current at OCP during injection of analyte indicated that adsorption of MPA and MEA occurred during the initial 5 - 10 s. As with the monolayers evaluated in perchlorate, the measured

current response stabilized prior to 200 s, however, the SAMs may not be as well organized as those evaluated when longer incubation times are employed.

5.4.1 MPA in NaOH

Under basic conditions, both the carboxylic and thiol groups are deprotonated in the bulk species. Figure 5.7 shows the typical CV obtained in 0.1 M NaOH with 200 μM MPA solutions at Au(111) with a scan rate of 30 mV s^{-1}. It has been shown that the desorption of smaller chain functionalized thiol species, occurs at different potential values as a function of the gold single crystal orientation in base [39]. MPA also gives rise to more than one cathodic wave at polycrystalline electrodes, where both (111) and (110) surfaces are available [40, 41, 42]. Figure 5.7 only indicates one sharp defined peak (circa – 0.71 V) hence only the Au(111) orientation is present. The surface coverage of MPA in 0.1 M NaOH as evaluated from the desorption peak was 39 ± 4 μC cm^{-2} (or Γ of 4.1 x 10^{-10} mol cm^{-2}) when numerous scan rates were evaluated, listed in Table 5.1. This result is very close to the coverage of 4.0 x 10^{-10} mol cm^{-2} obtained in 0.5 M KOH by Pedrosa *et al* [43]. The value is slightly lower than the coverage for MPA evaluated in 0.1 M $KClO_4$. However, evaluating the coverage from CVs recorded at 20 mV s^{-1}, indicated an increased surface charge of 49 ± 3 μC cm^{-2}, which coincides with the coverage observed in perchlorate. This value is still quite lower than the charge of 66 μC cm^{-2} reported by Kim *et al* after 1 hour of immersion [33]. Sawaguchi *et al* [24] noted a total charge of 65.8 μC cm^{-2} for MPA desorption in base, after 10 minutes of immersion. This may well be a result of the allotted time for monolayer organization, as noted in $KClO_4$ as well, where MPA coverage was less than MEA coverage.

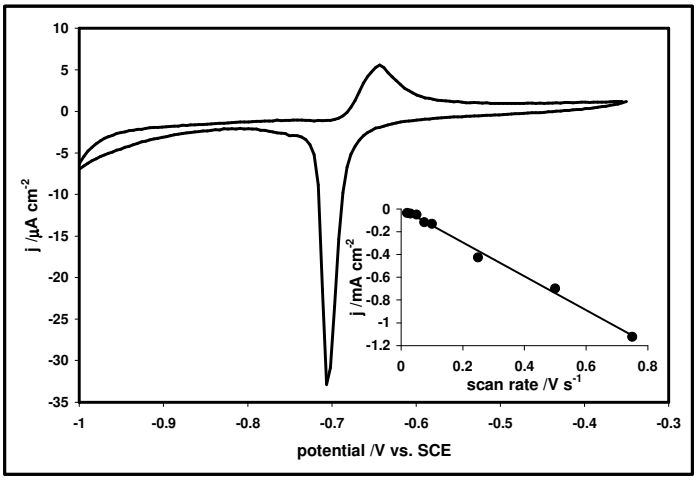

Figure 5.7: Cyclic voltammogram of MPA in 0.1 M NaOH recorded at 30 mV s^{-1} (after initial potential was held at -0.35 V for 200 seconds). The inset indicates the linearity of the peak current density for the desorption of MPA.

The inset of Figure 5.7 indicates that the peak current density for the desorption peak is linear in accordance with Equation 5.1. However, the determination of α yields an average value of 2.6 ± 0.1, which is not reasonable. Even if the surface charge were doubled (considering the values obtained at longer immersion times), α would still be greater than 1. To obtain α values within a reasonable range, a factor of 3 needs to be accounted for, and α would then approximate 0.85 ($\Gamma = Q/nFA$). This highlights that a simple one electron reduction model is not valid for all SAMs, and that a more complex solvent substitution reaction is occurring [30], although this was not noted for cys and $(cys)_2$ (Chapter 4). In contrast, the desorption peak potentials are in accordance with Equation 5.2 and linear with $\ln(\upsilon)$, providing a reasonable α value of 0.72 ± 0.05. The transfer coefficient evaluated from the peak potential is independent of the formal charge for the reaction. As has been commonly noted, the charging current in hydroxide leads to inflated surface coverage charges. The discrepancy between the α values obtained from the peak current and the peak potential values may well reflect that the charging current

contributes substantially due to a multi-step reduction. If a multi-step mechanism is indeed occurring, it does not appear to be reflected in the peak potential (E_p) relationship to the scan rate according to Equation 5.2.

It is also noted from Table 5.1 that the reported desorption potential of MPA in base is somewhat variable, and as expected, should correlate with the surface coverage. That is, the better formed the monolayer is, the more negative the required potential to induce desorption.

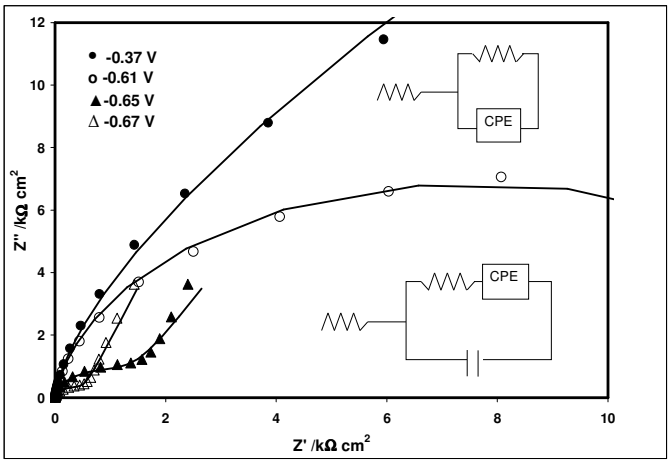

Figure 5.8: The Nyquist plots for MPA obtained in 0.1 M NaOH at select DC potentials: (•) at -0.37 V in the region of the capacitance minimum, (○) at -0.61 V, the onset of desorption, (▲) at -0.65 V and (Δ) -0.67 V during the desorption process. Data prior to desorption and at onset fit with ZARC, and once desorption had been initiated fit with circuit shown.

Figure 5.8 shows the typical Nyquist plots obtained for MPA in 0.1 M NaOH at various applied DC potentials: (•) at -0.37 V in the region near the capacitance minimum, (○) at -0.61 V where the onset of desorption is occurring, (▲) at -0.65 V and (Δ) -0.67 V during the desorption process. It is clear that even prior to desorption, a very well defined arc is present, and throughout the double layer region, the data fit very well with a simple ZARC circuit. In the potential region between -0.40 and -0.48 V, the double

layer capacitance was evaluated at 14.5 ± 0.5 μF cm^{-2} ($\alpha_f > 0.97$), in excellent agreement with reported values (Table 5.2). As the applied DC potential became more negative, an increase in the rate of desorption becomes evident as a compression of the arc. During the region of desorption, it was necessary to fit the data with the modified circuit shown in Figure 5.8. This circuit was also employed for the reduction of cys and $(cys)_2$ monolayers in 0.1 M NaOH [Chapter 4].

Figure 5.9 shows the Tafel slope obtained by plotting the ln of the inverse R_{CT} values. The slope values were found to range between 43 and 75 V^{-1}, and the inverse slopes of the log R_{CT} gave values of 30 to 48 mV per decade. This implies α values between 1.1 and 1.9, which again are higher than expected, as noted with the CV current data, as expected if the reaction is not a simple one electron transfer.

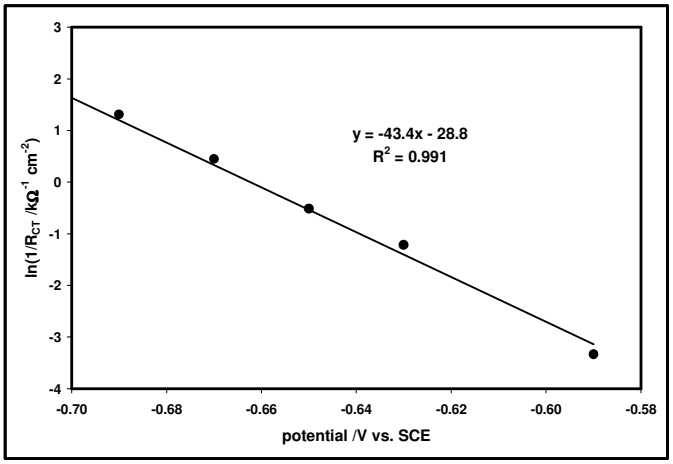

Figure 5.9: Tafel plot of the inverse R_{CT} during the desorption of MPA from Au(111) in 0.1 M NaOH.

5.4.2 MEA in base

In 0.1 M NaOH, bulk MEA is expected to be fully deprotonated at the amino and thiol moieties. A typical CV obtained in 0.1 M NaOH is shown in Figure 5.10, recorded at 0.02 V s^{-1}. Scans were always initiated at or near the OCP. At slow scan rates (0.05 V

s^{-1} or below), both cathodic peaks *a* and *b* are evident, attributed to trans and gauche species. At scan rates greater than 0.05 V s^{-1}, only peak *b* is evident, suggesting that under basic conditions the desorption is not equivalent as found in perchlorate. In determining the surface coverage for MEA, scan rates greater than 0.05 V s^{-1} were employed, where only peak *b* was present. The surface coverage for MEA from peak *b* was determined at 45 ± 3 μC cm^{-2} (Γ of 4.6 x 10^{-10} mol cm^{-2}) as listed in Table 5.1. Surface coverage in hydroxide from Au(111) has been given at 70 μC cm^{-2} (Γ of 7.3 x 10^{-10} mol cm^{-2}) [36] and 5.7 x 10^{-10} mol cm^{-2} [44], as well as other values noted in Table 5.1.

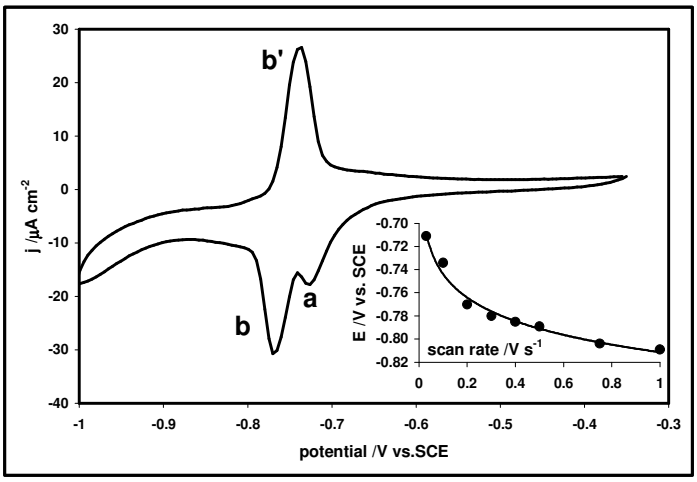

Figure 5.10: Cyclic voltammogram of MEA in 0.1 M NaOH recorded at 20 mV s^{-1} (after initial potential was held at -0.35 V for 200 seconds). The inset indicates the peak potential dependence for the desorption peak (b) as a function of scan rate.

The peak current density of peak *b* is linear with the scan rate, but as found with MPA, the α value using this method is not feasible. The determination of α yields an average value of 2.3 ± 0.2, much larger than what would be expected. Again, as found with MPA, α would still be greater than 1 if the MEA concentration were as much as doubled. Again, a factor of 3 would bring the value of α to a reasonable value of

approximately 0.76. However, as found with MPA, a more reasonable value for α is determined by using the desorption peak potential for process *b*. The inset of Figure 5.10 shows that the desorption peak potential is linear with ln(υ), as expected from Equation 5.2. For MEA, this provides an α value of 0.74 ± 0.09.

The double layer capacitance for a deprotonated or uncharged monolayer of MEA in base has been given as 15 μF cm^{-2} [16]. The Nyquist plots obtained for MEA were indistinguishable from those determined for MPA. In the double layer region prior to desorption, data were fit with a ZARC circuit, and values of 23.0 ± 0.1 μF cm^{-2} were obtained for the capacitance minimum in the region of -0.39 to -0.49 V where α_f was greater than 0.95 (Table 5.2). This is higher than expected for a deprotonated MEA layer, but compares well to the range of 20 to 26 μF cm^{-2} determined for cys and $(cys)_2$ derived monolayers in 0.1 M NaOH [Chapter 4].

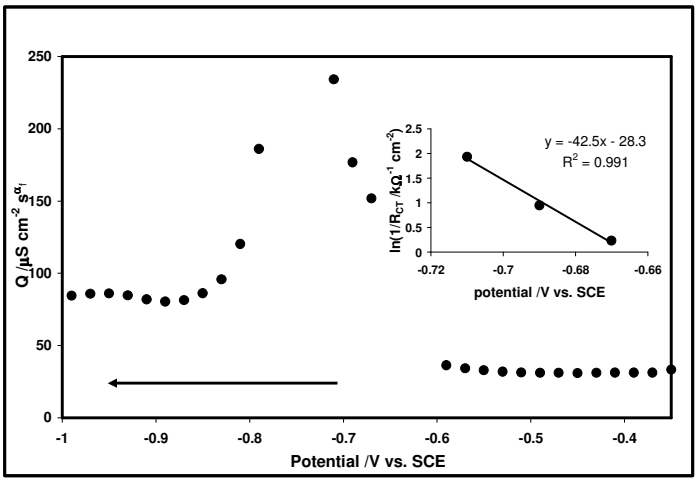

Figure 5.11: Approximation of the double layer capacitance in terms of *Q* for the reduction of cysteamine from Au(111) in 0.1 M NaOH. Data fit in same manner as for MPA. Inset shows the Tafel plot of the inverse R_{CT} during desorption.

Figure 5.11 shows the double layer capacitance values obtained at each DC potential. Although the double layer region prior to desorption (-0.35 V to -0.60 V) was

very reproducible, the region of desorption was quite difficult to fit, and varied for each data set. The inset of Figure 5.11 shows that the Tafel slope for MEA is quite similar to that obtained for MPA.

5.4.3 Summary in 0.1 M NaOH

Under basic conditions, the surface coverages appear to follow the same trend as noted for 0.1 M $KClO_4$. A lower coverage for MPA is obtained relative to MEA (if trans and gauche species are considered), and both single functionalized species have a higher coverage than cys (reported at 37 $\mu C\ cm^{-2}$) [10, 45, 46]. Since MEA CV's were characterized by two discrete waves at lower scan rates, coverage for the monolayer was determined at scan rates above 0.05 $V\ s^{-1}$, utilizing peak β. The desorption peak profiles for MPA were indistinguishable from those of cysteine, cystine and typical longer-chain alkanethiols, characterized by a single peak. The desorption peak due to the breakage of the thiol-Au bond is known to occur at differing potentials for differing gold faces and has been clearly demonstrated employing cysteine [39]. Similarly, MPA desorption from polycrystalline gold, displays numerous peaks as compared to desorption from Au(111) under alkali conditions [41, 42, 47]. Only the peak corresponding to the Au(111) face was evident in our evaluations of MPA. The desorption peak potentials in basic media are also known to correlate to alkane chain length, with more negative reduction potentials for longer chain thiols. The desorption peak potentials for the short chain functionalized species evaluated correspond to $(cys)_2$<MPA/cys<MEA.

The transfer coefficients for MPA and MEA when determined from the desorption peak potentials (using Equation 5.2) are 0.72 and 0.74, respectively. These values are the same within experimental error, and compare well to the α values determined for cys and $(cys)_2$ of 0.82. However, evaluations of α from both the CV current data, and the EIS charge transfer resistance, yield values in excess of 1. This was not found for cys and $(cys)_2$, where reliable values were extracted from the current data. Although cys and $(cys)_2$ fit with the model of a one electron transfer reduction, MPA and MEA clearly require a more complex solvent substitution reaction.

The inverse slopes of the log R_{CT} plots gave values of 30 to 48 mV per decade for MPA, and similar values are estimated for MEA. These values are smaller than the inverse slopes of 59 to 106 mV determined for cys and $(cys)_2$. However, the decrease in the slope values is anticipated based on chain length of the molecule [48]. The transfer coefficient for MPA and MEA evaluated from the R_{CT} indicates inflated values on the order of 1.1 to 1.9, whereas α determined for cys varied in the range of 0.55 to 0.99. It is apparent that contributions of the charging current are much more evident for the CO_2^- and NH_2 species, and less predominant for cys where both functional groups are present.

5.5 Conclusions

Evaluations of the MEA monolayers formed at 200 s under potential control indicate that in 0.1 M $KClO_4$ full saturation of MEA is achieved, as surface coverage charges approach maximum theoretical values, and the double layer capacitance is in agreement with previous studies. In contrast, SAMs formed under these conditions for MPA indicate lower surface coverage and increased double layer capacitance values,

suggesting that longer times for complete formation of the SAM are required. In the presence of 0.1 M NaOH the transfer coefficient evaluated from the desorption peak potential provides equivalent values on the order of 0.7. Evaluation utilizing either the peak current density or the charge transfer resistance greatly inflate the values of α, which had not been noted for cys SAMs where both functional groups are present.

5.6 Bibliography

[1] Vericat, C.; Lenicov, F. R.; Tanco, S.; Andreasen, G.; Vela, M. E.; Salvarezza, R. C. *Journal of Physical Chemistry B*, **2002**, *106(35)*, 9114.

[2] Zhang, J.; Welinder, A. C.; Hansen, A. G.; Christensen, E. M.; Ulstrup, J. *Journal of Physical Chemistry B*, **2003**, *107(45)*, 12480.

[3] Imbayashi, S.-i.; Mita, T.; Kakiuchi, T. *Langmuir* **2005**, *21(4)*, 1470.

[4] Bonanni, B.; Bizzarri, A. R.; Cannistraro, S. *Journal of Physical Chemistry B* **2006**, *110(30)*, 14574.

[5] Andolfi, L.; Bizzarri, A. R.; Cannistraro, S. *Thin Solid Films* **2006**, *515*, 212.

[6] Shervedani, R. K. and Mozaffari, S. A. *Analytical Chemistry* **2006**, *78(14)*, 4957.

[7] Phong, P. H.; Ooi, Y.; Hobara, D.; Nishi, N.; Yamamoto, M.; Kakiuchi, T. *Langmuir* **2005**, *21(23)*, 10581.

[8] Phong, P. H.; Sokolov, V. V.; Nishi, N.; Yamamoto, M.; Kakiuchi, T. *Journal of Electroanalytical Chemistry* **2007**, *600*, 35.

[9] Petri, M.; Kolb, D. M.; Memmert, U.; Meyer, H. *Electrochimica Acta* **2003**, *49*, 183.

[10] Hager, G. and Brolo, A. G. *Journal of Electroanalytical Chemistry* **2003**, *550-551C*, 291.

[11] Smith, C. P. and White, H. S. *Langmuir* **1993**, *9*, 1.

[12] Fawcett, W. R.; Fedurco, M.; Kovacova, Z. *Langmuir* **1994**, *10*, 2403.

[13] Andreu, R. and Fawcett, W. R. *Journal of Physical Chemistry* **1994,** *98(48)*, 12753.

[14] Hu, K. and Bard, A. J. *Langmuir* **1997**, *13*, 5114.

[15] Zhao, J.; Luo, L.; Yang, X.; Wang, E.; Dong, S. *Electroanalysis* **1999**, *11(15)*, 1108.

[16] Kakiuchi, T.; Iida, M.; Imbayashi, S-i.; Niki, K. *Langmuir* **2000**, *16*, 5397.

[17] Nishiyama, K.; Kunbo, A.; Ueda, A.; Taniguchi, I. *Chemistry Letters* **2002**, 80.

[18] Schweiss, R.; Werner, C.; Knoll, W. *Journal of Electroanalytical Chemistry* **2003**, *540*, 145-151.

[19] Burgess, I.; Seivewright, B.; Lennox, R. B. *Langmuir* **2006**, *22*, 4420.

[20] Zhang, J.; Demetriou, A.; Welinder, A. C.; Albrecht, T.; Nichols, R.; Ulstrup, J., *Chemical Physics* **2005,** *319(1-3)*, 210.

[21] Kudelski, A. *Journal of Raman Spectroscopy* **2003**, *34*, 853.

[22] Michota, A.; Kudelski, A.; Bukowska, J. *Surface Science* **2002**, *502-503*, 214.

[23] Lee, S. Y.; Noh, J.; Ito, E.; Lee, H.; Hara, M. *Japanese Journal of Applied Physics* **2003**, *42*, 236.

[24] Sawaguchi, T.; Sato, Y.; Mizutani, F. *Journal of Electroanalytical Chemistry* **2001**, *507(1-2)*, 256.

[25] Zhang, J.; Christensen, H. E. M.; Ooi, B. L.; Ulstrup, J. *Langmuir* **2004**, *20(23)*, 10200.

[26] Imbayashi, S.-i.; Iida, M.; Hobara, D.; Feng, Z. Q.; Niki, K.; Kakiuchi, T. *Journal of Electroanalytical Chemistry* **1997**, *428*, 33.

[27] Sawaguchi, T.; Sato, Y.; Mizutani, F. *Physical Chemistry and Chemical Physics* **2001**, *3*, 3399.

[28] Imae, T. and H. Torii, *Journal of Physical Chemistry B* **2000,** *104(39)*, 9218.

[29] Wirde, M.; Gelius, U.; Nyholm, L. *Langmuir* **1999**, *15(19)*, 6370.

[30] Laredo, T.; Leitch, J.; Chen, M.; Burgess, I. J.; Dutcher, J. R.; Lipkowski, J. *Langmuir* **2007**, *23(11)*, 6205.

[31] Bard, A. J.and Faulkner, L. R. Electrochemical Methods: Fundamentals and Applications; 2nd ed.; John Wiley: New York, 2001

[32] Shimazu, K.; Teranishi, T.; Sugihara, K.; Uosaki, K. *Chemistry Letters* **1998**,669.

[33] Kim, K. and J. Kwak, *Journal of Electroanalytical Chemistry* **2001**, *512(1-2)*, 83.

[34] Esplandiu, M. J.; Hagenstrom, H.; Kolb, D. M. *Langmuir* **2001**, *17(3)*, 828.

[35] Shervedani, R. K.; Bagherzadeh, M.; Mozaffari, S. A. *Sensors and Actuators B* **2006**, *115*, 614.

[36] Ooi, B. L.; Hobara, D.; Yamamoto, M.; Kakiuchi, T. *Langmuir* **2005**, *21(24)*, 11185.

[37] Carot, M. L.; Esplandiu, M. J.; Cometto, F. P.; Patrito, E. M.; Macagno, V. A. *Journal of Electroanalytical Chemistry* **2005**, *579*, 13.

[38] Boubour, E. and Lennox, R. B. *Langmuir* **2000**, *16*, 7464.

[39] Arihara, K.; Ariga, T.; Takashima, N.; Arihara, K.; Okajima, T.; Kitamura, F.; Tokuda, K.; Ohsaka, T. *Physical Chemistry and Chemical Physics* **2003**, *5*, 3758.

[40] Mendes, R. K.; Carvahal, R. F.; Kubota, L. T. *Journal of Electroanalytical Chemistry* **2008**, *612*, 164.

[41] Carvahal, R. F.; Freire, R. S.; Kubota, L. T. *Electroanalysis* **2005**, *17(14)*, 125.

[42] Shimazu, K.; Hashimoto, Y.; Kawaguchi, T.; Tada, K. *Journal of Electroanalytical Chemistry* **2002**, *534*, 163.

[43] Pedrosa, V. A.; Lowinsohn, D.; Bertotti, M. *Electroanalysis* **2006**, *18(9)*, 931.

[44] Zhang, J.; Bilic, A.; Reimers, J. R.; Hush, N. S.; Ulstrup, J. *Journal of Physical Chemistry B* **2005**, *109(32)*, 15355.

[45] Zhang, J.; Chi, Q.; Nielsen, J. U.; Friis, E. P.; Andersen, J. E. T.; Ulstrup, J. *Langmuir* **2000**, *16*, 7229.

[46] Matsunaga, M.; Nakanishi, T.; Asahi, T; Osaka, T. *Chirality* **2007**, *19*, 295.

[47] Hobara, D.; Miyake, K. ; Imbayashi, S.-i.; Niki, K.; Kakiuchi, T. *Langmuir* **1998**, *14(13)*, 3590.

[48] Sahalov, H.; O'Brian, B.; Stebe, K. J.; Hristova, K.; Searson, P. C. *Langmuir* **2007**, *23*, 9681.

Chapter 6: Summary and Conclusions

6.1 In the Presence of 0.1 M $KClO_4$

It is clear that the direct comparison of the various species in 0.1 M $KClO_4$ is not ideal, since large changes in the solution pH occur due to the acid and/or base functional groups of the analyte upon addition. Future work in this area should incorporate stable and controllable pH conditions, as afforded by the use of a readily purifiable buffer system. As expected, the solution pH in perchlorate media was slightly acidic (~5.6) for the cys and $(cys)_2$ species, alkaline for MEA, and acidic for MPA.

However, some generalizations can be made. Table 6.1 highlights the major electrochemical parameters determined in this study. The desorption potential (E_p) is mostly a function of solution pH (with contributions of monolayer stability). The short incubation times for the SAMs (200 s near the OCP) indicated low surface coverage for cys and $(cys)_2$ both having CO_2^- and NH_2 groups, with coverage for $(cys)_2$ being the lowest. Intermediate coverage was observed for MPA (CO_2^- containing species) and near to full attainable coverage for MEA (NH_2 containing species).

Table 6.1: Electrochemical parameters obtained for all four types of SAMs in 0.1 M $KClO_4$.

	Final solution	E_p	Coverage (Γ)	C_{DL}	Transfer coefficient (α)		
SAM	pH	/V vs SCE	/x 10^{-10} mol cm^{-2}	/μF cm^{-2}	$CV_{(Ep)}$	$CV_{(current)}$	$EIS_{(Rct)}$
cys	5 - 6	-0.63	3.0 - 3.4	15	n/a	n/a	0.85
$(cys)_2$	5 - 6	-0.64	2.4	15	n/a	n/a	n/a
MPA	3.3 - 4	-0.52	4.9	15	0.94	0.81	n/a
MEA	7.6 - 8	-0.70	6.9	15.5	n/a	n/a	n/a

The double layer capacitance for all SAMs was determined at approximately 15 μF cm^{-2} as shown in Table 6.1. These values are lower than the capacitance in the presence of electrolyte only (~22 μF cm^{-2}), and do not seem to be affected by the degree of surface coverage or functional group presence of the species.

Cys and $(cys)_2$ derived SAMs indicate two very different processes during monolayer reduction in 0.1 M $KClO_4$. Prior to the main desorption, there is an additional surface reaction attributed to a de-protonation step of the NH_2 group. Since cys species have a tendency to form dimerized subunits, whereby the CO_2^- and NH_2 groups hydrogen bond, disruption of the hydrogen bond would be facilitated by de-protonation of the amine. This may be coupled with a re-orientation of the molecules, as has been noted on silver surfaces. SAMs formed from MPA indicated no additional process prior to desorption. However, in the presence of bulk MPA, a passifying reaction occurs post-desorption. The two surface isomers known for MEA (trans and gauche) are shown to have the same mechanistic and kinetic desorption.

6.2 In the presence of 0.1 M NaOH

Under basic conditions (pH ≥ 11), the solution pH is in a range where none of the surface species would be protonated. Desorption of the SAMs indicated that a simple one electron transfer was occurring based on dynamic and steady-state measurements.

Table 6.2 lists the comparative electrochemical parameters determined in basic solution. The cys SAMs provided the same coverage as typically reported for longer incubation times, suggesting assembly is complete after 200 s. The $(cys)_2$ SAMs which

were found to provide much lower coverage than cys, indicate that this is a result of longer binding and organization times required for the disulfide species. The same differences in surface coverage were noted in perchlorate. MPA surface coverage was higher than that observed for cys and $(cys)_2$ SAMs, but lower than MEA SAMs. Surface coverage was highest for MEA, when both the gauche and trans isomers were considered. This is attributed to the fact that the NH_2 group further facilitates binding, and coverage at 200 s was optimal and comparable to much longer incubation times.

Table 6.2: Electrochemical parameters obtained for all four types of SAMs in 0.1 M NaOH.

	E_p	Coverage (Γ)	C_{DL}	Transfer coefficient (α)		
SAM	/V vs SCE	/x 10^{-10} mol cm^{-2}	/μF cm^{-2}	$CV_{(Ep)}$	$CV_{(current)}$	$EIS_{(Rct)}$
cys	-0.72	3.9	20 - 26	0.82	0.90	0.55 - 0.99
$(cys)_2$	-0.67	2.4	20 - 26	0.82	0.78	0.55 - 0.99
MPA	-0.71	5.1	14.5	0.72	2.6	1.1 - 1.9
MEA	-0.76	8.3	23	0.74	2.3	~1

In terms of the desorption potentials, these correlate to the surface coverage in 0.1 M NaOH of the respective species, and were determined proceeding towards more negative potentials as: $(cys)_2$<MPA/cys<MEA. Both CV and EIS measurements show that $(cys)_2$ desorbs at more positive potentials than cys, further supporting that the disulfide requires longer SAM formation times.

The transfer coefficients obtained for all species using the desorption potentials from CV measurements are found to be very similar, as shown in Table 6.2. However, evaluations of α from EIS measurements only provided realistic values for cys and $(cys)_2$, as MEA and MPA values were found to be inflated. An apparent factor of 3 for

MPA and MEA derived SAMs was noted in the determination of α from CV peak current data. It is quite possible that since MPA and MEA are somewhat smaller in size than cys, that charging currents associated with the strongly adsorbed OH^- electrolyte contribute significantly. This data also supports that the assumptions of a simple one-electron transfer reaction during the reduction process are not always valid. As in perchlorate, MEA clearly showed the presence of both trans and gauche isomers.

The double layer capacitance (C_{DL}) was found to be lowest for MPA (14.5 μF cm^{-2}) and approximately 5 - 10 μF cm^{-2} higher for cys, $(cys)_2$ and MEA. This result is somewhat unexpected, as typically the C_{DL} increases with increasing charge on the monolayer. Since MEA afforded full theoretical coverage, and no charge should be carried on the NH_2 group at the potentials evaluated, this observation can only be attributed to more complex double layer structures involving the hydroxide ions.

For future work it is recommended that these systems be evaluated at a basic pH, but in the absence of the strongly binding hydroxide ions.

6.3 Conclusions

Based on the overall results, the following final conclusions are drawn. Electrochemically induced SAMs obtained from MEA are found to provide the most consistent results in comparison to SAMs formed by long incubation times. It is likely that the presence of the NH_2 group greatly enhances binding to the surface. Thus, even SAMs prepared from cys were consistent with expected values in 0.1 M NaOH, even at the very short incubation times. Use of $(cys)_2$ provided the least well formed SAMs, as a

consequence of the disulfide adsorption, indicating that this species is not amicable to rapid monolayer formation. MPA as well, does not provide sufficiently well formed SAMs when short term potential controlled adsorbtion is induced.

Use of impedance spectroscopy, and the requirement of a CPE component, highlight that the desorption process is much more complex than a simple one electron transfer. Although in general the simplified circuits used in this study were suitable for an initial investigation, much more work in this area is warranted. Assumptions of a simple one-electron transfer process are adequate, yet it is clear that the surface reactions are much more complex. Since the formal charge associated with monolayer desorption varies more in hydroxide solutions, the evaluation of MPA and MEA clearly show that different treatments of the desorption mechanism are needed.